STUDY OF SINTERING AND STRUCTURE-PROPERTY RELATIONSHIPS IN BORON SUBOXIDE (B_6O) – ALKALINE EARTH METAL OXIDE, COBALT, AND NICKEL COMPOUND

ENOCH NIFISE, OGUNMUYIWA

A dissertation submitted to the Faculty of Engineering and the Built Environment, University of the Witwatersrand, Johannesburg, in fulfillment of the requirements for the degree of Master of Science in Engineering.

2009

DECLARATION

I declare that this dissertation is my own unaided work. It is being submitted for the degree of Master of Science in Engineering to the University of the Witwatersrand, Johannesburg. It has not been submitted before for any degree or examination to any other university.

…….

Enoch Nifise, OGUNMUYIWA

…….Day of …… Year ……

ABSTRACT

Recently some progress has been reported in improving the fracture toughness of boron suboxide (B_6O). This involved the introduction of second phases in it at low levels of doping. This study extends this work through the addition of different additives and through the improvement of densification, by controlled sintering.

Boron suboxide powders were sintered with and without additives. Pure B_6O powders were sintered at a temperature of 1900^oC under a load of 50 MPa for 20 minutes in an argon environment. B_6O powders mixed with different additives, including alkaline-earth metal oxide, nickel and nickel compounds, cobalt compounds and chromium boride. These powders were sintered at a temperature of 1850^oC under loads from 50 -80 MPa, for 20 minutes in an argon environment. Microstructure, phase composition and properties were investigated.

Boride secondary phases were formed when hot pressing B_6O admixed with nickel and nickel compounds, cobalt compounds and chromium boride additives while the alkaline earth metal oxide additives resulted in the formation of boride and borate phases, depending on the oxide used. The mechanisms leading to the achievement of increased toughness and the possible reasons for toughness variation with the different additives are critically analyzed.

Good combinations of mechanical properties were achieved for B_6O-cobalt compound additive with hardness values from 32.6 – 34.9 GPa and fracture toughness from 5.2 to 5.8 $MPa.m^{0.5}$ for B_6O-Co_2B and B_6O-CoO materials respectively.

DEDICATION

To the Almighty God and the most important people in my life: my parents, brothers and sisters, and most especially, my dear wife, Motunrayo.

ACKNOWLEDGEMENTS

I would like to acknowledge the following people for the valuable contributions which facilitated the completion of this research work.

(i). Prof. I. Sigalas for suggestions and supervising this work.

(ii). Dr. M. Herrmann for his advice, useful comments, time and constructive criticism.

(iii). Johnson, for assistance with the SEM works – you are a friend indeed.

(iv). Support staff of the School of Chemical and Metallurgical Engineering (University of the Witwatersrand) namely, Aubrey, Graham, Gift, Johnson, Bruce and Theo for their assistance with specimen preparation.

(v). Element Six (Pty) Ltd – Diamond Research Laboratory for their financial support.

(vi). NRF for financial assistance.

(vii). The ceramics group for their special friendship and all postgraduate students in the School of Chemical and Metallurgical Engineering for their friendship

(viii). My family, especially Engr. Ogunmuyiwa M.O., for the support and sacrifices throughout this period.

(ix). Finally, to my wife, Motunrayo. For your continued love, understanding, support and above all patience - Ngiyabonga.

TABLE OF CONTENTS

Chapter Three

Chapter Four

Chapter Five

Chapter Six

References

LIST OF FIGURES

LIST OF TABLES

LIST OF SYMBOLS

SEM	=	Scanning Electron Microscopy
EDX	=	Energy Dispersive X-ray Spectroscopy
TEM	=	Transition Electron Microscopy
XRD	=	X-ray diffraction
ICSD	=	International Centre for Diffraction Data
ICP-OES	=	Inductively coupled plasma optical emission spectroscopy
Hv	=	Vickers hardness
K_{IC}	=	Fracture toughness
GPa	=	GigaPascal
MPa	=	MegaPascal
hr(s)	=	hour(s)
min(s)	=	minute(s)
μm	=	micron
m	=	meter
wt%	=	Weight percent
^{o}C	=	degrees Celsius
K	=	degrees Kelvin

CHAPTER ONE

1 Introduction

The synthesis of new materials with hardness comparable to or even harder than that of diamond is of considerable fundamental and technological interest and is a great challenge to chemists, physicists, and material scientists. Most of the known ultrahard materials, including diamond and cubic boron nitride (cBN), were first synthesized in the 1950s and industrially manufactured using a high pressure – high temperature process (Bundy et al., 1955; Wentorf 1957, 1961). Extensive research in this domain continues and recently a number of new ultrahard materials have been discovered (Zerr and Reidel, 2000).

Diamond and cubic boron nitride (cBN) combine excellent mechanical, chemical, and physical properties. However, owing to its instability at high temperatures, diamond cannot be used, for example, as a cutting tool for steel, due to its chemical interaction with that metal. cBN, owing to the attributes of great hardness and abrasion resistance, coupled with a higher chemical stability than diamond when in contact with ferrous alloys, can be used to machine both steel and cast iron. However, as temperature increases cBN weakens due to diffusion wear and transformation to its hexagonal structure (hBN) (Zerr and Reidel, 2000). The synthesis of diamond and cubic boron nitride materials also require high pressures and temperatures, which make their production expensive and limit the sizes and geometric forms possible.

For this reason and because of the need to replace expensive diamond in many other applications, new hard materials with comparable or even superior properties are required.

Boron suboxide is third in hardness after diamond and cBN (31 to 38 GPa) (Ellison-Hayashi et al, 1994; Itoh et al., 1998; Itoh et al., 2000; Kayhan and Inal, 1999; Olofsson and Lundström, 1997; Sasai et al., 2001 and Veprek, 2000). Boron suboxide (nominally B_6O) qualifies as a "superhard phase", with a single crystal having a hardness of 45 GPa and with abrading properties compared to those of diamond, of H_V = 70-100 GPa (Ellison-Hayashi et al, 1994) and cubic boron nitride, H_V = 60 GPa (Zhongwu and Yusheng, 2005: Itoh et al., 1998). In addition to this hardness, the fracture toughness of this material (single crystal) has been found to be 4.5 MPa.$m^{0.5}$, which approaches that of single crystal diamond at 5 MPa.$m^{0.5}$ (Duanwei et al., 2002) and is significantly better than that of a single cubic boron nitride crystal at 2.8 MPa.$m^{0.5}$ (Brookes, 1986). Boron suboxide has a better thermal stability compared to that of diamond (He et al., 2002) and can be produced without high pressure. These properties suggest that B_6O may be a good candidate for cutting tool and other wear part applications where abrasive wear resistance is important. The strong covalent bonds and short interatomic bond length contribute to exceptional physical and chemical properties such as great hardness, low mass density, high chemical inertness and excellent wear resistance (Itoh et al., 1998; Olofsson and

Lundström, 1997; Garvie et al., 1997; He et al., 2002; Hubert et al., 1998; Yu et al., 2000 and Itoh et al., 2000).

B_6O powders can be produced without any pressure being applied, at moderately high temperatures (1380^{o}C) (Shabalala, 2007), under argon, by reducing B_2O_3 with B or by oxidation of boron with zinc oxide or other oxidants. It has been established that boron suboxide powders formed at or near ambient pressures are generally oxygen deficient (B_6O_x, $x<0.9$). High pressure applied during the synthesis of B_6O can significantly increase the crystallinity, oxygen stoichiometry, and crystal size of the products (Hubert *et al*., 1998). Boron suboxide powders of nominal composition B_2O, B_3O, B_4O, B_6O_{1-x} ($0.72\leq x\leq 0.96$), B_8O, $B_{12}O$, $B_{15}O$, $B_{18}O$, $B_{20}O$ and $B_{22}O$ have been reported (Badzain, 1988; Brodhag and Thévenot, 1986; Ellison-Hayashi et al, 1992; Hall and Compton, 1965 and Kharlamov et al., 2002). Although boron suboxide is reported as having nominal compositions, it is widely accepted to be non-stoichiometric and the reported compositions range from $B_6O_{0.72}$ to $B_6O_{0.86}$ at ambient temperature. Thus, the formula is best reported as B_6O_x where $x < 1$ (Ellison-Hayashi et al, 1992).

In spite of the high fracture toughness (4.5 MPam$^{0.5}$) of a single crystal of B_6O, the fracture toughness for polycrystalline B_6O is less than 1.5 MPam$^{0.5}$ which limits industrial applications. The low fracture toughness obtained in the sintered

compacts is not completely clear. Efforts have been made to increase the fracture toughness by forming B_6O composites with other ultrahard materials such as diamond, boron carbide (B_4C), and cBN (Itoh et al., 2000; Sasai et al., 2001). Despite good hardness values, the fracture toughness of the B_6O materials was either not reported or it was very low. In other words, the B_6O sintered compacts produced till now usually were found to be very brittle.

Hot pressed B_6O materials have yielded a good hardness of between 30 and 38 GPa (Holcombe and Ottis, 1972; Goosey, 1974; Bairamashvili *et al*., 1979), but no value of fracture toughness have been reported. Promising mechanical properties, especially fracture toughness, for hot pressed B_6O materials, have only been reported by Kayhan and Inal (1999). However, property measurements involved the use of a rather high radius crack, and a high level of porosity in the produced compact, thus rendering them quite suspect.

Studies were made by Itoh et al. (2000) to improve the mechanical properties of B_6O materials by introducing other hard materials, such as B_4C and cBN, as a binder in the materials. Maximum microhardness $H_{v0.1}$ of 46 GPa was obtained from B_6O-30vol%B_4C sintered composite under the sintering conditions of 4 GPa, 1700^{o}C for 20 minutes. The fracture toughness was approximately 1 MPa.m$^{0.5}$. The fracture toughness of the B_6O-x-cBN composites increased as the cBN content

increased; the maximum fracture toughness (1.5-1.8 MPa.$m^{0.5}$) was observed for x = 40-60vol%. Crack deflection along the B_6O-cBN grain boundary contributed to increasing the fracture toughness. The fracture toughness attained is too low to make ultrahigh pressure sintering a commercially attractive option for these materials.

Furthermore, studies by Shabalala et al. (2006) to improve the mechanical properties of B_6O material by introducing a small amount of aluminium using the hot pressing technique at 1900^oC for 20 minutes with an applied pressure of 50 MPa reported a hardness of 29.3 ± 0.5 GPa (2.2wt % of Al) and a potentially useful fracture toughness of 3.0 ± 0.12MPa.$m^{0.5}$. He also reported that doping B_6O with a small volume fraction of Al_2O_3 resulted in a pronounced improvement of the mechanical performance of the hot-pressed material and in particular, a marked increase in fracture toughness (4.25 ± 0.25 MPa.$m^{0.5}$ with 7.2wt% Al), but with low hardness (24.5 ± 0.8 GPa).

Andrews et al. (2007) prepared B_6O composites by hot pressing B_6O powder with varying weight percentages of alumina, aluminum and carbon additions. Dense materials with a hardness of 30.2 ± 0.6 GPa and fracture toughness of 3.2 ± 0.2 MPa.$m^{0.5}$ were achieved at 1900^oC.

1.1 Justification of the study

It is very difficult to sinter B_6O powders to full density, but a careful selection of additives in combination with controlled sintering conditions could result in the production of B_6O materials having unique combination of mechanical properties for industrial applications. Hot pressed B_6O materials have not produced a combination of good mechanical properties, having hardness values between 30 and 38 GPa (Holcombe *et al*., 1972; Goosey, 1974; Bairamashvili *et al*., 1979), but the fracture toughness measurements were not reported.

The composition of the grain boundary phase and the grain sizes of the phases in the sintered material are the main features in the microstructure that influence the mechanical properties of the material, especially fracture toughness. The presence of secondary phases in the sintered compacts allows the activation of toughening mechanisms such as crack bridging and crack deflection. This is assumed to occur because of mismatch in thermal expansion between the grain boundary phases and the B_6O phases, which places the grain boundary and the grains under residual stress (Shabalala, 2007; Peterson and Tien, 1995). In some of the B_6O sintered composites investigated, the sintering additives acted as liquid phase at sintering temperature which could have an added advantage of lowering the sintering temperature, rate of grain growth and the cost of production and hence a finer grain size could be obtained. This results in a material with higher hardness, strength and wears

resistance (Shabalala T.C (2007), Kayhan *et al*. (1999)). This research work is therefore aimed at improving the mechanical properties, especially fracture toughness of B_6O-based composites by incorporating suitable secondary phases.

The research carried out in this MSc is aimed at addressing the following questions

- ✓ Can the introduction of Ca, Mg, Ni, Co oxides and compounds improve the mechanical properties of the B_6O-based composites?
- ✓ To what extent would the secondary phase(s) affect the grain boundaries of the composites?
- ✓ What toughening mechanisms are involved?
- ✓ Which phase(s) produces the optimum hardness-toughness relationship in the B_6O-based composite?
- ✓ What would be the relationships between the structure of the resulting composites and their mechanical properties?

1.2 Aim of the research

This research work is aimed at investigating the properties and structure of various hot pressed B_6O powders with and without selected additives (alkaline earth metal oxide, nickel and nickel compounds, cobalt compounds and chromium boride) and

the effect of the additives on the overall mechanical properties of the B_6O composites.

To achieve the above stated aim, a detailed literature review on boron suboxide-based ultrahard materials together with their properties are presented in chapter 2. Chapter 3 outlines the methodology and equipment used for the experiments. The results and discussions of the experiments are presented in chapters 4 and 5 respectively, while chapter 6 outlines the conclusions and recommendations based on the experimental results.

CHAPTER TWO

2 Introduction

This chapter reviews the available knowledge on boron-based superhard materials with particular emphasis on boron suboxide materials, B_6O.

2.1 Hard materials

Generally, hard materials are solids with high hardness in the range of 8 – 10 on the Mohs' scale of hardness, given by the sequence of minerals which can be scratched by the next (Table 2.1). Usually, common hard materials are subdivided into compounds with metallic (TiN or WC), ionic (Al_2O_3), or covalent bonding (diamond, Si_3N_4) (Holleck, 1986).

Hardness

Hardness is one of the quantitative parameters that describe the resistance of a material towards plastic (irreversible) deformation. Plastic deformation starts when the shear component of the stress applied to a material exceeds some value called "the yield stress". There are many ways to create a plastic deformation and consequently many ways to define and to measure the resistance of a material towards such deformations. Hardness can thus be determined by scratching, grinding and indentation methods. The indentation method of measuring hardness is

considered for the purpose of this study. The Vickers hardness is defined by equation 2.1

$$H_v = 1854.4 \times \frac{P}{d^2} \qquad \textbf{[2.1]}$$

Where H_V = Vickers hardness, measured in GPa

P = load applied, measured in MPa

d = diagonal of square based indentation, measured in mm.

Table 2.1: Knoop hardness ranking of minerals and some prominent synthetic ceramic materials (*Spear, 1989; Binder 1975)*

Mineral /Synthetic materials	Microhardness, Knoop 100 GPa
β-Si_3N_4	17
Al_2O_3	21
SiC	26
α-Si_3N_4	26 – 35
TiC	28
B_4C	30
TiB_2	30
B_XO	30 – 59
SiO_2	33
cBN	45
Diamond (C)	75 – 100

Superhard/ ultrahard materials

Superhard materials can be defined as materials having a Vickers hardness of H_v > 40GPa. In addition to high hardness – the capability of a material to withstand imprinting or scratching by another material – they usually possess other unique properties, such as compressive strength, shear resistance, low mass density, high mechanical strength, high thermal conductivity, high chemical inertness, high melting temperature, large bulk moduli (a measure of resistance to volume change created by applied pressure) and excellent wear resistance (Torsten, 1997). They are phases of compounds with short bond lengths with high cohesive energies (Brazhkin et al., 2002). They are formed between light elements and often contain boron, carbon, nitrogen and oxygen, as one component, for example, cBN, B_4C and B_6O. The materials include semiconductors, useable also at high temperatures (Torsten, 1997).

This combination of properties makes the materials highly desirable for a number of applications (Zerr and Riedel, 2000). Ultrahard materials are widely used as wear parts, grinding, and cutting tools. Currently, only diamond and cubic boron nitride (cBN) are used in industry as ultrahard materials. Table 2.2 shows the properties of some selected hard materials.

Table 2.2: Density, hardness, bulk and shear modulus of some selected hard materials.

Material	**Density (g/cm^3)**	**Hv_1 (GPa)**	**Bulk modulus (GPa)**	**Shear modulus (GPa)**	**Reference**
Diamond	3.52	70	443	535	Cook et al., 2000
c-BN	3.48	45-50	400	409	Cook et al., 2000
B_4C	2.52	30-50	250	-	Cook et al., 2000
TiB_2	4.50	30-33	244	263	Cook et al., 2000
AlB_{12}	2.58	26	-	-	Cook et al., 2000
$AlMgB_{14}$	2.66	32-35*	212	231	Cook et al., 2000; Tadeka et al, 2004

*Load not specified

Structurally these materials either belong to the tetrahedrally coordinated, diamond-related group of compounds or they belong to the icosahedral, boron-rich group of compounds. The former group includes representatives of the zinc blende and wurtzite types of structure, for instance BN, BP, $BeSiN_2$ (superstructure), and SiC (Hall and Compton, 1965). The second group includes representatives of many structure types, although the most prominent ones are structures related to that of boron carbide and boron modifications (Uno and Higashi, 1994, Lundström and Bolmgren, 1994, and Lundström, 1997). Figure 2.1 illustrates a map of such materials in the phase diagram of the B-C-N-O system.

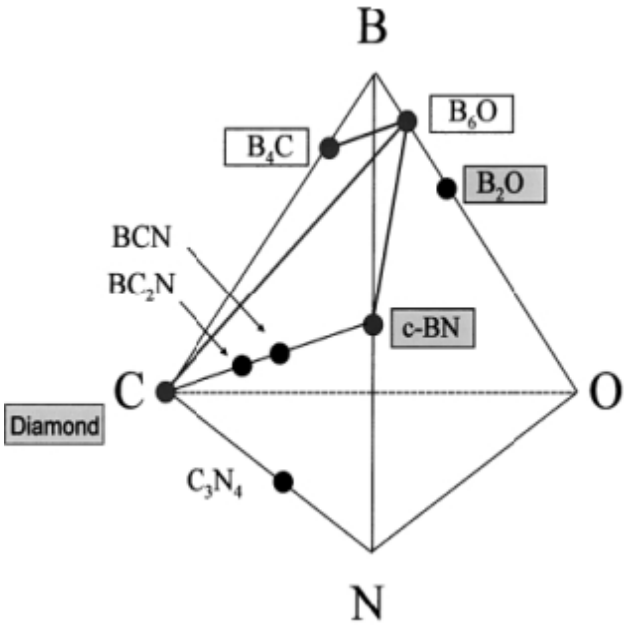

Figure 2.1: Map of superhard materials in the phase diagram of the B-C-N-O system. (Itoh, 2004)

2.2 Boron-based hard materials

Elemental boron is very hard and in its extremely pure form has a microhardness of 30 GPa, but is much too brittle for practical use (www.chemtopics.com). At high temperatures it is a good conductor but at room temperature and below it is an insulator. This behaviour as well as many of its other properties earns it the classification of a *metalloid*. The high hardness is related to a low molar volume of $5cm^3$ and a covalent bonding of the rhombohedral crystal structure. Boron compounds have exceptional properties in respect of their chemical bonding, crystal structure, and phonon and electron conduction (Gao et al., 2005).

Boron exists in many polymorphs for example two rhombohedral forms, α and β-boron containing 12 and 105 atoms in the rhombohedral unit cell respectively, α and β tetragonal boron, and an amorphous form. The different phases depend on the temperature, pressure, and reactants present during formation (Ellison-Hayashi et al., 1992) Boron atoms form very stable clusters such as an octahedron, an icosahedron, and other polyhedrons. Such structure characteristics resulting from the covalent nature of the bonding and forming a rigid three-dimensional framework, determine their bulk properties of high hardness and refractory nature.

The crystal structures of α- and β-boron are shown in figure 2.2. Both have a rhombohedral Bravais lattice with a space group of $R\bar{3}m$ in its perfect form. The icosahedral unit B_{12} is a common building block (Badzian, 1988; Masago et al., 2006). The structure of β-boron is complex with a unit cell consisting of 105 atoms, which can be classified into 15 nonequivalent atomic sites on the assumption of $R\bar{3}m$ symmetry (Hoard et al., 1970). Site B(13) in figure 2.2 is only partially occupied with an occupancy of 73.4%. The missing boron atoms appear at extra site B(16) with an occupancy of 26.6%. The most easily available modification of boron that is found commercially or made within the laboratory is the β phase (Masago et al, 2006). Hence, this phase is considered to be the thermodynamically stable phase (Badzian, 1988; Masago et al., 2006).

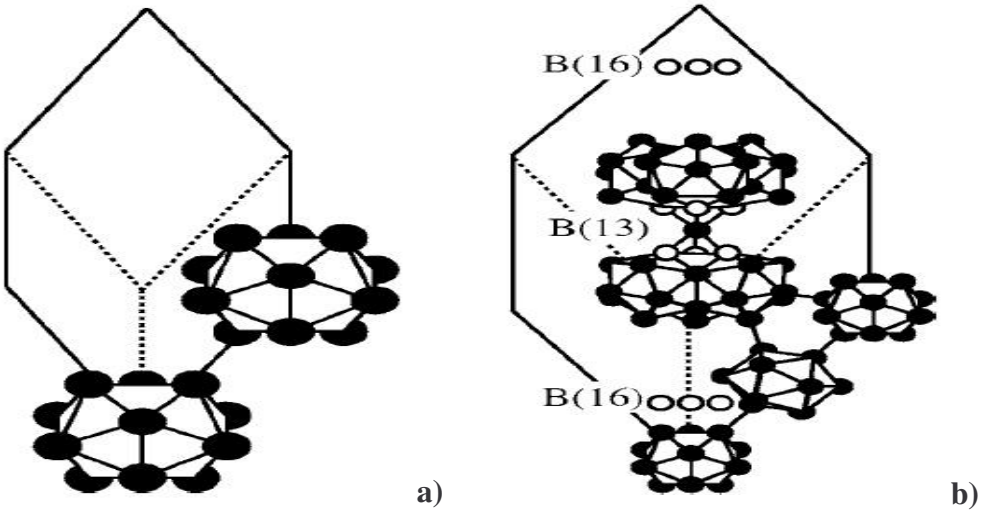

Figure 2.2: Crystal structure of α- (a) and β-boron (b). α-boron has a rhombohedral structure (space group $R\bar{3}m$) with 12 atoms in a cell. β-boron has the same space group, but it contains 105 atoms in a cell. The closed (open) circles represent atomic sites with full (partial) occupancy. Atomic sites with partial occupancy are indicated (Masago et al., 2006).

The different modifications of elementary boron and a number of its compounds belong to the group of materials called **"boron-rich solids"**. These boron-based hard materials can be of the binary or ternary systems (B-C, B-O). They exhibit a close relationship in view of their crystal structures, because all of them contain B_{12} icosahedra or related aggregates of atoms as essential common structural elements. These icosahedra determine essentially the electronic structure and hence the chemical bonding of these solids; a large similarity of their chemical and physical properties can be expected. Because this assumption can be taken as proved, at least as far as such investigations have been performed, the generalization of properties determined on single representatives for the entire group of solids seems admittable

to a certain extent. The examples of these hard materials include $B_{22}O$, B_2O, B_6O, and B_4C.

Table 2.3: General properties of boron-rich solids (extracted from www.uni-duisburg.de)

Properties	Boron-rich solids
Melting point	High melting points e.g. B_4C about 2900K
Hardness	Great hardness at ambient temperatures e.g. 2000 – 4500 kp/mm^2
Density	Generally low density e.g. B_4C = 2.5 g/cm^3
Thermal expansion coefficient	Small thermal expansion coefficient e.g. $B_4C = 5.73*10^{-6}K^{-1}$
Resistance to chemical attack	High resistance to chemical attack, hence low corrosivity
Neutron absorption	High neutron absorption cross section, caused by ^{10}B isotope
Others	Semiconducting behaviour

Some of these properties offer the prerequisites for technical use under extreme conditions, which are not admittable for most other materials. Moreover, the relationship of properties of this large group of structurally related solids allows the selection or tailoring of specific properties for particular uses. But this needs a detailed knowledge of the properties and their relation to the structural details.

The crystal structure of $AlMgB_{14}$ is based on B_{12} icosahedral units bonded together with Al and Mg (Matkovich and Economy, 1970). Computational results on $AlMgB_{14}$ suggest that the high hardness of the material is a result of the intrinsic hardness of the B_{12} icosahedral units and is not related to the linkage of the B_{12} icosahedra by Al and Mg (Lowther, 2002). The microhardness of single crystal $AlMgB_{14}$ was

determined by Higashi to be between 27.4 and 28.3 GPa(Higashi and Ito, 1983). The findings of Cook *et al* found the microhardness of $AlMgB_{14}$ prepared by hot-pressing elemental atomic compositions of 1:1:14 respectively to be between 32-35 GPa (Cook et al., 2000). The increased hardness is not unusual since the measurement by the Ames group was done on a polycrystalline material and probably with a very low load. Due to the impedance of dislocation movement as a result of polycrystalline samples, largely dependant on the grain size of the polycrystals, the hardness of polycrystalline samples is usually slightly higher than the hardness of the corresponding single crystal (Krell and Blank, 2000).

Crystal structure of boron suboxides

Boron suboxides are formed as a result of oxygen atoms dissolving into an electron deficient α-rhombohedral boron structure. This decreases the c/a ratio of the boron structure (Hubert et al., 1998; Itoh et al., 2000). Structure models of boron suboxides suggest oxygen occupancy of the 6*c* positions with coefficients depending on the composition (table 2.4). Table 2.4 shows the cell parameters for α-boron, boron carbide and selected samples of B_6O. For instance, the unit cell parameters for samples produced by Hubert et al. (1998) were refined from powder X-ray diffraction data to a = 5.3902(1) Å, c = 12.3125(2) Å, which gives a c/a ratio of 2.284.

Table 2.4: Cell parameters for α-boron, boron carbide and selected samples of B_6O (Space group $R\bar{3}m$, hexagonal axes).

Compound	**a_h ($\AA$)**	**c_h ($\AA$)**	**c_h: a_h**	**V($\AA^3$)**	**O-occupancy in position 6*c*.**	**Prep. Method**	**Reference**
α-rh B	4.927(3)	12.564(7)	2.55	-	-	-	Lundström and Andreev, 1996
B_4C	5.5991(5)	12.074(2)	2.156	-	-	-	Lundström and Andreev, 1996
$B_6O_{0.72}$	5.361(1)	12.340(1)	2.301	307.44	0.72[a]	Amb. P.	Lundström and Bolmgren (1994)
$B_6O_{0.76}$	5.367(1)	12.328(2)	2.297	307.53	0.76[a]	Amb. P.	Kobayashi et al., (1993)
$B_6O_{0.77}$	5.3696(4)	12.3258(6)	2.295	307.77	0.77	Amb. P.	Hubert et al., (1998)

Table 2.4: Cell parameters for α-boron, boron carbide and selected samples of B_6O (Space group $R\bar{3}m$, hexagonal axes). (*Continued*)

Compound	**a_h ($\mathring{A}$)**	**c_h ($\mathring{A}$)**	**c_h: a_h**	**V($\mathring{A}^3$)**	**O-occupancy in position 6*c*.**	**Prep. Method**	**Reference**
$B_6O_{0.78}$	5.3824(4)	12.322(1)	2.289	309.15	0.787 [a]	Amb. P.	Lundström and Andreev (1996)
$B_6O_{0.839}$	5.3761(7)	12.326(3)	2.293	308.52	0.839 [a]	Amb. P.	Lundström and Andreev (1996)
$B_6O_{0.89}$	5.3872(1)	12.3152(3)	2.286	309.53	0.89	5.5 GPa 1800 °C	Hubert et al., (1998)
$B_6O_{0.95}$	5.3902(2)	12.3125(4)	2.284	309.78	0.95	5.5 GPa 1700 °C	Hubert et al., (1998)
B_6O_x	5.395	12.342	2.288	311.10	-	hot P.	Rizzo et al., (1962)
B_6O_x	5.435	12.415	2.284	317.60	-	3.5 GPa 1200 °C	Liu et al., (1995)

The structure of boron suboxide (nominally B_6O) is built up of eight B_{12} icosahedra units situated at the apices of the rhombohedral unit cell (space group $R\bar{3}m$). The structure can be viewed as a distorted cubic close packing (ccp) of B_{12} icosahedra.

Figure 2.3 shows the structure of B_6O. B_6O has an α-rhombohedral boron type of structure consisting of a B_{12} cluster as the fundamental frame. Two oxygen atoms are located in the interstices along the [111] rhombohedral direction, replacing the 3-centre, 2-electron bond that links the icosahedra in this direction (Itoh et al., 1998; He et al., 17, 2002; Hubert et al., 1998; Lundström and Andreev, 1996). The O-O bonding distance is 0.307 nm, which prevents direct O-O bonding (Hubert et al., 1998; Lundström and Andreev, 1996). Consequently, each oxygen atom is only bonded to three equatorial boron atoms belonging to three different boron icosahedra. There have even been reports that samples of material with nominal composition near '$B_{22}O$' scratch the softer {100} faces of diamond (Badzian, 1998). However, boron suboxide is non-stoichiometric (He et al., 2002; Badzian, 1998). Reported compositions range from $B_6O_{0.72}$ to $B_6O_{0.86}$ at near ambient pressures (McMillan et al., 1999; Lundström, 1997; Petrak et al., 1974).

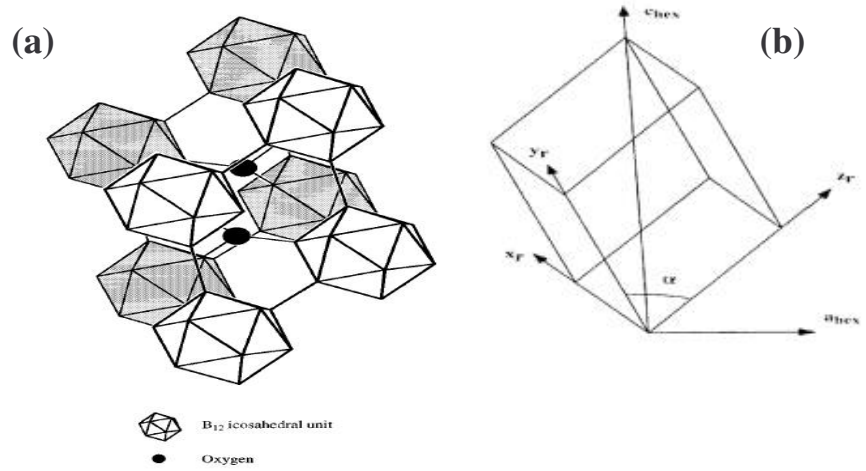

Figure 2.3: (a) Structure of B_6O built of eight icosahedral units situated at the vertices of the rhombohedral unit cell. Gray icosahedra are in the background. The icosahedra are composed of 12 B atoms situated at the corners of a slightly distorted icosahedron. Oxygen atoms are three-coordinated to boron atoms in separate icosahedra in the (001) plane (McMillan et al., 1999; Hubert et al., 1998).

(b) An outline of the rhombohedral unit cell with the rhombohedral (x_r, y_r, z_r) and hexagonal (c_{hex}, a_{hex}) axes shown. The base of the rhombohedron defines a tetrahedral figure in which the angle α may be distorted from the ideal value (70.5°), depending upon the ratio c_{hex}: a_{hex} (Hubert et al., 1998).

Compared to room-temperature synthesis, high-pressure high-temperature (HPHT) techniques produce B_6O much closer to the ideal composition (highest O occupancy, $B_6O_{0.96}$) with improved crystallinity (Hubert et al., 391, 1998; Hubert et al., 10, 1998; McMillan et al., 1999). Pressures up to 10 GPa have been used. Structural investigations have shown that there is only partial occupancy of the oxygen position (Olofsson and Lundström, 1997; Kobayashi et al., 1993). An investigation by Lundström and Andreev (1996) has shown that the oxygen occupancy varies from 0.787(5) at 1450°C to 0.831(5) and 0.839(4) at 1350°C and 1250°C respectively. High pressure synthesis of boron suboxide in the presence of an oxidizing agent results in an increase in the oxygen chemical potential, as should be expected, and that drives

the composition of the B_6O phase closer to the nominal stoichiometry (Olofsson and Lundström, 1997; Hubert et al., 391, 1998; McMillan et al., 1999; Hubert et al., 10, 1998). The formula of the suboxide is therefore more conveniently written as B_6O_{1-x} (Olofsson and Lundström, 1997).

B_2O was reported to have crystallised in the space group P3 with the hexagonal unit cell a = 2.879 Å and c = 7.052 Å, containing four boron and two oxygen atoms (Endo et al., 1987). The structure was suggested to have consisted of buckled atomic layers (consisting either of boron atoms or of boron and oxygen atoms), stacked in the c direction (corresponding to [111] direction of the sphalerite cell) in the sequence BB layer and double OB-BO layer. Lundström (1997) calculated the interatomic distances using space group $P\bar{3}m1$ with boron at the atomic positions 2c (z = 0.375) and 2d (z = 0.042), respectively, and oxygen at 2d (z = 0.292). It was assumed that $d_{BB} = d_{BO}$. The calculations show that the B-B distances within and between the buckled boron layer are normal, namely 1.765 Å. The B-O distances are, however, larger within the two halves of the B-O double layer, namely 1.765 Å, a consequence of the assumption made. If the half layers of the double layer are assumed to be plane, the B-O distance is 1.66 Å, which is more reasonable considering the interatomic distances in other B-O solids. In B_6O for instance, the distance is slightly less than 1.50 Å.

The shortest B-O distance between a boron atom in the buckled boron layer and an oxygen atom in the buckled layer is, however as large as 2.35 Å, which indicates a very weak bonding between these two types of layers. This distance will be even larger if the B-O half layers are assumed to be plane. This means that the structure suggested by Endo *et al*. (1987) for B_2O has mainly properties characteristic of layer structures, including no great hardness. Based on the calculations conducted by Lundström (1997), it was concluded that the proposed structure of B_2O is unstable. This means that the crystal structure of B_2O needs to be investigated more closely. In addition to the most studied form of boron suboxide (B_6O_{x-1} and B_2O), other boron suboxides (B_xO) of nominal composition B_2O, B_7O, $B_{13}O_2$, $B_{20}O$, and $B_{22}O$ have been reported. (Badzian, 1998; Brodhag and Thévenot, 1986; Ellison-Hayashi et al., 1992; Hall and Compton, 1965; Kharlamov et al., 2002). Table 2.5 gives the data of some of the selected boron suboxides.

Table 2.5: Site Occupancies and the number of atoms per hexagonal unit cell for some selected B_6O materials (Space group, $R\bar{3}m$, hex. axes)

Compound	$\mathbf{a_h}$ (Å)	$\mathbf{c_h}$ (Å)	$\mathbf{c_h}$: $\mathbf{a_h}$	**Reference**
B_2O	2.879	7.052	2.449	Endo et al., 1987
B_7O	0.0545	0.1242	2.279	Liu et al., 1995
$B_{13}O_2$	0.5392	1.2341	2.289	Kharlamov et al., 2002

Crystal structure of boron carbide (B_4C)

Boron carbides are among a number of materials with crystal structures derived from that of α-rhombohedral boron. The crystal structure of boron carbide (B_4C), which is better represented as $B_{13}C_2$, is built up of B_{12} icosahedra linked together by C-B-C chains (figure 2.4).

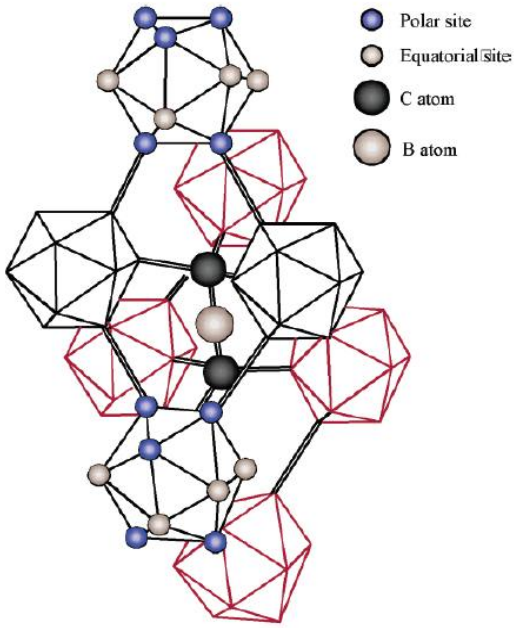

Figure 2.4: Crystal structure of $B_{13}C_2$ (Gao et al., 2004)

The space group is $R\bar{3}m$ (No. 166) similar to boron suboxide. The incorporation of carbon in boron carbide is understood to supply the extra two electrons to the crystal of α-boron, replacing the weak three-centre bond with strong covalent bonds. These

relatively weak three-centre bonds are mainly responsible for the cohesion in the *ab* plane. The arrangement is such that an elongated hole is formed between two three-centre bonded triangles along the trigonal axis (Lundström and Andreev, 1996; Lundström, 1997). The structures belonging to the structural family of B_4C differ mainly in the number and type of atoms accommodated in the elongated holes occurring along the hexagonal *c* axis (rhombohedral space diagonal) of the unit cell.

Even though boron carbide and boron suboxide are related to the same rhombohedral structure, the difference is somewhat connected to the inter-icosahedral atoms (Nieto-Sanz et al., 2004). In boron suboxide and boron carbide, O and C atoms are placed between icosahedra, linking them with strong covalent bonds. These intracluster bonds are stronger in boron suboxide than in boron carbide due to the higher electronegativity of oxygen relative to carbon. With the development of the first-principles approach, Gao *et al*. (2004) predicted the hardness of a number of boron-rich phases. It is believed that boron-rich materials formed by adding some element to boron icosahedra have great potential as new superhard materials for industrial use.

2.3 Synthesis of boron suboxide (B_6O) powders

The synthesis of boron suboxide powders and a description of its properties have been extensively reported in literature. Most of these reports attribute the formula

B_6O or B_7O to the suboxide being investigated. Although several techniques have been used in the past, there are two major ones which have gained wide applications.

Boron suboxide powders can be produced by reacting stoichiometric amounts of elemental boron and boron oxide under controlled conditions ($1000^oC \leq$ Temperature $\leq 2200^oC$; $1hr \leq$ Time $\leq 12hr$; argon atmosphere) (Itoh et al., 1998, 2000; He et al., 2002; Hubert et al., 1998; McMillan et al., 1999; Ellison-Hayashi et al., 1992). Alternatively, boron suboxide powders can be produced by reacting boron with *M*O where *M* is Mg or Zn and O is oxide (Kayhan and Inal, 1999; Ellison-Hayashi et al., 1992; Holocombe et al., 1972; Liu et al., 1995) or by reducing other oxides such as SnO, Ga_2O_3, In_2O_3, Bi_2O_3, $Li_2B_4O_7$, $KClO_3$ and CdO (Brodhag and Thévenot, 1986; Hall and Compton, 1965; Lundström and Andreev, 1996).

The specific form of B_xO produced depends on the process conditions and the ratio of elemental boron to boron oxide loaded into the reaction cell (Ellison-Hayashi et al., 1994). The reaction of boron and boron oxide can generally be represented as (Ellison-Hayashi et al., 1994);

$$16B_{(s)} + B_2O_3 \rightarrow 3B_6O \qquad \textbf{[2.2]}$$

The high temperature solid-liquid reaction [2.2] is achieved by wet mixing powdered boron and powdered B_2O_3 using a molar ratio of $B:B_2O_3$ = 16:1.03 in a mixer.

Ethanol/hexane or any other non-oxygenated dispersion liquid is normally used as solvent. The excess B_2O_3 takes into consideration that a small amount of B_2O_3 does not react with B, but rather volatilises during the heat treatment (Itoh et al., 1998). Nevertheless, this excess B_2O_3 can be removed after synthesis by washing in warm ethanol and/or water (He et al., 2002). Furthermore, while the B_2O_3 starting material is assumed to be essentially pure, it has been found that if the elemental boron used as starting material is less than 95% pure, a B_6O material which is harder than previously reported in literature can be formed (Ellison-Hayashi *et al.,* 1992). It has been claimed that the impure B contains about 6% Mg, which serves as a sintering aid for the B_6O and improves the hardness property of the final material. An alternative method of producing B_6O of high hardness is to use pure raw materials and separately add a suitable quantity of the desired sintering aid. Other materials such as Ca and Y are also expected to act as sintering aids.

The alternative route whereby boron suboxide powder may be produced is by the reduction of metal oxides, usually ZnO (Holcombe et al., 1972; Brodhag and Thévenot, 1986; Liu *et al.,* 1995) or other oxidants such as MgO, SnO,Ga_2O_3, CdO, In_2O_3, CuO and $Li_{12}B_4O_7$ (Lundström and Andreev, 1996) with boron under argon atmosphere to a temperature range of 1200^{o}C- 1600^{o}C. The chemistry of the reaction is generally given as:

$$xB + MO \rightarrow B_xO + M \qquad [2.3]$$

Liu et al., 1995 synthesized boron suboxide B_7O by the oxidation of boron with an excess of zinc oxide ZnO under a pressure of 3.5 GPa and a temperature of 1200°C, according to the following reaction;

$$7B + ZnO \rightarrow B_7O + Zn \uparrow \qquad [2.4]$$

It was observed that this route produces a single phase product of B_7O, as compared with other routes which give a mixture of boron suboxide B_7O with either boron or boron oxide B_2O_3. The zinc (melting point of 419°C) produced in the course of synthesis is beneficial in bringing about the complete solid state reaction. Although there are many oxidizing agents used in high pressure and high temperature experiments, for example, CrO_3, $KClO_3$, MgO, Ga_2O_3 etc., ZnO was chosen to avoid working with gas at high pressure and high temperature.

$$4CrO_3 \rightarrow 2Cr_2O_3 + 3O_2 \uparrow \qquad [2.5]$$

$$2KClO_3 \rightarrow 2KCl + 3O_2 \uparrow \qquad [2.6]$$

With each of these procedures there are attendant shortcomings or drawbacks which detract from the usefulness of the procedure in the production of B_6O. For example, one of the more successful procedures involves the reduction of molten B_2O_3 with boron, but the high volatilization and vapour pressure of this oxide at the reaction temperatures of 1200^0- 1500^0C respectively increase the likelihood of producing non-stoichiometric B_6O and inhibit the sealing of the reaction vessel. The molten B_2O_3

also reacts with the metal or ceramic reaction vessel and thereby contaminates the B_6O. With respect to other known procedures, the reduction of B_2O_3 with magnesium produces a solid solution of magnesium boride contaminant in the suboxide while the reduction of magnesium oxide with boron produces only a relatively small and insufficient yield of B_6O.

A method of preparing a boron suboxide material is disclosed in U.S. Patent No. 3,660,031 (Holocombe et al., 1972). Here, the boron suboxide material is formed by reducing ZnO with elemental boron at a temperature in the range of 1200 – 1500^oC. However, the material produced by this method is reported as having the formula B_7O. It was characterized with an average Vickers hardness of 3820 $kg.mm^{-2}$ (under a load of 100g) and a density of about 2.60$g.cm^{-3}$. The material is described as highly refractory and suitable for use on surfaces subject to abrasion.

U.S. Patent No. 3,816,516 (Goosey, 1974) also disclosed a method of fabricating boron suboxide products. According to this patent, a mixture of elemental boron and boron oxide was cold pressed in a tantalum lined metal die. After the pressure on the compacted mixture was released, it was coated with a mixture of boron nitride and boron oxide, and was subjected to a second pressing step while heating at a temperature sufficient to melt the boron oxide in the compacted mixture. This was followed by a cooling step and another hot pressing step. The boron suboxide product made by this method was reported as being smooth, sound, free of flaws and

contaminants, and suitable for a variety of applications, e.g., cutting tools, ceramic bearings, and grinding media. Upon analysis, the boron suboxide product gave 80.1 weight percentage boron and 19.9 weight percentage oxygen, which corresponds to the stoichiometry B_6O.

The preparation of boron suboxide (B_6O) in small quantities can also be carried out by the oxidation of boron (directly or platinum catalyzed) with oxygen gas at ambient pressure and at 1100-1800^{o}C (Rizzo et al., 1962).

The synthesis of boron suboxide (B_6O) by reactive sintering can be carried out either at ambient/near ambient pressure or high pressure conditions. Boron suboxide powders produced at or near ambient pressure are generally nonstoichiometric with the reported compositions ranging from $B_6O_{0.72}$ to $B_6O_{0.86}$ (He et al., 2002; Lundström and Andreev, 1996; Petrak et al., 1974; Gladkaya et al., 2001). Additionally, the synthesis typically produces fine-grained powders mixed with amorphous boron material (McMillan et al., 1999).The synthesis of boron suboxide at high pressures (4–5.5 GPa) results in near perfect icosahedra particles, euhedral (trigonal) grains (up to 40 μm), and multiple-twinned particles (MPTs) (He et al., 2002; McMillan et al., 1999; Hubert et al., 1998). These results are unexpected because the X-ray powder diffraction pattern remains fully consistent with the $R\bar{3}m$ space group, which does not allow the presence of five-fold symmetry (Hubert et al., 1998; McMillan et al., 1999; Hubert et al., 1996).

The presence of re-entrant faces on some particles allows the identification of these icosahedra as multiple-twinned particles rather than quasi-crystalline materials. Figure 2.5 shows the morphology of B_6O MTPs. Icosahedral MTPs of B_6O serve as the nucleus for the icosahedral packing of B_{12} units. Growth occurs by the addition of successive layers of B_{12} icosahedra to each triangular face. The icosahedral morphology of the grains makes them potentially useful for high-wear-resistance applications. Other morphologies that have been reported include intergrown subhedral to anhedral icosahedral grains, and rounded anhedral sintered masses (He et al., 2002; Hubert et al., 1998).

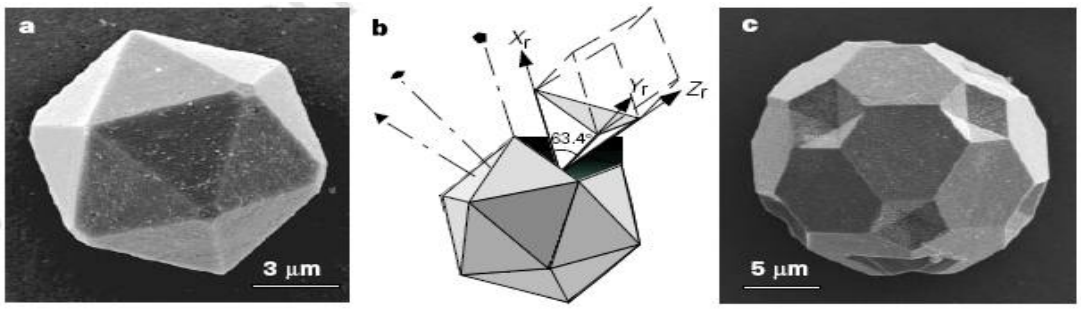

Figure 2.1: Morphology of B_6O MTPs. (a) SEM image of an isolated icosahedron. (b) Descriptive model of a regular icosahedron consisting of 20 tetrahedral individuals, illustrating the relationship between a tetrahedral individual and a rhombohedral cell. (c) SEM image of B_6O MTPs with well developed faces forming re-entrant angles at the apices, indicative of twinning (McMillan et al., 1999; Hubert et al., [10] 1998).

2.4 Sintering of boron suboxide (B_6O) materials

Under normal pressure conditions, boron suboxide (B_6O) materials remain unsinterable. High pressure sintering techniques, such as hot pressing or isostatic hot pressing, also cannot produce a fully dense compact of the materials (Brodhag and Thévenot, 1986). No appropriate sintering aid has been found because this material is easily oxidized to form B_2O_3 with the mechanical strength of the resultant sintered compact degraded (Saisai et al., 2001). Sintering of boron suboxides, like other sintering processes, is believed to occur in stages. The sintering mechanism of boron suboxide in the B-B_2O_3 system is summarized in section 2.4.1. Additionally, work carried out on B_6O powder sintered via low-pressure high-temperature (LPHT) and high-pressure high-temperature (HPHT) conditions and their properties are summarized in sections 2.4.2 and 2.4.3, respectively.

2.4.1 Low pressure – high temperature conditions (LPHT)

The sintering mechanism of boron suboxide at low-pressure (20 to 29 MPa) and high-temperature (up to 2000^{o}C) has been studied by Brodhag and Thévenot (1986). 'Sound' pellets were reactively hot pressed from a mixture of boron and boron anhydride. Additionally, B_6O powder was prepared by boron reduction of zinc oxide. Boron nitride lining was used to avoid carbon diffusion in the sample during hot pressing in graphite dies. No densification effect was observed for the B_6O powder

below the sintering temperature of 1600^{o}C. Nevertheless, three important variations in density (i.e. volume) for reactive hot pressing were observed (figure 2.6).

The first variation at about 290^{o}C is believed to be due to the fusion of B_2O_3 and the liquid penetrating between the solid particles. The reaction at about 1200^{o}C leads to further densification, and proper sintering starts at 1800^{o}C (Brodhag and Thévenot, 1986). The absolute and relative volume compositions showed that a higher pressure provides better penetration by the liquid phase and therefore a better reaction. The figure 2.6a curves show densification during reactive hot pressing in terms of absolute densities. As expected the curve with the highest pressure, 29 MPa, has a higher final density.

Figure 2.6b gives details of the densification kinetics during the reaction which seems to have three steps in the range 1000 - 1400^{o}C. From their investigations, it was concluded that the boron suboxide powder sinters better than the reactive one (about 200^{o}C lower). The reason was attributed to traces of zinc remaining in the powder as well as other microstructure-related reasons. For the reactive hot pressing experiments, the de-agglomeration (* on figure 2.6) leads to a lower green density, but the sintering rate is higher and the sintering temperature is lower. Homogeneity of the mixture improves the reaction and the disappearance of large pores due to initial B_2O_3 agglomerates (Brodhag and Thévenot, 1986).

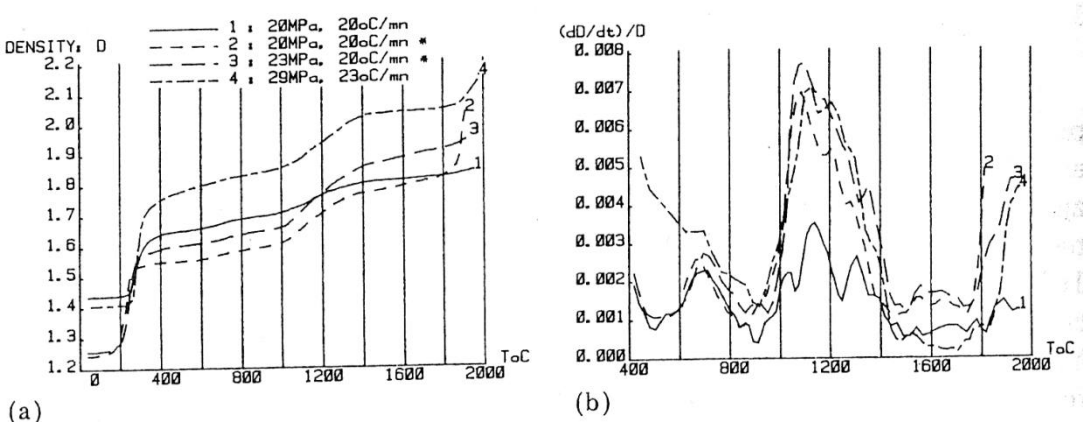

Figure 2.6: Densification during reactive hot pressing (a) absolute density, (b) densification rate (* for screened reactive mixtures) (Brodhag and Thévenot, 1986)

Although the synthesis of boron suboxide (B_6O) at or near ambient pressure comes with the advantage of reduced cost of production and avoids the risk of working with gases at high pressure, it leaves an option of forming a non-stoichiometric B_6O compound, generally oxygen deficient (B_6O_x, $x < 0.9$). Hence, the formula of the suboxide is commonly expressed as B_6O_{1-x}, where $x \leq 1$. (Duanwei et al., 2002; McMillan et al, 1999; Garvie et al., 1997).

Badzian (1998) produced boron suboxide via high temperature sintering (about 2000^{o}C), under pressures from 100 to 1000 MPa from boron and B_2O_3. The sintered bodies were melted in an induction furnace in an argon atmosphere and their properties measured. The melted material was found to be black in colour. Chemical analysis performed on the powder assumed a $B_{22}O$ composition. The melted material had a microhardness measured by Hanemann indentation (80g load) of 60 GPa. This

material showed polycrystalline morphology, could easily wear a diamond tip parallel to the (001) plane, or scratch a (111) diamond face in any direction.

Bairamashvili et al., (1979) synthesized boron suboxide (B_6O) by the hot pressing technique in a compaction press and in vacuum at high temperature (exact temperature and pressure not reported). The physicomechanical properties of this material were measured and compared with SiB_4 and B_4C which belong to the same family and are prepared in the same way as the B_6O. Although the load applied was not indicated, the resulting materials had more than 90% of the theoretical densities. A summary of the measured properties are given in table 2.6. The compression strength measured for B_6O varied from 63 GPa at 20^oC to 39 GPa at 1000^oC. The microhardness values for B_4C and B_6O were nearly identical and SiB_4 were slightly lower, however the fracture toughness was not reported. The elastic moduli of B_4C, B_6O and for SiB_4 were measured in air at room temperature by the dynamic specimen – bending method.

Table 2.6: Physicomechanical properties of B_6O, B_4C and SiB_4 (Bairamashvili et al., 1979).

Sample	**Density (g/cm^3)**	**σ_{comp} (GPa) at RT**	**Hardness (GPa)**	**Young's modulus (GPa)**	**Linear thermal expansion coefficient ($\times 10^{-6}$ K^{-1}) [RT-1000 ^oC]**	**Thermal conductivity at 100^{o}C, W/mK**
B_6O	2.4	63	32	440	5.5	10.2
B_4C	2.4	79	35	480	4.5	14.7
SiB_4	2.35	50.2	27	280	6.0	5.9

Ellison-Hayashi et al. (1994; 1992; 1994[EU]; 1995) produced boron suboxide (B_6O) by hot pressing a stoichiometric mixture of elemental boron and boron oxide powders at temperatures in the range of about 1800 - 2200^{o}C and at a pressure of about 14 - 40 MPa for a period of about 5 minutes to 3 hours while encapsulated by hBN. An average Knoop hardness (100g load) of about 38 GPa was reported and for some materials that property was bound to be about 42 GPa. It was claimed that the powder could be crushed into granules and used as abrasive grit, or grit bonded to tools which require highly abrasive surfaces. The high hardness was attributed to the presence of Mg in boron starting powder which aids in densification. The fracture toughness was not reported.

Goosey and Anderson (1974) fabricated boron suboxide by hot pressing at about 2000^{o}C under a pressure of about 40 MPa. The boron suboxide (B_6O) was fabricated

by forming a compacted article from a mixture of boron and boron oxide in a metal die lined with graphite and tantalum. The compacted article was coated with a mixture of boron nitride and boric oxide and was subjected to a second pressing step while being heated at a temperature sufficient to melt the boron oxide in the compacted mixture. After allowing the metal die to cool, the compacted article was removed and placed in a graphite die also coated with boron nitride and lined with tantalum and then hot pressed. The resulting material was reported to be a 'sound' boron suboxide article, free of contaminants. The product possesses outstanding physical properties (Knoop hardness of 30 GPa at 100g load and modulus of elasticity of about 480 GPa) that render it suitable for a variety of applications such as cutting tools, ceramic bearings, and grinding media. The measured density of the material was 2.60 g/cm^3. The fracture toughness for this material was however not reported.

Holcombe et al., (1972) produced boron suboxide (B_7O) by blending zinc oxide powder with boron powder. The blended powders were isostatically pressed at about 140 MPa into pellets and heated in the presence of inert atmosphere to a temperature in the range of 1200-1500^{o}C to effect the reduction of zinc oxide by the boron. This material was characterized as having a density of 2.80 g/cm^3, an average Vickers hardness value of 38.2 GPa at 100g load but the fracture toughness was not reported. It is surprising that the measured density is higher than the theoretical density of B_6O (2.59 g/cm^3). This is an indication that the zinc oxide did not react completely with

the boron powder and therefore the B_6O powder produced contained zinc impurities. Since the density of zinc (7.1 g/cm^3) is higher than the theoretical density of B_6O, the density of the resulting sintered compact would be higher than that of B_6O. This material is described as highly refractory, resistant to oxidation and acids and suitable for use on surfaces subject to abrasion, e.g., grinding wheels, drill bits, machine tools and in structures employed in high temperature applications.

Kayhan and Inal (1999) fabricated a B_6O compact from B_6O powder produced by reacting boron and zinc oxide. Hot pressing was carried out at 1600^{o}C in vacuum under pressure of 40 MPa for 2 and 4 hours respectively. An inductively heated graphite die was used. An intermediate barrier layer of boron nitride was used between the green sample and the graphite die and rams to prevent carbon diffusion from the die to the sample. During pressing, the pressure was maintained at 10 MPa up to the sintering temperature and then was increased to 40 MPa. The densities measured were 2.15 and 2.18 g/cm^3 respectively. The samples were then given a high temperature treatment at 1800^{o}C under vacuum with no pressure applied for full densification (densities measured were 2.31 and 2.39 g/cm^3, respectively). The Vickers microhardness (100g load), fracture toughness and flexural strength values measured for these materials are summarized in table 2.7. The fracture toughness was calculated from a three-point bend testing with a notch radius of 0.4 mm.

Table 2.7: Summary of properties of B_6O hot pressed at 1600°C in vacuum under 40 MPa (**Kayhan and Inal 1999**).

Material	**Density (g/cm^3)**	**Hardness (GPa)**	**Fracture toughness ($MPam^{0.5}$)**	**Flexural strength (MPa)**	**Phases**
2h hot pressed	2.15	35	5.35	57.18	B_6O, B, B_2O_3
4h hot pressed	2.18	35	5.52	59.07	B_6O, B, B_2O_3
2h hot pressed & heat-treated	2.31	36	5.84	62.43	B_6O, B
4h hot pressed & heat-treated	2.39	37	6.23	66.70	B_6O, B
4h hot pressed, heat-treated & infiltrated	2.53	40	8.12	86.88	B_6O, Al_2O_3, $Al_{1.67}B_{22}$

From table 2.7 the properties measured for pure B_6O materials are very surprising and unexpected since the fracture toughness was already high (6.23 $MPam^{0.5}$) for the pure hot pressed material even before infiltrating with aluminium. This is contradictory to what has been reported in literature to date, that pure B_6O sintered compacts have low fracture toughness values. Using the fracture toughness (K_{IC}) and reported strength values (σ), the defect size (a) can be estimated as (Wachtman, 1996):

$$a = Y\left[K_{IC}/\sigma\right]^2 \qquad \textbf{[2.7]}$$

Where Y ≈ 1. This gives a very large defect (≈ 0.8cm), thus questioning the validity of the data.

Olofsson and Lundström (1997) synthesized non-stoichiometric B_6O powders from a mixture of amorphous boron or α-rhombohedral boron and B_2O_3 in excess. They found that the use of α- boron, under some conditions, resulted in a more crystallized boron suboxide, which was utilized to study the homogeneous range of the suboxide in the temperature range 1250°C - 1450°C. The oxygen content of solid was determined from Rietveld analysis of X-ray powder diffraction intensities and it was claimed that the oxygen concentration in solid B_6O decreases with temperature in the range 1250°C- 1450°C as anticipated (figure 2.7). The unit cell dimensions, occupancy of the 6c position by oxygen, and some interatomic distances are shown in table 2.8 for materials prepared at different temperatures and presumably not too far from equilibrium. At temperatures lower than 1250°C it was progressively more difficult to reach equilibrium, since the reaction rate decreases. They concluded that stoichiometric B_6O cannot be prepared using oxygen at ambient pressure.

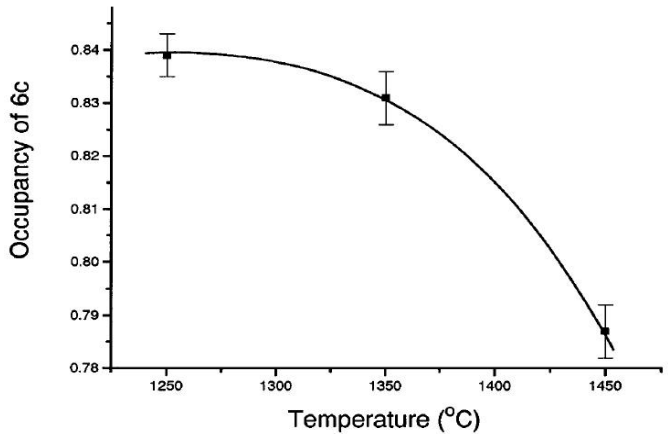

Figure 2.7: Oxygen content (occupancy of position 6c) of B_6O vs. temperature (Olofsson and Lundström, 1997)

Table 2.8 Crystallographic data for boron suboxide sample (Olofsson and Lundström, 1997)

Sample composition	**a axis (Å)**	**c axis (Å)**	**Temperature (^oC)**	**Occupancy of position 6c**	**Distance (Å) O(1) –O(1)**	**Distance (Å) O(1) - 3B(1)**	**Starting materials**
B_6O_{1-x}							
I, $B_6O_{0.79}$	5.3824(4)	12.322(1)	1450	0.787(5)	3.007(5)	1.463(1)	Amorphous boron and B_2O_3
II, $B_6O_{0.83}$	5.3761(7)	12.326(3)	1350	0.831(5)	3.025(5)	1.476(1)	α-Boron and B_2O_3
III, $B_6O_{0.84}$	5.3774(7)	12.322(3)	1250	0.839(4)	3.004(5)	1.476(1)	α-Boron and B_2O_3

Petrak et al., (1974) produced B_6O by reactive hot pressing from a mechanically mixed boron and anhydrous boron powder (the actual pressing temperature and pressure were not reported). Phases observed in the hot pressed samples were boron suboxide and boron. Nevertheless, a slight amount of B_2O_3 was also observed in some of the samples. Measured densities were more than 99% of the theoretical density. The linear expansion coefficient for this material increased with increasing temperature and had an average value of 5.69 x $10^{-6}/^oC$ for the temperature range of 20 - 900^oC, which is greater than that of B_4C. Knoop hardness of B_6O measured at a load of 100g was 30.4 GPa, similar to B_4C (30.2 GPa) prepared and measured under the same conditions. The Young's modulus value was about 470 GPa with Poisson's ratio of 0.155 and flexural strength of about 350 MPa with an average grain size of 2 µm.

Srikanth et al., (1991), attempted to determine the nature of the B_xO phases that occurred in the field defined by pressure of 0 to 1.5 GPa, temperature between 1200-1700^oC, and the compositional range $2/3 \leq x \leq 24$. Amorphous boron powder and boric acid were the starting reactants. After processing at elevated temperature and pressure, for compositions over the range $2/3 \leq x \leq 6$, B_2O_3 and B_6O ($R\bar{3}m$) were the dominant phases present. For the compositions $6 \leq x \leq 24$, B_6O and rhombohedral B were the primary phases identified. Densities obtained ranged from 2.20 to 2.46 g/cm^3. The hardness values obtained were dominated by the occurrence of B_6O. However, there were some suggestions of high values of hardness on localized scale in specimens near the $B_{22}O$ composition. Fragments of processed specimen containing B_6O were observed to scratch Al_2O_3 (easily) and SiC.

2.4.2 High pressure-high temperature conditions

Researchers have began to explore these conditions with the aim of synthesizing boron suboxide powders with improved purity, crystallinity as well as obtaining a lower degree of oxygen deficiency. They intend to get closer to the nominal composition of B_6O.

He et al., (2002) produced B_6O single crystals at high pressure (~ 5.5 GPa) and high temperature (2100^oC) for 60 minutes with grain sizes over 100 µm. This made it possible to measure the Vickers hardness on separate single crystals. The Vickers

hardness was measured using a pyramidal diamond indentation method, after the samples had been polished using diamond abrasive disks and slurries. The average Vickers hardness was 45 GPa under a load of 0.98N (He et al., 2002). The corresponding fracture toughness, measured using Anstis' equation, was 4.5 $MPam^{0.5}$.

Hubert et al., (1998), synthesized B_6O at high pressure and high temperature using a Walker-type multianvil apparatus. The pressure medium consisted of a cast MgO octahedron and force was applied by eight tungsten carbide cubes with corners truncated to triangular faces. The cell assembly is illustrated in figure 2.8. Amorphous boron (B) was mixed with B_2O_3 and the samples were pressurized between 1 to 10 GPa at 1200^{o}C -1800^{o}C.

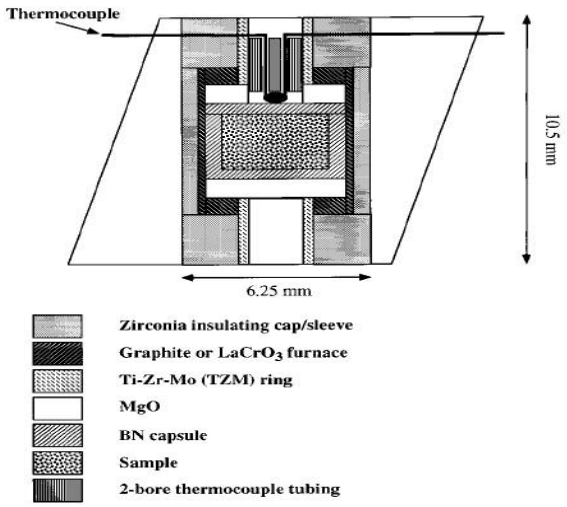

Figure 2.8 Cell assembly containing the B and B_2O_3 mixture, used for the synthesis of B_6O at high pressure. This assembly is placed at the center of MgO octahedron to which pressure is applied isostatically (Hubert et al., 1998)

Their best materials were obtained from a starting mixture containing an excess of B_2O_3 reacted at 1700^{o}C, between 4 and 5.5 GPa. After the products had been washed in water, a well-crystallized single-phase product dominated by icosahedrally twinned particles up to 30 μm in diameter were easily recovered. Oxygen occupancies ascertained from Rietveld refinements showed data consistent with the chemical compositions determined by Parallel electron energy- loss spectroscopy (PEELS). The highest oxygen occupancy, $B_6O_{0.96}$, was obtained for the micrometer-size icosahedral particles prepared. The refined hexagonal cell parameters and oxygen occupancies for B_6O_{1-x} are given in table 2.8.

Itoh et al., (1998) produced a B_6O compact via high-pressure (3-6 GPa) high-temperature (1400-1800^oC) techniques from powdered B_6O synthesized from amorphous boron and boron oxide (B_2O_3) for 10 to 20 minutes in inert atmosphere. The specimen chamber was surrounded by an hBN capsule and a graphite heater was used for heating purposes. A single phase sintered compact having a Vickers microhardness (200g load) of between 31 and 33 GPa under pressures of 3-5 GPa and 1700^oC for 20 minutes could be produced. It was found that the B_6O sintered compact was of internal grain fracture type while the toughness was low. The B_6O sintered compact had superior oxidation resistance in air at high temperatures (up to 1000^oC) in comparison with a B_4C sintered compact prepared under the same conditions (5 GPa, 1700^oC and 20 minutes). The B_2O_3 layer formed during oxidation functioned as a protective layer and oxidized mildly up to about 1000^oC. The synthesis of B_6O single crystals at high pressure and high temperature was discussed in section 2.4. However, properties of these materials were not mentioned.

Macmillan et al., (1999) found that for higher synthesis pressures, the particle compositions were found to be much closer to the stoichiometric value. It therefore appears that increasing the synthesis pressure in the presence of an oxidizing agent will result in an increase in the oxygen chemical potential, and that this drives the composition of the B_6O phase closer to the nominal stoichiometry.

2.5 Properties of boron suboxide materials

It has been established in literature that boron suboxide (B_6O) displays a range of interesting physical and chemical properties such as great hardness, low mass density and high chemical inertness due to its short interatomic bond lengths and strong covalent character. This section reviews some of the properties reported for boron suboxide material.

Makarov and Ugai (1986), studied the thermochemical properties of boron suboxide (B_6O). They found the standard enthalpy of formation of B_6O which was determined by calorimetric dissolution of B_6O and strong nitric acid to be: $\Delta H_f^{\Theta}(B_6O_S, 298.15K) = (527 \pm 32) KJmol^{-1}$, but this study was limited to temperatures up to 800K.

Itoh et al., (1998) studied the oxidation resistance properties of B_6O and found that the B_6O compact exhibited an oxidation resistance in air of up to 600^{o}C and a mild oxidation behaviour in the temperature range of 700-1000^{o}C, resulting in the formation of a liquid film of B_2O_3. It was also found that this B_6O compact had a superior oxidation resistance in air at high temperatures in comparison with the B_4C compact, sintered under the same conditions. The porosities in both materials were not reported, but the B_6O compacts were reported to have densities higher than 95%

of the theoretical. Figure 2.9 shows the results of the thermal analyses that were performed using TGA-DTA on both single phase compacts.

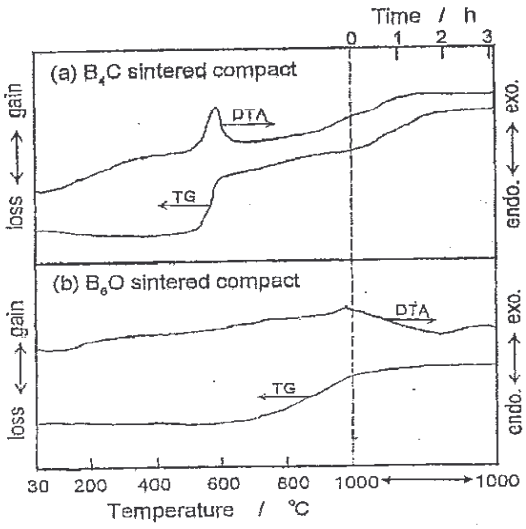

Figure 2.9: TGA and DTA analyses of single phase compacts (a) B_4C and (b) B_6O prepared at 5GPa, 1700°C and 20 minutes. Heating rate: 3°C/min, atmosphere: air (Itoh et al., 1998)

The B_2O_3 film thickness after the oxidation of the B_6O sintered compact is shown in figure 2.10. It was found from the graph that the thickness of the oxidation film increased by a small amount until the treatment temperature reached 1100°C, however, when the treatment temperature reached 1200°C or more, the thickness of the oxidation film increased despite the fact that the B_2O_3, which played a role as a protective film, volatilised rapidly. This indicates that when the treatment temperature is 1200°C or greater, the B_6O sintered compact is rapidly oxidized whether or not a protective film is present.

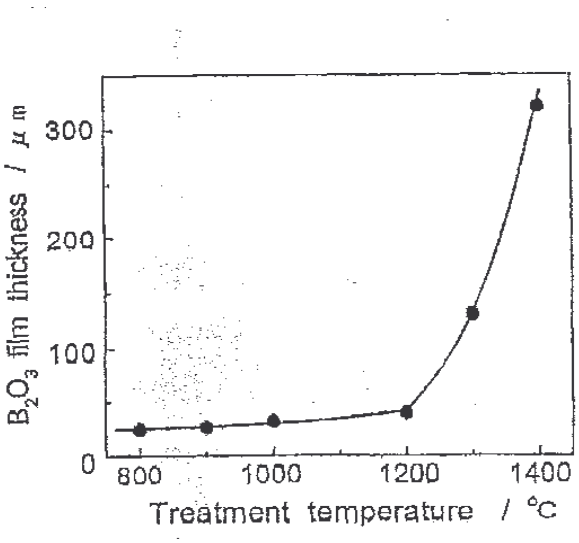

Figure 2.10: B_2O_3 film thickness after oxidation in air for 4 hours as a function of treatment temperature. (Itoh et al., 1998)

Duanwei et al., (2002) grew B_6O single crystals (at pressures of about 5.5 GPa) with grain sizes greater than $100\,\mu m$ which enabled them to measure the intrinsic properties of B_6O. The Vickers hardness of the B_6O single crystals was measured using a diamond indentation method, after the samples had been polished using diamond abrasive disks and slurries. Under a loading force of 0.98 N, an average hardness of 45GPa was obtained. The fracture toughness was found to be very promising at 4.5 $MPa.m^{0.5}$ which approaches that of single crystal diamond at 5 $MPa.m^{0.5}$.

Shabalala et al., (2007), reported an elastic constant of hot pressed B_6O measured using the ultrasonic pulse-echo technique, the result given in table 2.9. The data obtained in this work was slightly higher than the data found in other literature

(Petrak et al., 1974, Goosey 1974). Shabalala claimed that the difference was due to the amount of boron oxide (B_2O_3) and oxygen content of the synthesized powder.

Table 2.9: Elastic properties of hot pressed B_6O

Material	**Elastic Modulus *E*** (GPa)	**Shear Modulus** (GPa)	**Bulk Modulus** (GPa)	**References**
B_6O	540	227	300	Shabalala *et al.,* 2007
B_6O	470	206	230	Petrak *et al.,* 1974
B_6O	483	-	-	Goosey 1974

Recently, Andrews et al., (2008) approximated the thermodynamic properties of boron suboxide (B_6O) over the temperature range of 800K to 2300K. This study was based on the assumption that B_6O has similar heat capacity to B_6Si since both compounds have a similar structure, composition, and chemical bonding. The heat capacity of B_6O at 2300K was estimated to be 204J/mol.K.

Boron suboxide (B_6O) additives

The low fracture toughness obtained in the sintered compacts is not completely clear. Efforts have been made to increase the fracture toughness by forming B_6O composites with other ultrahard materials such as diamond, boron carbide (B_4C), and

cubic boron nitride (cBN). B_6O composites have also been produced with aluminium and carbon additions.

B_6O-B_4C materials

Itoh et al., (2000) produced B_6O composites in the B_6O-xB_4C (x = 0-40 vol. %) system under high pressure-high temperature conditions (3-5 GPa, 1500-1800^oC) from a mixture of in-laboratory synthesized B_6O powder and commercially available B_4C powder. The relationship among the formed phases, microstructures and mechanical properties of the sintered composites was investigated as a function of sintering conditions and added B_4C content. It was found that neither solid solutions nor new compounds were formed under the sintering conditions and that the sintered composite consisted of the mixed phases of B_6O and B_4C. Under these sintered conditions, strong interparticle bonding between B_6O and B_4C increased the hardness and toughness of the sintered composites. A maximum microhardness of ~46 GPa (200g load) was reported from B_6O-30 vol. % B_4C powder under sintering conditions of 4 GPa, 1700^oC and 20 minutes. Fracture toughness was less than 1 $MPam^{0.5}$.

B_6O-cBN materials

Itoh et al., (2000) investigated high-pressure sintering behaviour in the B_6O-cBN system using in-laboratory synthesized B_6O and commercially available cBN powders. The phase relation, microstructure and mechanical properties of the

composites were examined by varying the added cBN amount and its average grain size as well as the sintering conditions. No reaction occurred between the two components under high pressure (4-6 GPa) and high temperature (1500-1800^{o}C) conditions. Well dispersed B_6O-*x*(cBN) sintered composites of almost full density were prepared in the range of x = 0-50 vol.% by sintering at 6 GPa and 1800^{o}C for 20 minutes. A maximum Vickers microhardness of 46 GPa (200g load) was attained by adding 40 vol. % cBN with an average grain size of 0.5 µm. A maximum fracture toughness of about 1.8 MPam$^{0.5}$ (using Niihara's equation) was obtained at 60 vol. % cBN addition. It is believed that crack deflections along the B_6O-cBN grain boundary contributed to the increase in fracture toughness.

B_6O-diamond materials

Sasai et al., (2001) prepared sintered material in the B_6O-*x*diamond (*x* = 0-80 vol.%) system under high pressure and high temperature conditions (3-5 GPa, 1400-1800^{o}C) from a mixture of in-laboratory synthesized B_6O powder and commercially available diamond powder with various grain sizes for 20 minutes. The phases formed, microstructures and mechanical properties of the sintered composites were investigated on varying the added diamond content and sintering conditions. It was concluded that neither solid solutions nor new chemical compounds were formed under the sintering conditions. Sintered composites of full density consisted of mixed phases of B_6O and diamond. A maximum microhardness of 57 GPa (200g load) was measured in the B_6O-60 vol. % diamond (grain size < 0.25 µm) sintered composite

under the sintering conditions of 5 GPa, 1700°C and 20 minutes. The fracture toughness, however, was less than 1 $MPam^{0.5}$ (measured using Niihara's equation).

B_6O- materials with Al_2O_3 additives

Shabalala (2007) produced B_6O composites using Al-B-O and C-containing compounds at low-pressure high-temperature (hot pressing) conditions (1600-1900°C, 50 MPa, 20 minutes). The composite powders were prepared by mixing in-laboratory synthesized B_6O powder with commercially available Al, Al_2O_3, and by coating it with Al_2O_3 using a Chemical Vapour Deposition (CVD) process. The relationship among the formed phases, microstructures, and mechanical properties of the sintered composites were investigated. Measured densities were higher than 97% of theoretical density. The Al_2O_3 addition via mixing and CVD produced B_6O composites with better mechanical properties, especially fracture toughness. Increasing the amount of Al (or Al_2O_3) slightly reduces the hardness but significantly increases the fracture toughness of the B_6O composites. The sample with the lowest amount of Al (2.2 wt.% Al) had a Vickers hardness of 31.1 GPa (500g load) and fracture toughness of 3.1 $MPam^{1/2}$. The increase in fracture toughness was attributed to the formation of aluminium borate, $Al_{18}B_4O_{33}$, as a secondary phase at grain boundary interfaces. Crystallization of the $Al_{18}B_4O_{33}$ led to the formation of nanosized residual porosity in close proximity to the Al-containing phase, acting as crack-arrest sites. Also, a further toughening mechanism was connected to the slight crack deflections and bridging of the propagating cracks through the $B_6O/Al_{18}B_4O_{33}$

interface which is under high thermal stress arising from the thermal expansion coefficients mismatch between B_6O and $Al_{18}B_4O_{33}$. Composites produced from the addition of C decreased Vickers hardness in the range of 22.8 - 25.9 GPa (500g load) but increased fracture toughness in the range of 5.25 - 5.48 $MPam^{0.5}$. The increase in fracture toughness was attributed to the formation of B_4C phase as well as some traces of $Al_{18}B_4O_{33}$ from the starting B_6O powders.

2.6 Potential applications of boron suboxide-based (B_6O) materials

The most widely used superhard materials in industry for drilling, cutting, milling and grinding includes diamond, cBN and their sintered composites. However, diamond transforms to graphite at high temperature when it is used to machine steel while cBN weakens as temperature increases as a result of diffusion wear and it is more difficult to synthesize.

Boron suboxide-based materials reviewed in this chapter possess good physical and mechanical properties comparable to diamond and cBN. B_6O has similar thermostability as cBN (He et al., 2002). The oxidation resistance of single phase B_6O and B_4C sintered compacts have been compared and found that the oxidation resistance of B_6O in air at high temperatures is far superior to that of B_4C and comparable to cBN which has a similar crystal structure and hardness to B_6O (Itoh et al., 1998; 2002). The product of the oxidation of B_6O (B_2O_3) during the initial stages

serves as a protective layer and thus oxidizes mildly until about 1000^{o}C. For these reasons, B_6O has an advantage over the use of diamond in certain applications.

Boron suboxide therefore becomes a potentially good candidate for cutting tools and other industrial applications where abrasive wear resistance is essential (Ellison-Hayashi et al., 1994, 1995; Kayhan and Inal, 1999; Holocombe et al.,, 1972; Kurisuchiyan et al., 1995). B_6O also has potential applications as semiconductor due to an estimated band gap of 2 eV based on photoluminescence, theoretical calculations and consistency with its red-orange colour (Barry, 1999; Lee et al., 1991). Nevertheless, commercial applications have not yet been realized due to its low fracture toughness.

2.7 Toughening mechanism in ceramic materials

In ceramic materials, stress applied to a material does not result in limited plastic deformation and therefore stress relaxation does not occur by this mechanism. Instead, the stresses become concentrated at flaws/cracks in the material. The critical stress intensity factor (K_{IC}) for a material is defined to be the critical stress/energy at a crack tip in the material required to cause further propagation of the crack. Fracture toughness may be defined to be the resistance to fracture and therefore K_{IC} is a measure of fracture toughness of a ceramic material.

Traditionally, engineering ceramics have been considered for heat containment, wear resistance, static load bearing, and electro-optical applications owing to the generalized properties of ceramics which include hardness, corrosion resistance, high temperature stability, creep resistance, high elastic modulus, and electrical and thermal resistivity. Unfortunately, these properties come at the expense of toughness. While metals typically have toughness values of 15 to 150 $MPa.m^{0.5}$, most ceramics usually have toughness values below 5 $MPa.m^{0.5}$ (Evans, 1988).

Significant research effort has been directed toward the development of tough ceramics, since such materials have the potential to open up a large range of specialized engineering applications. A general solution is to engineer the microstructure of ceramics in such a way so as to inhibit crack propagation (Lee et al., 1993).

A number of toughening mechanisms such as crack deflection, crack branching, crack bridging, transformation toughening, frictional interlocking and micro-cracking have been suggested in literature, but there is an ongoing debate about the relative importance of each of these mechanisms (Hansson et al., 1993, Seung and Chong, 1994). Some authors have proposed that crack deflection is the main toughening mechanism (Meguid, 1996). The more commonly active mechanisms have been

classified in a general way by Wachtman (1996) and are given for the present discussion in table 2.10.

Table 2.10: A general classification of some of the toughening mechanisms in ceramics. (Wachtman,1996)

Class of effect	**Mechanism**
Crack deflection	Generation of out of plane components by a tilting or twisting of a crack plane around grains and secondary –phase inclusions.
Crack bowing	Pinning of a crack front by secondary-phase pinning points, leading to an in plane bowing of the crack front
Crack branching	Subdivision of a crack into multiple propagation fronts.
Crack bridging	Inhibited crack opening and enhanced crack energy dissipation around ligamentary grains that span the crack wake.
Crack-tip shielding	A reduction of the crack-tip stress intensity, through direct stress modifications, or through crack-tip blunting by ductile deformation, phase transformation, or micro-cracking processes.
Transformation Toughening	Occurs as a result of a stress-induced phase transformation of particulate inclusions in a ceramic matrix. Residual stresses surround each particle which acts across the projected fracture plane, and have to be nullified for the crack to propagate through the transformed zone.

In their studies, Clarke and Farber (1987), discussed a concept of impeding the growth of a crack by placing inhomogeneities (obstacles: second phase particles, whiskers and fibres) in the crack path, thereby increasing the fracture toughness of ceramics. Although the presence of such obstacles would encourage the pinning of the crack, the crack path could deviate from the obstacle by either bowing around the obstacle (figure 2.11(a)) or by deflecting out of the crack plane (figures 2.11 (b) and

(c)). Crack deflection takes place whenever the crack path adopts a least resistant path. This may occur as a result of the presence of residual stresses and different phase elastic moduli.

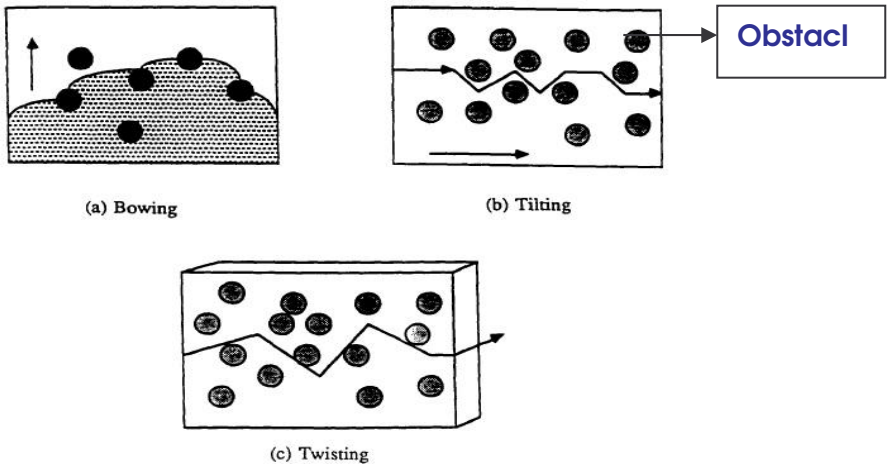

Figure 2.21: Effect of obstacles upon crack-tip interaction. (Meguid, 1996)

Lange (1970) and Evans (1972) examined the effect of crack bowing on the fracture toughness of brittle materials and claimed that the extent of the toughening is strongly influenced by the stress state.

This mechanism serves as the motivation for introducing some obstacles as second phase into the B_6O matrix, to interact with the crack front and impede the growth of such cracks, thereby improving the fracture toughness of the B_6O-based composite produced in this work

CHAPTER THREE

3 Experimental procedure

3.1 Introduction

This chapter describes the details of the materials, the methodology, the equipment, and relevant formulae used in this project.

3.2 Materials and chemicals used

Boron suboxide (B_6O) powder produced at IKTS – Dresden was used for the major part of the hot pressing investigations carried out in this project. MgO, CaO, Ni, NiO, Ni_2B, CoO, Co_2B and CrB_2 powders were used as sintering additives. Additionally, $CaCO_3$ obtained from IKTS – Dresden was used instead of CaO, because of it is more stable than CaO. A summary of all the materials and chemicals used are tabulated in table 3.1.

Table 3.1: Materials and chemicals used in this project

Materials/ chemicals	**Form**	**Purity (%)**	**Colour**	**Particle size (µm)**	**Density @ 20°C (g/cm^3)**	**Supplier**
Boron suboxide (B_6O)	Powder	-	Brown	< 212	-	IKTS – Dresden
Calcium carbonate ($CaCO_3$)	Powder	p.a	White	-	-	Merck
Magnesium oxide (MgO)	Powder	96	White	44	3.58	Industrial analytical
Calcium oxide (CaO)	Powder	99.95	Off-white	-	3.25-3.38	Industrial analytical
Nickel (Ni)	Powder	99.996	Grey	127	-	Industrial analytical
Nickel oxide (NiO)	Powder	99	Dark green	-	-	Industrial analytical
Nickel boride (Ni_2B)	Granules	99	Grey	-	-	Industrial analytical
Cobalt oxide (CoO)	Powder	95	Green	-	-	Industrial analytical
Cobalt boride (Co_2B)	Powder	99	Grey	-	-	Industrial analytical
Chromium boride (CrB_2)	Powder	99	Grey	-	-	Industrial analytical
Hexagonal boron nitride (hBN)	Rods	-	White	-	-	H.C. Stark
Sodium hexametaphos-phate	Liquid	-	Colourless	-	-	Saarchem
Propan-2-ol (C_3H_8O)	Liquid	99	Colourless	-	-	Saarchem
Ethanol (C_2H_5OH)	Liquid	99	Colourless	-	-	Saarchem

Table 3.1: Materials and chemicals used in this project (*Continued*)

Materials/ chemicals	**Form**	**Purity (%)**	**Colour**	**Particle size (µm)**	**Density @ 20°C (g/cm^3)**	**Supplier**
Methanol (CH_3OH)	Liquid	99	Colourless	-	-	Saarchem
Hydrochloric acid (HCl)	Liquid	32	Colourless	-	1.16	Saarchem
Acetone (CH_3COCH_3)	Liquid	99	Colourless	-	-	Saarchem
Distilled water	Liquid	-	Colourless	-	-	-
Diamond spray	Liquid	-	Colourless	1, 3, & 9	-	Leco
Diamond extender	Liquid	-	Blue	-	-	Leco
Argon	Gas	UHP	Colourless	-	-	Afrox

3.3 Equipment

The following equipment was used in the course of the investigations:

3.3.1 Attrition ball mill

The Attritor is often referred to generically as a "stirred ball mill." The operation of an Attritor is simple and effective. The material to be ground is placed in a stationary tank with the grinding media. Carbon steel, stainless steel, chrome steel, tungsten carbide and ceramic balls are commonly used media. The material and media are then agitated by a shaft with arms, rotating at high speed. This causes the media to exert

both shearing and impact forces on the material. The final result of this remarkably efficient process is an extremely fine material, measured in microns or fractions of microns, distributed on a very narrow curve. The attrition ball mill was used for size reduction of the synthesized B_6O powder from the micron grain to the sub-micron grain size. Figure 3.1 shows the attrition ball mill used in this work.

Figure 3.1: Attrition ball mill

3.3.2 Planetary ball mill

A planetary mill, Fritsch Pulversette 6, was used during the wet mixing of powders, using ethanol or methanol as a solvent. The mixing vessel used inside the planetary ball mill was made from alumina with a capacity of 250 ml. Steel balls of 2.5 mm in

diameter were used as milling media. The mill was operated at a speed of 200 rpm for 2 hours. Figure 3.2 shows the planetary ball mill.

Figure 3.2: Planetary ball mill

3.3.3 Particle size analyzer

The Malvern Mastersizer 2000 particle size analyzer was used to determine the particle size distribution of the milled powders. The Mastersizer 2000 was designed to measure the distribution of different sizes within a sample. The Mastersizer combines the principles of the Fraunhofer model and the Mei theory and works backward from the above theories by using the optical unit to capture the actual scattering pattern from a field of particles. It then uses the theory to calculate the size

of the particles that created the pattern. Figure 3.3 shows the Malvern Mastersizer 2000 particle size analyzer.

Figure 3.3: Malvern Mastersizer 2000

Particle size determination

The size and size distributions of milled boron suboxide particles as well as other powders were determined using the Malvern Mastersizer 2000. In order to obtain an average particle size with narrow particle size distribution, tests were conducted using sodium hexametaphosphate (NHMP) as a surfactant and water as dispersant. B_6O powders were dispersed in 0.05% NHMP solutions using external ultrasound for 2 minutes. The background measurement was done using a NHMP solution with the

same concentration (0.05%) exercising extreme care in order to achieve a clean background. About 10 mg of powder was prepared and put in a 1L beaker containing about 800 ml of solution for the size distribution tests. Obscuration was less than 16%. Particles added to the NHMP solution in the beaker were homogenized using a stirrer at a pump speed of 2000 rpm. A refractive index of 2.43 and an absorption value of 0.04 were used to determine the size distribution of the milled powder.

3.3.4 Rotary evaporator (Rotavap evaporator)

The Heidolph laborota 4010 digital rotary evaporator used has a speed range of 20 – 270rpm, a power dissipation of 1410W, a 1000mL evaporating flask and a 1000mL receiving flask. The water bath operates from 20°C to 180°C. It came with a digital display of water bath and rotation speed. This was used to dry the milled powder from the washing process. Figure 3.4 show the diagram of the Heidolph laborota 4010 digital rotary evaporator.

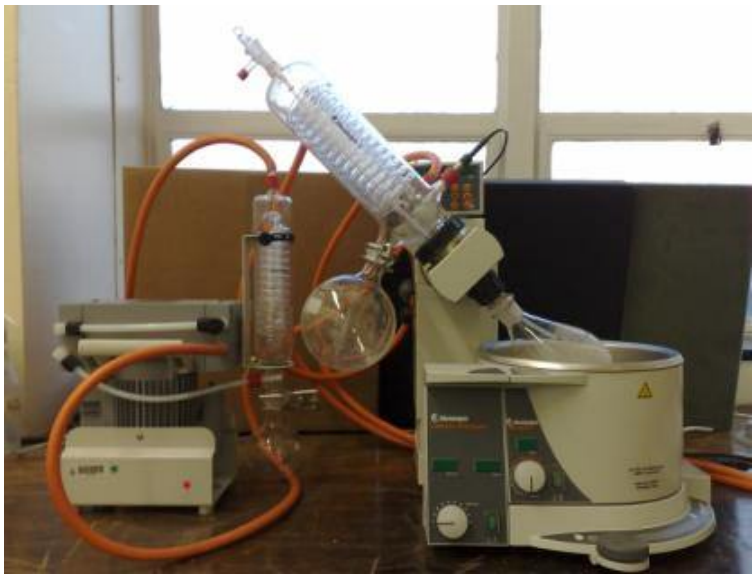

Figure 3.4: Heidolph laborota 4010 digital rotary evaporator

3.3.5 Uniaxial hot press

A Uniaxial hot press (HP20 Thermal Technology), from Thermal Technology Industries, was used for sintering and densification of samples. It consists of a furnace which is heated by a carbon element and circulated with water to cool the system. The maximum obtainable furnace temperature is 2100^{o}C and the maximum pushing force that can be applied to compacts during hot pressing is 100 KN. The force is applied through graphite punches uniaxially from the bottom graphite punch. A rotary vacuum pump is attached to the hot press and is capable of vacuum levels of 10 mTorr. Figure 3.5 below shows the picture of this Uniaxial hot press.

Figure 3.5: Uniaxial hot press

The graphite components that were placed in the hot-zone of the furnace were coated before sintering with an h-BN suspension, which was stabilized using poly-vinyl pyrrolidone (PVP). The suspension was made by mixing 37g of h-BN and 100 ml of water, with poly-vinyl pyrrolidone (2g) used as a stabilizer. All the ingredients in the suspension were stirred together vigorously, in a 250 ml beaker, using a magnetic stirrer until the constituents of the entire suspension was uniform. The suspension was then applied by paint brush to the clean hot graphite components.

Capsule

Hexagonal-BN was chosen as a crucible material in this work because of its high temperature stability (decomposition temperature around 3000^{o}C), chemical inertness

(stability in argon gas atmosphere up to 2200°C), high thermal shock resistance and high thermal conductivity. The sample cell was made from h-BN, while the piston was a graphite rod coated with layers of h-BN suspension. A 3mm h-BN cylindrical plate was placed between the graphite piston and the sample to avoid any carbon contamination. Figure 3.6 shows the drawing of the capsule used in this work.

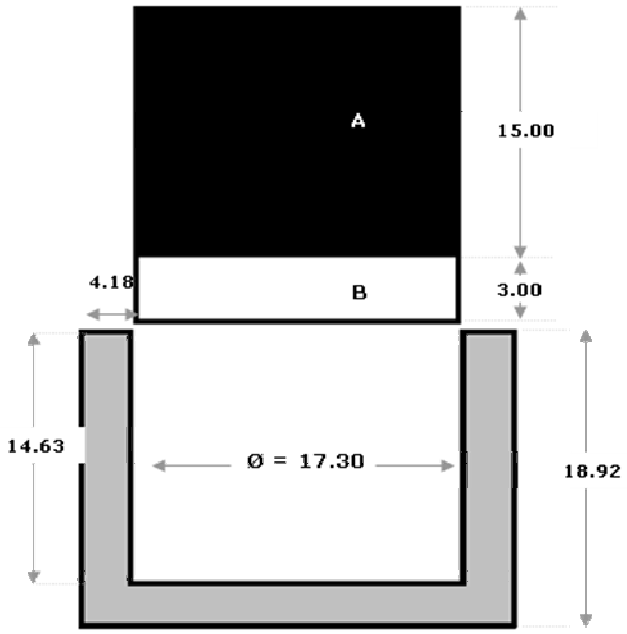

Figure 3.6: Drawing of the hBN capsule used. (A) Graphite (B) hBN

3.4 Milling of boron suboxide (B_6O) powder

Synthesized boron suboxide powder with an average agglomerate particle size of 3 µm (at d_{50}) was charged in a stainless steel attrition mill (S/N 200603, Szegvari Attritor System having 750 ml capacity). Steel balls of 2.5 mm diameter were used.

The ratio by weight of charge to ball was varied for different milling batches. Mill speed was kept in the range of between 200 and 400 rpm at room temperature. Propan-2-ol was used as the grinding media, to reduce wear of the balls. The weight of the balls was measured before and after milling to determine weight loss during milling. The attrition mill was stopped at selected milling times of 5, 8, 10, 12, 15, 18, 20, 30, 33 and 40 hours. After every requisite time interval, required amounts of powders were withdrawn for washing and particle sizing, taking due care to avoid sampling errors.

After milling, the milled powder was withdrawn and washed to remove the contaminants. In order to recover pure B_6O powder for further processing, contaminants (mainly Fe and Cr) introduced during milling were minimized by washing the milled B_6O powders in 1 M HCl followed by washing in ethanol and warm methanol to remove any B_2O_3 remaining in the powder. For every 100g of milled powder, 2.5 litres of 1 M HCl were used for the washing. The HCl solution was changed after every 6 hours. The washing did not remove the impurities completely. (see table 4.3) Nevertheless, the levels of impurities were strongly reduced by increasing the time of washing for the second batch of milled powder. After the washing, B_6O powders were dried in a rotary evaporator and kept in desiccators for further processing. The washed and dried B_6O powder samples were taken for ICP-OES analysis to determine the level of impurities left in the powders.

3.5 Chemical analysis of milled boron suboxide (B_6O) powder

An inductively coupled plasma optical emission spectrometer, ICP-OES (SPECTRO CIRUS CCD), was used to determine the level of concentrations of Fe and Cr in the washed powders. 0.1g weight of the samples was digested in a solution containing 3 ml HNO_3 (55%), 2 ml HCl (32%) and 3 ml HF (40%) by the microwave digestion technique (Multiwave 3000 SOLV). The digestion was done at 260^{o}C for 30 minutes. The analytical wavelengths chosen were 259.941 (nm) for Fe, and 267.716 (nm) for Cr. These wavelengths showed a good linear response between concentration and intensity and were free of interferences in the range of concentrations used in the present study. The actual quantitative results will be discussed in detail in chapter 4.

3.6 Mixing boron suboxide (B_6O) powder with other compounds

To improve the mechanical properties, especially the fracture toughness of the 'pure' polycrystalline B_6O hot pressed compacts, different sintering additives were used. These additives were expected to reduce and/or replace the existing B_2O_3 on the surfaces of B_6O particles by reacting with them to form oxide/boride phases.

The washed B_6O powder was mixed with different compounds from the alkaline earth oxide (MgO and CaO), as well as nickel and cobalt derived compounds, in methanol for 2 hours using the planetary ball mill. The mixing speed was kept at 200 rpm, while using 2.5mm steel balls as the media. The calculation of the weight

percentage of each additive was carefully done in order to retain the same volume percentage in the B_6O powder. After mixing, the slurry was dried using the rotavap, and then characterized using X-ray powder diffraction to identify the phases present and then SEM/EDS to check the homogeneity of the admixed powder.

3.7 Hot pressing of powders

For pure B_6O

The furnace was heated to 1700^{o}C at 15^{o}C/min and held at this temperature for 20 minutes, the applied pressure was increased gradually to 30MPa at this temperature, after which the temperature was increased at a rate of 10^{o}C/min to 1900^{o}C. The holding time at 1900^{o}C was 20 minutes during which time the applied pressure was kept constant at 50 MPa. The furnace was then cooled to room temperature at 20^{o}C/min. During cooling, furnace temperature lagged behind the programmed temperature at temperatures lower than 800^{o}C. At temperatures lower than 500^{o}C the load was removed from the sample. At room temperature the sample cell was removed from the graphite die/insert and the sample was then removed from the h-BN crucible for analysis. A typical hot pressing cycle is shown in figure 3.7. The maximum load applied for hot pressing of pure B_6O was 50MPa.

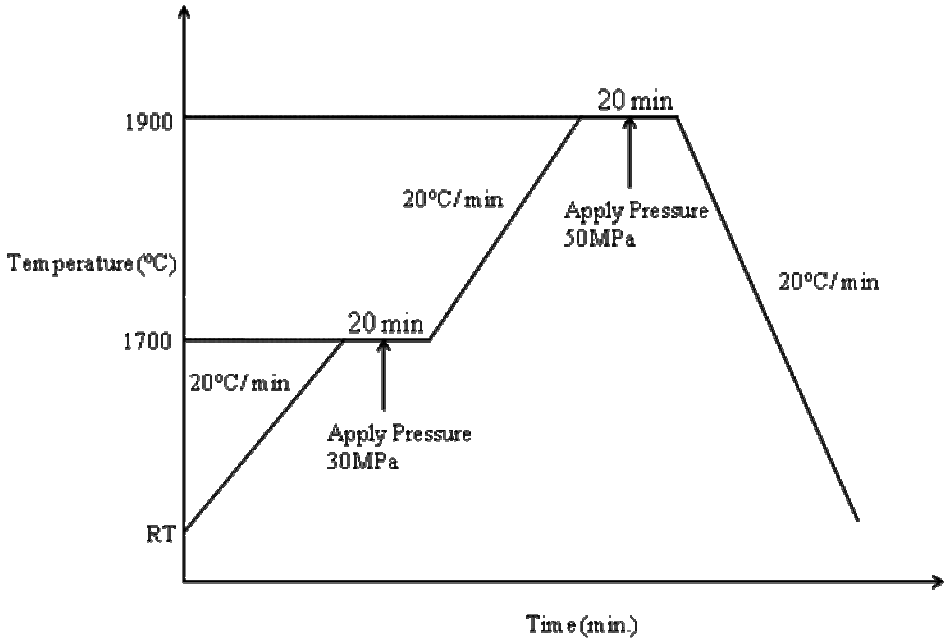

Figure 3.7: Hot pressing profile used for pure B_6O materials. (RT = room temperature)

For B_6O with sintering additives

The above profile was also used for sintering B_6O composites, but high densification was not achieved due to the heterogeneity of the samples. Many other profiles were tried to achieve high density, until one was arrived at that gave a good densification in the sintered product. Here, the furnace was heated to 1400°C at 20°C/min and held at this temperature for 5 minutes, to apply a load of 80 MPa (this load was maintained throughout the hot pressing). The furnace was further heated to 1850°C (sintering temperature) at 20°C/min and held at this temperature for 20 minutes. The furnace was then cooled to room temperature at 20°C/min. Figure 3.8 shows the hot pressing profile for the B_6O composites.

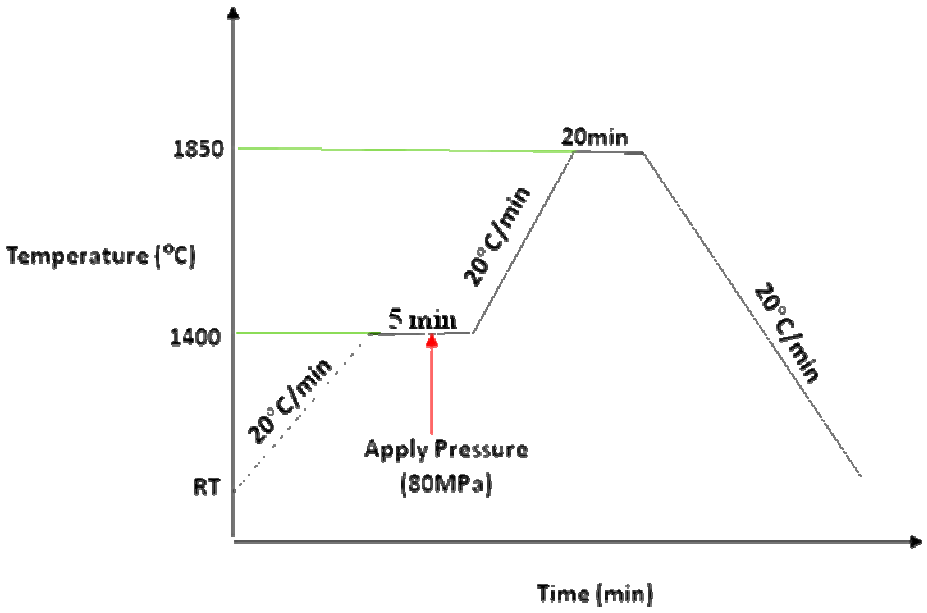

Figure 3.8: Hot pressing profile for B_6O materials.

3.8 Characterization techniques

Before characterization, all hot-pressed materials were ground on the surface to remove any hBN material adhered to the hot-pressed material. Densities of the materials were measured immediately after hot pressing. Materials were then cut into 2 pieces using a diamond saw for further analyses. The following were the characterization techniques employed in this work.

3.8.1 X-Ray diffraction (XRD)

A Philips PW 1713 X-ray diffractometer fitted with a monochromatic Cu Kα radiation set at 40 kV and 20 mA was used to determine the phase composition of

powders and hot-pressed materials. The scan was taken between 10^{o} and 80^{o} 2 theta (2Θ) with a step size of 0.02 degree. Phase identification was done using Philips Analytical X'Pert HighScore® software with an in-built International Centre for Diffraction Data (ICSD) database. B_6O and other peaks were identified by comparing the acquired d-values with the values obtained from the database as well as from previous investigation.

3.8.2 Polishing of the samples

Cross-sections of hot-pressed materials were carefully polished after hot mounting in bakelite powder followed by lapping on Struers 80, 120, 220, 600 and 1200 grit. Grinding was carried out to achieve a flat surface and to remove any scratches. Materials were then polished on pan clothes of 9, 3 and 1 μm respectively, using diamond spray and diamond extender to remove surface stress raisers and machining damage such as microcracks and to increase the reproducibility of data, especially, crack size. Samples were rinsed with ethanol and dried. Polishing was performed for 15 minutes on each of the polishing cloths.

3.8.3 Determination of density, hardness and fracture toughness

Density measurements

The density of the samples was determined using the Archimedes method. The samples were immersed in distilled water (in a beaker) and then boiled for 3 hours, using a hot plate, in order to displace air from the pores in the sample. The thickness of the sintered samples was about 4 mm. The boiled water containing the material was then allowed to cool to room temperature.

The density of the material was calculated by first determining the mass of the water impregnated sample, i.e. suspended mass (m_s). The sample was then removed from the water and dried lightly on the surface using a paper towel to remove excess water from the surface, and the water saturated mass (m_w) was then determined. Finally, the dry mass (m_d) of the sample was measured after the sample had been dried in an oven for about 20 minutes, and then cooled to ambient temperature. For accuracy each mass was determined five times in order to calculate a mean value which was then used to determine the density (ρ_s) and the porosity (P_o) of the samples. The following formulae were used to calculate the densities and the open porosities.

$$\rho_s = \frac{m_d \rho_{water}}{(m_s - m_w)} \qquad \textbf{[3.1]}$$

$$P_o = \left(\frac{m_w - m_d}{m_w - m_s} \right) \times 100 \qquad \textbf{[3.2]}$$

Where, m_s = suspended mass

m_w= water saturated mass $\rho_{water} = 1.000 g cm^{-3}$

m_d = dry mass

P_o= open porosity, Temperature = RT

Theoretical densities of the hot pressed B_6O materials were calculated based on the rule of mixtures according to the formula given in appendix A2.

Hardness and fracture toughness determination

The hardness and fracture toughness of the hot pressed materials were measured by the indentation technique using a Vickers indenter (LECO V-100-A2 Vickers Hardness Tester machine) with a load of 1kg for pure B_6O, and 5kg for B_6O sintered materials. The length of the cracks generated by the indentation was measured (figure 3.9) and the crack lengths were used to calculate the fracture toughness (K_{1C}) of the materials.

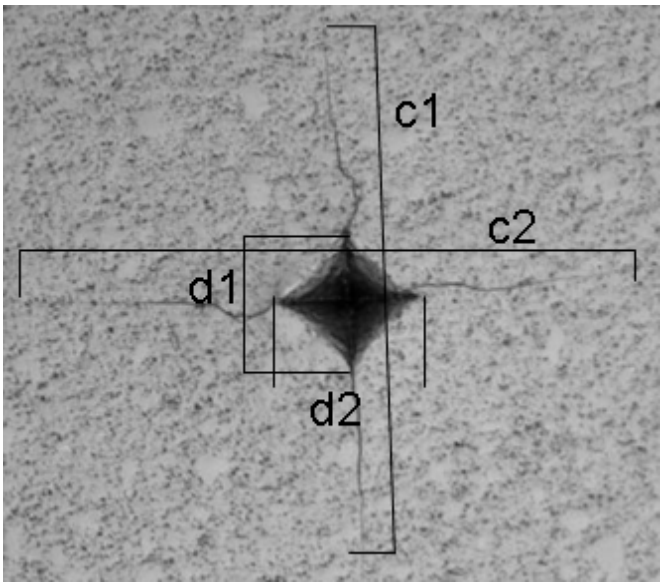

Figure 3.9: Schematic representations of a Vickers indent. (Shabalala, 2007)

Where, d_1 = vertical indentation length

d_2 = horizontal indentation length

c_1 = vertical length spanned by indentation cracks

c_2 = horizontal length spanned by indentation cracks

d = average indentation length

c = average length spanned by indentation cracks

The hardness values were calculated from the equation 3.3

$$H_v = 1854.4 \times \frac{P}{d^2} \qquad \textbf{[3.3]}$$

Where P is the applied load in Newton (N) and d is the arithmetic mean of the two diagonals in micrometers (μm). The hardness is then given in GPa.

Also, the fracture toughness was calculated from equation 3.4 given below:

$$K_{IC} = \xi\left(\frac{E}{Hv}\right)^{1/2}\left(\frac{P}{c^{3/2}}\right) \qquad \textbf{[3.4]}$$

Where, ξ is the calibration constant (0.016), E is the Young Modulus of Elasticity (GPa) and c the radial crack length (in micrometer) (Anstis et al., 1981).

3.8.4 Analysis of microstructure

The microstructures, composition, and morphology of powders and hot-pressed materials were analyzed by means of scanning electron microscopy (SEM). A Philips scanning electron microscope (ESEM XL30) equipped with energy dispersive X-ray spectrometer (EDX) was used to analyze the various elemental compositions found in the materials. An AxioCam MRc AV31-KS optical microscope was used to view the polished sintered B_6O materials. The microscope was fitted to a computer which uses the Axiovision 3.1 software for image analyses.

Chapter Four

4 Experimental results

4.1 Introduction

This chapter presents the results obtained from milling, chemical analysis, mixing, and hot pressing of the sintered pure B_6O and B_6O sintered materials.

4.2 Milling of boron suboxide (B_6O) powder

The milling procedure was discussed in section 3.4. The milling conditions are presented in table 4.1. From these investigations it was concluded that the optimum milling conditions are: 20 hours milling time at 400 rpm using 2.5 mm balls for the fourth milling (E4). These conditions were used for the other batches of milling experiments and the result was reproducible.

Contamination is unavoidable during milling although the extent can be minimized under certain conditions. Increasing the milling time increases the weight loss of the balls during milling. This indicates that contamination occurs during milling. Iron (Fe) and chromium (Cr) in the steel balls were the major contaminants in the milled powder.

Table 4.1: Milling conditions of boron suboxide powders

Batch	**Initial mill speed (rpm)**	**Final mill speed (rpm)**	**Diameter of steel ball (mm)**	**Ball to powder ratio**	**Time intervals (hours)**	**Initial particle size (µm) @ d_{50}**	**Final particle size (µm) @ d_{50}**
E1	200	400	2.5	3:1	8, 10, 15, 18, 20, 30, 33, 40	3.0	0.72
E2	400	400	2.5	5:1	5, 12, 15, 20, 25	3.0	0.76
E3	400	400	2.5	10:1	10, 15, 20	3.0	0.51
E4	400	400	2.5	10:1	20	3.0	0.54

All the milling was carried out at room temperature.

The size distribution of the milled powder was determined using a refractive index of 2.43 and particle absorption value of 0.04. Increase in the mill speed and the ball to powder ratio, increases the percentage impurity during the milling (appendix B). The dependence of the particle size distribution of B_6O powders on milling time, for batches E1 and E3, are shown in figures 4.1 (a) and (b).

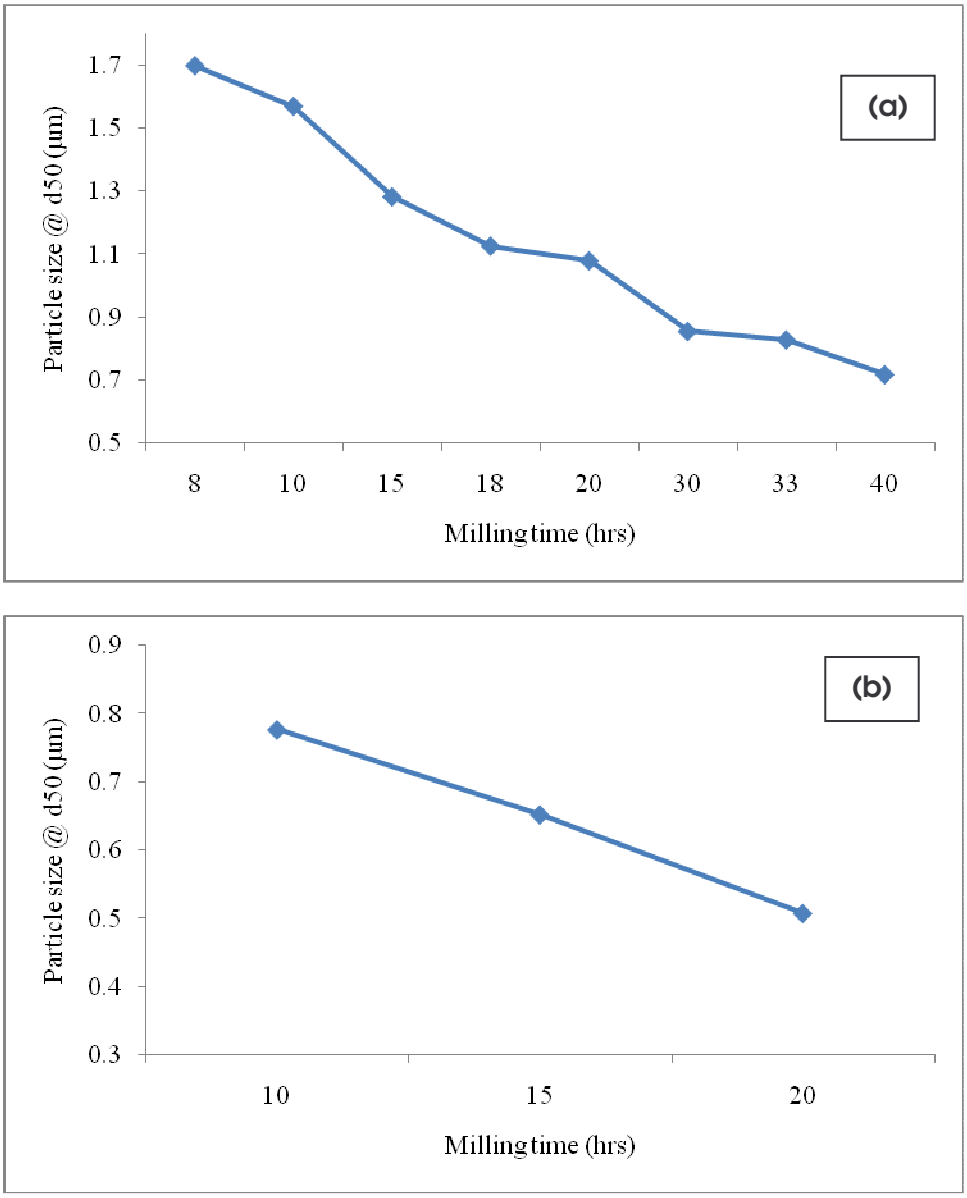

Figure 4.1: The dependence of the particle size distribution of B_6O powders on milling time (a) E1 (b) E3; It could be observed that increasing the milling time decreases the particle size.

The volume was expressed in the cumulative percentage undersize. Figure 4.2 shows also the comparison between the milled batches after 20 hours of milling under the same conditions.

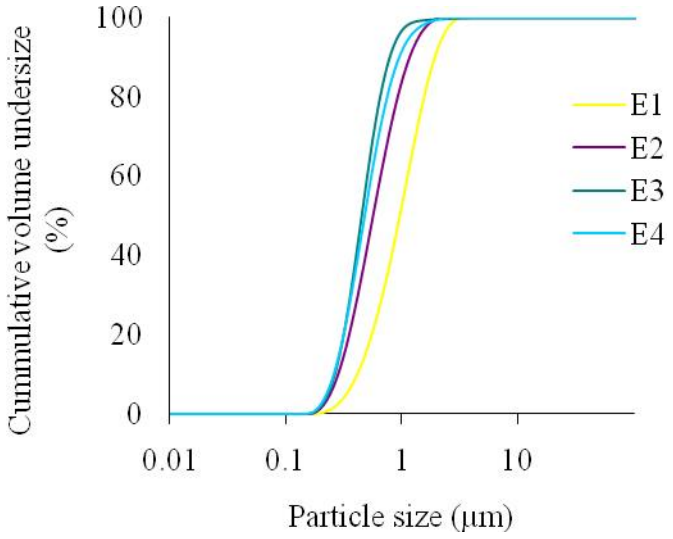

Figure 4.2: Comparison of milled B_6O powder batches after 20 hours.

Figure 4.3 shows the XRD pattern of B_6O powder milled for 20 hours before washing. Continuous washing of milled powder in 1 M HCl reduced Fe and Cr concentrations strongly.

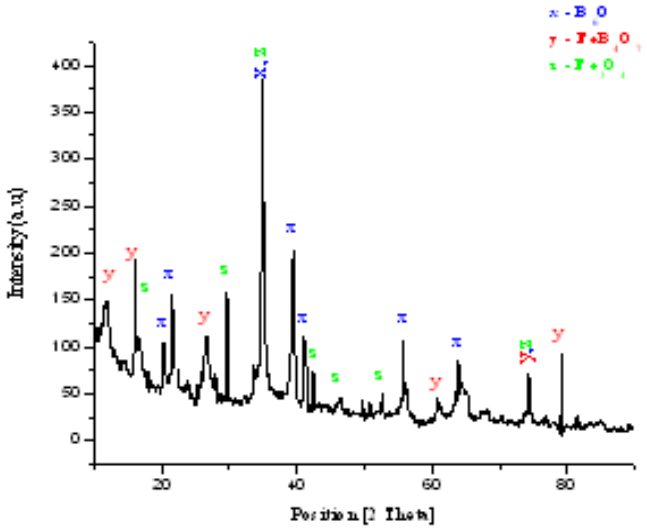

Figure 4.3: XRD pattern of B_6O powder milled for 20 hours before washing.

Figure 4.4 shows the XRD pattern of milled and washed B_6O powder. The peaks shown are those of B_6O only.

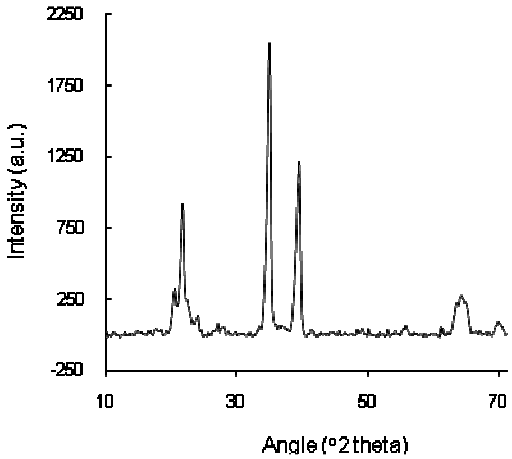

Figure 4.4: XRD pattern of milled and washed B_6O powder showing only B_6O peaks.

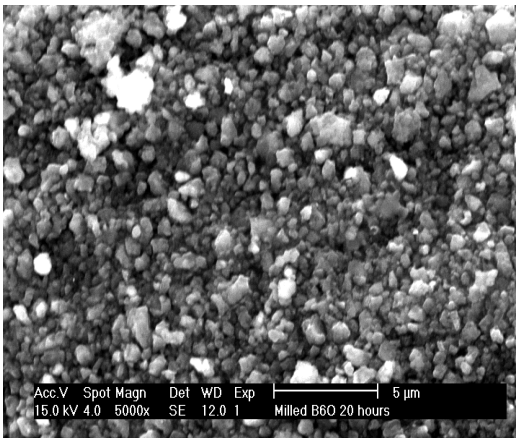

Figure 4.5: SEM image of B_6O powder milled for 20 hours.

After the milling, the boron suboxide (B_6O) powders were washed and dried in the rotavap evaporator and the results obtained for the recovery of the powder are given in table 4.2

Table 4.2: Weight loss and percentage recovery of milled, washed and dried boron suboxide (B_6O) powders.

Batch	**Initial powder weight (g)**	**Final powder weight (g)**	**Ball to powder ratio**	**Weight loss (%)**	**Recovery (%)**
E1	100	98.7	3:1	1.30	98.7
E2	100	93.1	5:1	6.90	93.1
E3	50	48.25	10:1	3.50	96.5
E4	50	49.3	10:1	1.40	98.6

4.3 Chemical analysis of the boron suboxide (B_6O) powder

As discussed in section 3.5, the basis for dilution of the B_6O powder for ICP-OES analysis was 0.1g of sample in 100ml of solution. Table 4.3 gives the result of the chemical analysis of the different batches of milling.

Table 4.3: Chemical analysis (ICP-OES) of B_6O, for the four batches after washing in 1 M HCl.

Milling batch	**Milling time (hours)**	**Fe (wt. %)**	**Cr (wt. %)**
E1	40	0.040	0.017
E2	25	0.090	0.026
E3	20	0.046	0.033
E4	20	0.057	0.039

4.4 Sintering and properties of boron suboxide (B_6O) powders

The sintering conditions have been discussed in section 3.7. The material was sintered with and without additives and their properties were investigated. The purpose of the additives was to enhance the mechanical properties of the B_6O material. The detailed results of the sintering are presented in this section:

4.4.1 Pure boron suboxide (B_6O) powder

B_6O powders were hot pressed at 1900°C for 20 minutes under a pressure of 50 MPa using a uniaxial hot press as described in section 3.7. Table 4.4 summarizes the properties of the hot-pressed materials. Loads of 1kg and 5kg were used to determine the Vickers hardness for sintered materials. At loads higher than 1kg chipping of the B_6O grains occurred in the pure B_6O material, hence, the fracture toughness was not measured for this material.

Table 4.4: Properties of pure B_6O material hot pressed at 1900°C, 50MPa and 20 minutes

Material	**Measured density (g/cm^3)**	**Percentage Theoretical density (%)**	**Open porosity (%)**	**Vickers hardness, H_v (GPa)**		**Fracture toughness ($MPa.m^{0.5}$)**
				5kg	**1kg**	
Pure B_6O	2.45	96.1	0.9	-	30.5 ± 2.1	Brittle

Figure 4.6 shows the XRD pattern of the hot pressed pure B_6O materials. XRD patterns are similar for the washed B_6O powder as for the hot pressed B_6O sample, but there was a reduction in the width of the peaks and the crystallinity had increased during hot pressing.

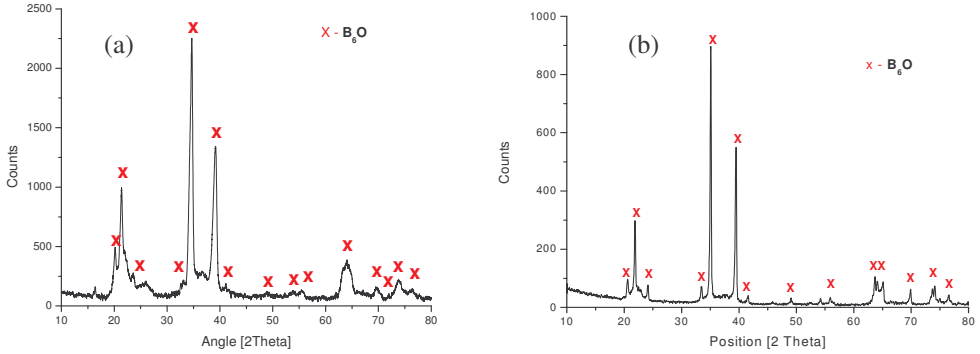

Figure 4.6: XRD pattern of B_6O powders (a) milled powder (b) sintered powder.

Figure 4.7 shows the SEM images of the hot pressed B_6O materials at different magnifications. EDX analysis carried out on the material showed that the secondary phases constituted mainly Fe and Cr, which is in agreement with the ICP result. The grain size of the hot pressed compacts could not be determined from the SEM images due to a lack of good etchant for this material. Small holes assumed to be pores were observed in the B_6O sample, but it must be mentioned that some of them came from the removal of the remaining B2O3 during polishing or due to bad polishing, which also influences the high porosity. Further optical analysis showed that this hot pressed B_6O sample had porous edges, which were caused by slight decomposition at the sintering temperature.

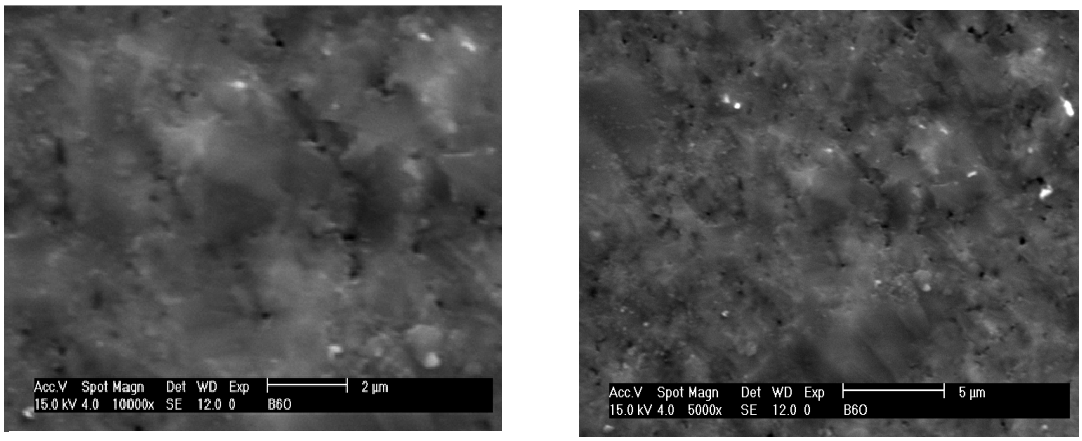

Figure 4.7: SEM images of hot pressed B_6O sample at different magnifications

4.4.2 B_6O with alkaline earth oxides additives

Mixing of the boron suboxide (B_6O) with various additives was described in section 3.6. The MgO powder was fine and white. The CaO and $CaCO_3$ powders are also white in appearance but they show a similar (modal) distribution pattern as observed from the SEM images. Figure 4.8 shows the SEM images of the alkaline earth oxide additives.

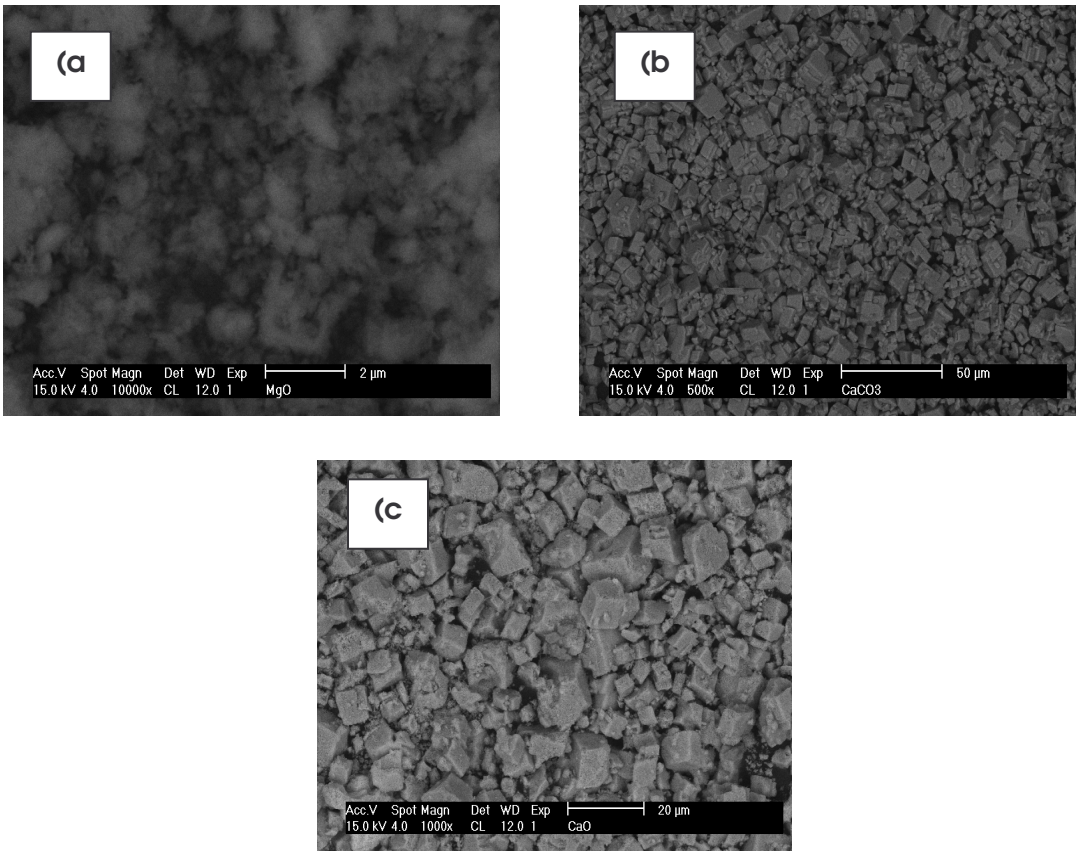

Figure 4.8: SEM images of alkaline-earth metal oxide additives (a) MgO (b) $CaCO_3$ and (c) CaO.

Different weight percentages of the additives were used in order to understand the densification mechanisms. The mixed and sintered B_6O powders were analysed using XRD and SEM to check the homogeneity of the secondary phase in the B_6O material. The weight percentage of the additives are given in table 4.5. The hot pressing profile for these materials has been described in section 3.7. Materials were hot pressed at 1850^{o}C under a pressure of 80 MPa for 20 minutes except for the MgO additive (sintered at 50 MPa). Mechanical properties and densities measured on the hot pressed materials are given in table 4.5.

Table 4.5: Densities and mechanical properties of B_6O-alkaline earth oxide materials hot pressed at 1800°C for 20minutes.

Materials	**Wt % of additive**	**Vol % of additive**	**Load (MPa)**	**Density (g/cm^3)**	**% Theo. density**	**Open porosity (%)**	**Hardness, H_v (GPa)**	**Fracture toughness, K_{ic} ($MPa.m^{0.5}$)**	**Secondary phases**
B_6O + CaO	1.4	1.08	80	2.44	95.7	1.5	32.1 ± 1.9	6.8 ± 1.6	CaB_6
B_6O + $CaCO_3$	0.7	1.08	80	2.50	98.0	1.0	31.6 ± 1.0	6.1 ± 1.7	B_4C, CaB_6
B_6O + MgO	1.5	1.08	50	2.49	97.6	0.9	31.5 ± 2.1	6.1 ± 1.3	$Mg_2B_2O_5$, HBO_2

Sub-micron B_6O powders were mixed separately with 1.5 wt% MgO powder, 1.4 wt% CaO powder and 0.7 wt% $CaCO_3$ powder respectively, these amounts corresponding to a constant value of 1.08 vol% of additives (and all other additives used in this study), which was predetermined and is shown in appendix A3. The mixtures were, after mixing and sintering, characterized using XRD, while the morphologies were observed with the SEM.

It can be observed that the densities obtained for the sintered B_6O materials were higher than those obtained for the pure B_6O, except for the CaO additive at 2.44 g/cm^3. The reason for the increase in densities could be as a result of the load applied during sintering. When compared with the rest of the materials in this group, it can be concluded that the CaO additive is not as dense as that of the others. The reason for this could not be determined here.

The Vickers hardness values measured for these materials were slightly higher than that of pure B_6O (even for the MgO-B_6O material sintered at the same load, 50 kg) and there are significant increases in the fracture toughness of the produced materials. For instance, B_6O materials containing 1.5 wt% MgO, 1.4 wt% CaO and 0.7 wt% $CaCO_3$ have a Vickers hardness of 31.5 GPa, 32.1 GPa and 31.9 GPa respectively, compared with 30.5 GPa of pure B_6O. Their corresponding fracture toughness values were 6.1 $MPa.m^{0.5}$, 6.8 $MPa.m^{0.5}$ and 6.1 $MPa.m^{0.5}$, respectively. For any small addition of the binder there was a significant increase in the fracture toughness compared to pure B_6O, which was found to be brittle.

The XRD of the mixed powders before sintering are shown in appendix C1. Only B_6O crystalline phases were observed in the mixtures with MgO and CaO except that with the $CaCO_3$ additive, which confirm the presence of $CaCO_3$. After hot pressing, a borate crystalline phase was formed in the MgO-doped composite and with an additional HBO_2 phase. The HBO_2 is probably the result of the reaction of residual B_2O_3 with H_2O (moisture). A boride crystalline phase was formed in CaO, and a carbide phase with traces of boride phase (CaB_6) in the $CaCO_3$ additives. The formation of B_4C could be as a result of carbon pick-up from the graphite dies by diffusion during cooling.

The XRD for the sintered B_6O-alkaline earth oxide materials are shown in figure 4.9, 4.10 and 4.11 respectively. XRD analysis shows the main peak of CaB_6 in the CaO

additive at 2Θ = 30.3°. In the $CaCO_3$ additive, the major peak of B_4C is at 2Θ = 37.6° while that of CaB_6 is at 2Θ = 30.3°. In the MgO addition, the major peaks for the secondary phases are 2Θ = 27.0° and 28.9°, for HBO_2 and $Mg_2B_2O_5$ respectively.

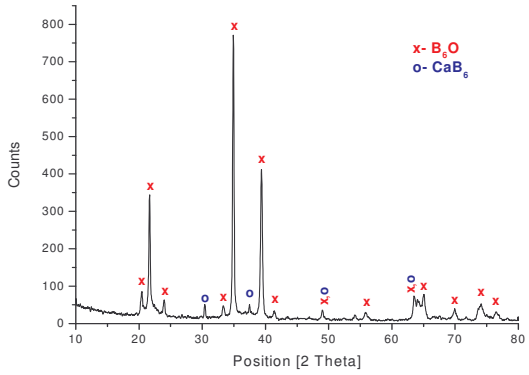

Figure 4.9: XRD pattern of sintered B_6O with CaO additive

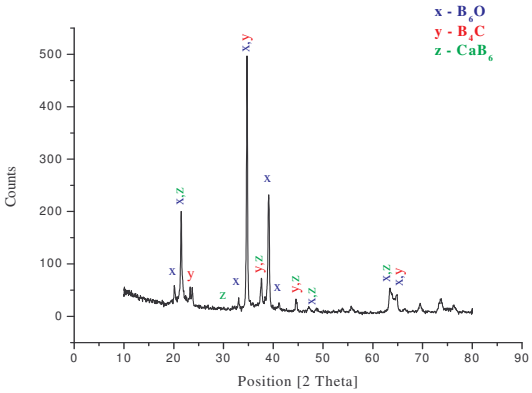

Figure 4.10: XRD pattern of sintered B_6O with $CaCO_3$ additive

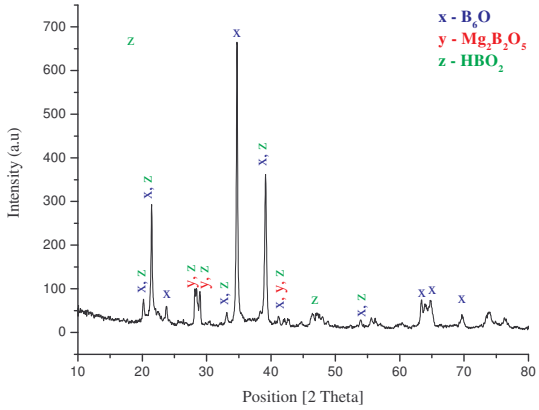

Figure 4.11: XRD pattern of sintered B_6O with MgO additive

The SEM/EDX images of the hot presssed B_6O-alkaline earth oxide materials produced are shown in figures 4.12, 4.13, 4.14, and 4.15 respectively. It can be observed from the micrographs that a homogeneous distribution of the minority phase was not obtained in these materials. There were segregations of the secondary phase scattered in pockets in the microstructure. Pores which could be inherent in these materials due to decomposition reactions at the sintering temperature were seen as dark spots in the samples. There were no differences in the distribution of the additives between the centre and the near surface area of the sintered materials. At higher magnifications, no evidence of any grain growth was observed in the hot pressed materials. The iron pickup in the EDX analysis of $CaCO_3$ and MgO additives-derived composites must have originated in the starting B_6O material.

The segregation of boride secondary phase in the B_6O-CaO-derived composite (figure 4.15) additive suggests variation in the properties of the materials at different points

in the sample. An EDX analysis of this sample confirms that the grey phase represents B_6O, while the white represents the boride phase, in agreement with the phase composition obtained from the XRD analysis.

The formation of the B_4C phase in the $CaCO_3$ additive-derived B_6O composite, as one of the secondary phases must have been a result of carbon diffusion from the graphite dies during cooling. This is confirmed by the existence of carbon on the EDX image, see figure 4.13.

The MgO additive-derived B_6O composite shows the formation of a borate phase, $Mg_2B_2O_5$. The non-homogeneous distribution of this phase on the material must have been as a result of the poor wettability of the secondary phase present. The pores on this material are more pronounced at higher magnifications (figure 4.14).

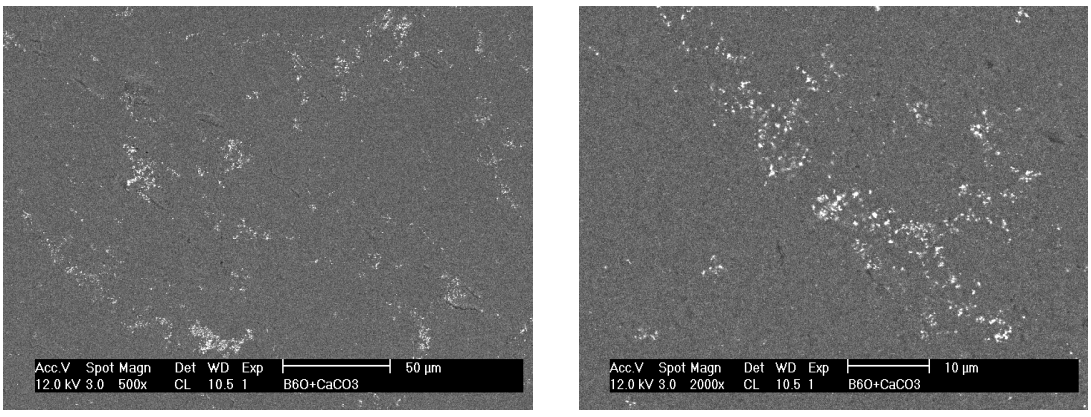

Figure 4.12: SEM images of B_6O + $CaCO_3$ at different magnifications

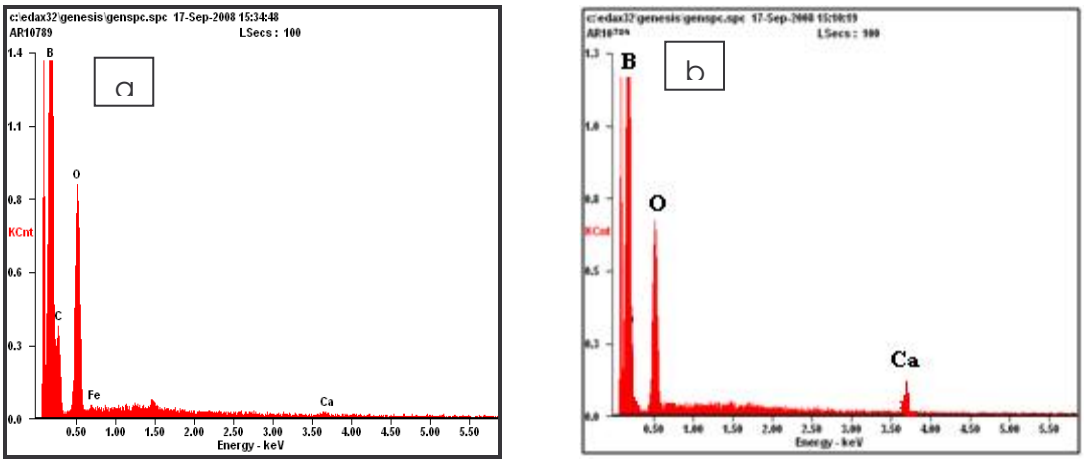

Figure 4.13: EDX from B_6O + $CaCO_3$ additives showing (a) Grey phase (b) White phase

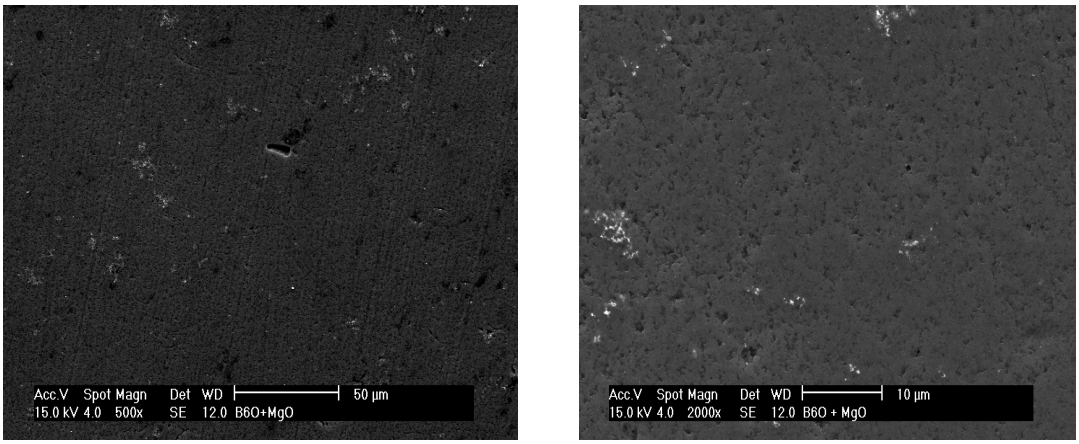

Figure 4.14: SEM images of B_6O + MgO at different magnifications

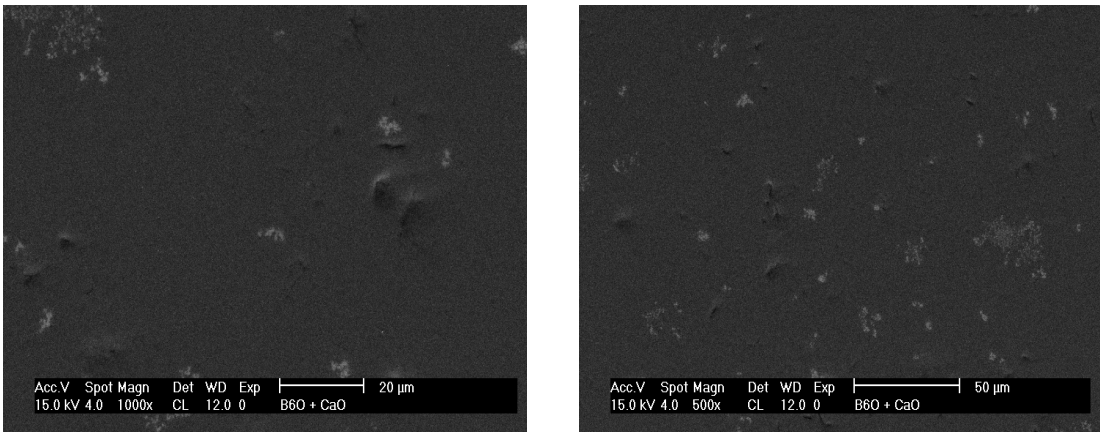

Figure 4.15: SEM images of B_6O + CaO at different magnifications

4.4.3 B_6O with nickel and nickel compounds

B_6O powder was mixed with nickel (Ni), nickel boride (Ni_2B), and nickel oxide (NiO) in the ratios 3.7, 1.5 and 2.8 respectively. The mixtures were hot pressed as discussed in section 3.7 of chapter 3. The results obtained after hot pressing are presented in table 4.6

Table 4.6: Densities and mechanical properties of B_6O powder with nickel and nickel derived compounds, hot pressed at 1800oC for 20minutes.

Materials	**Wt % of additive**	**Vol % of additive**	**Load (MPa)**	**Density (g/cm^3)**	**% Theo density**	**Open porosity (%)**	**Hardness, H_v (GPa)**	**Fracture toughness, K_{ic} ($MPa.m^{0.5}$)**	**Secondary phase**
B_6O + Ni	3.7	1.10	80	2.53	96.5	1.97	30.7 ± 1.1	6.4 ± 0.6	NiB
B_6O + Ni_2B	1.5	0.75	80	2.57	99.2	0.75	31.1 ± 1.1	6.5 ± 0.8	NiB
B_6O + NiO	2.8	1.10	80	2.54	98.1	3.97	27.1 ± 2.1	6.1 ± 0.9	NiB

The densities of these sintered materials can be observed to be higher than that of the pure B_6O material, which can be as a result of the different hot pressing profiles used. The densities obtained are above 95% of the theoretical densities of the different compounds added.

The Vickers hardness values measured for these materials except for NiO, show a slight increase when compared with that of pure B_6O. The Vickers hardness value for the Ni and Ni_2B additives are 30.7 and 31.1 GPa respctively, while that of NiO is 27.1 GPa, which also has the highest porosity, 3.97%. All the materials show a significant increase in the fracture toughness as compared with pure B_6O, which is brittle. The fracture toughness values range from 6.1 to 6.5 $MPa.m^{0.5}$.

XRD analyses of the mixed powders are shown in appendix C2, which confirm the presence of the additive phases in the different mixtures. The position of the main peak results from nickel addition was at $2\Theta = 39.2°$, that for nickel boride at $2\Theta = 39.0°$, and that of nickel oxide at $2\Theta = 38.9°$. The formation of boride secondary phase in the matrix after sintering (figures 4.16, 4.17, and 4.18) was observed by XRD. The unlabelled peaks are those of BN, which could be as a result of diffusion from the BN capsule used. Comparing the mixed powders to the hot pressed material, it was obvious that the Ni, Ni_2B and NiO additives reacted completely, thus oxidizing the B_6O to form the boride phase in the final composite. The advantage of this oxidation reaction is that there is a possibility of improving the oxygen content

and the crystallinity of boron suboxide. The reactions are presented in equations 4.1, 4.2 and 4.3 respectively.

$$3B_6O + 16Ni \rightarrow 16NiB + B_2O_3 \qquad [4.1]$$

$$3B_6O + 16Ni_2B \rightarrow 32NiB + B_2O_3 \qquad [4.2]$$

$$5B_6O + 16NiO \rightarrow 16NiB + 7B_2O_3 \qquad [4.3]$$

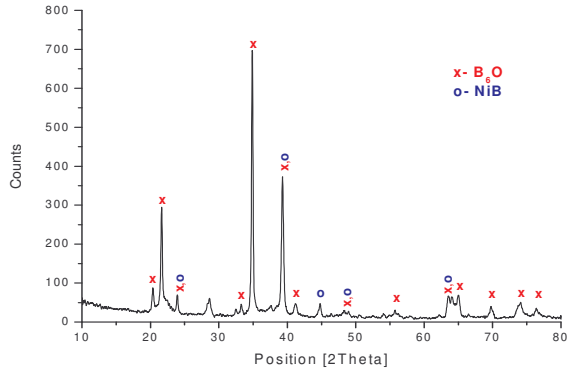

Figure 4.16: XRD pattern of sintered B_6O with Ni additive (unlabelled peak = BN)

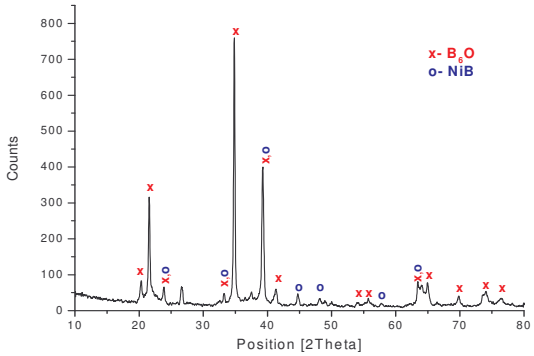

Figure 4.17: XRD pattern of sintered B_6O with Ni_2B additive (unlabelled peak = BN)

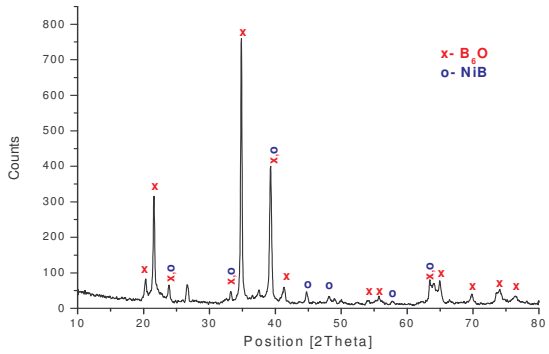

Figure 4.18: XRD pattern of sintered B_6O with NiO additive (unlabelled peak = BN)

Figures 4.19, 4.20 and 4.21 show the SEM photographs of the polished sintered materials. It can be observed from the micrographs that a homogeneous distribution of the binder phase was not obtained in these materials. There were segregations of the secondary phase scattered in pockets on the microstructure. The segregation of the boride secondary phase suggests variation in the properties of the materials at different points in the sample. There are no differences in the distribution of the additives between the centre and the near surface area of the sintered materials. The three materials showed a similar materials distribution. EDX analysis on each sample confirms that the grey phase represents B_6O, while the white represents the respective borides of the additives, in agreement with the phase composition obtained from the XRD analyses. Pores which could be inherent in the matrix due to the decomposition reactions at the sintering temperature were seen as dark spots in the samples. At higher magnifications, no evidence of any grain growth was observed in the hot

pressed materials. The iron pickup in the EDX analysis of Ni_2B-derived B_6O composite must have originated in the starting B_6O material.

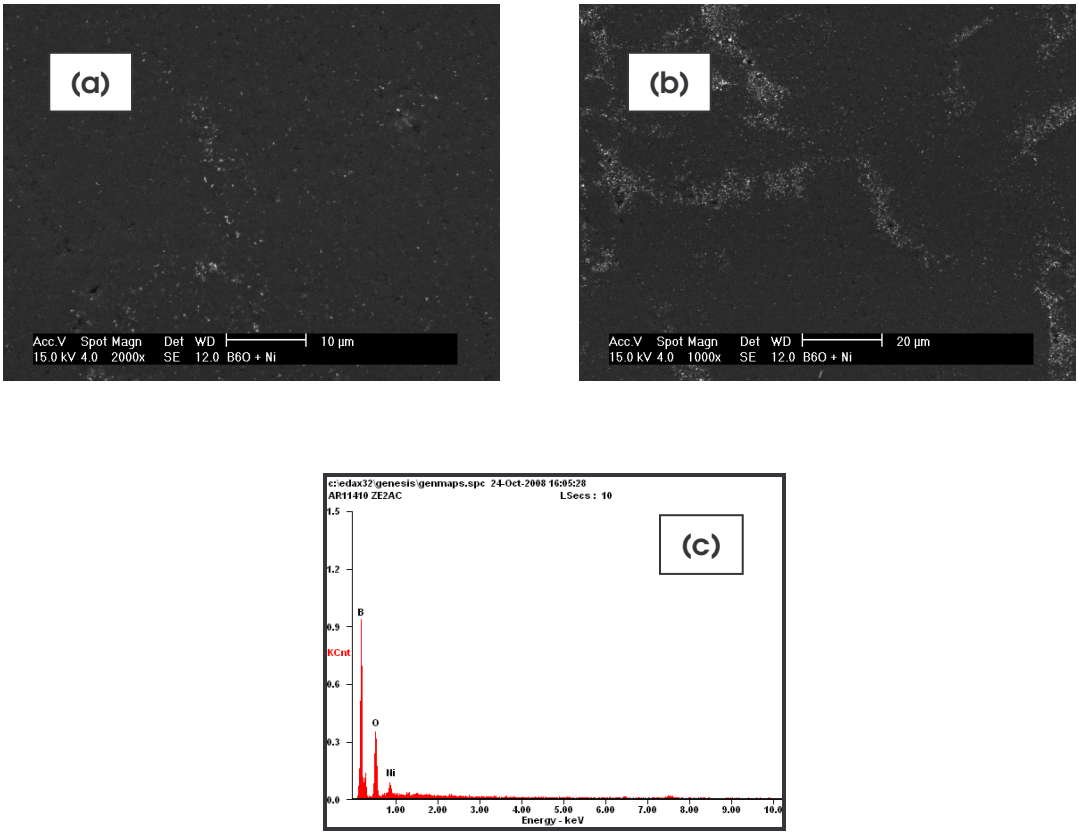

Figure 4.19: SEM image of B_6O + Ni sintered material. (a) *x*2000, (b) *x*1000, and (c) EDS on white phase.

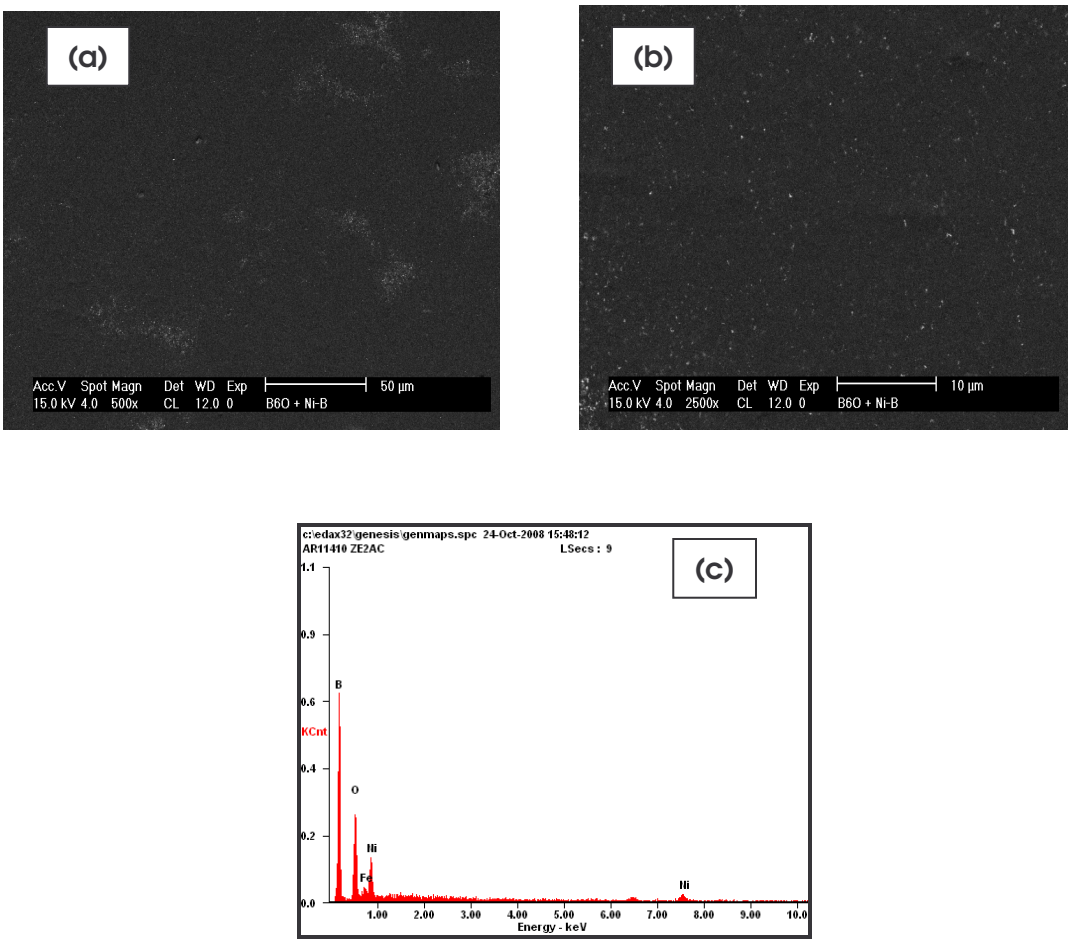

Figure 4.20: SEM image of B_6O + Ni_2B sintered material. (a) *x*500, (b) *x*2500, and (c) EDS on white phase.

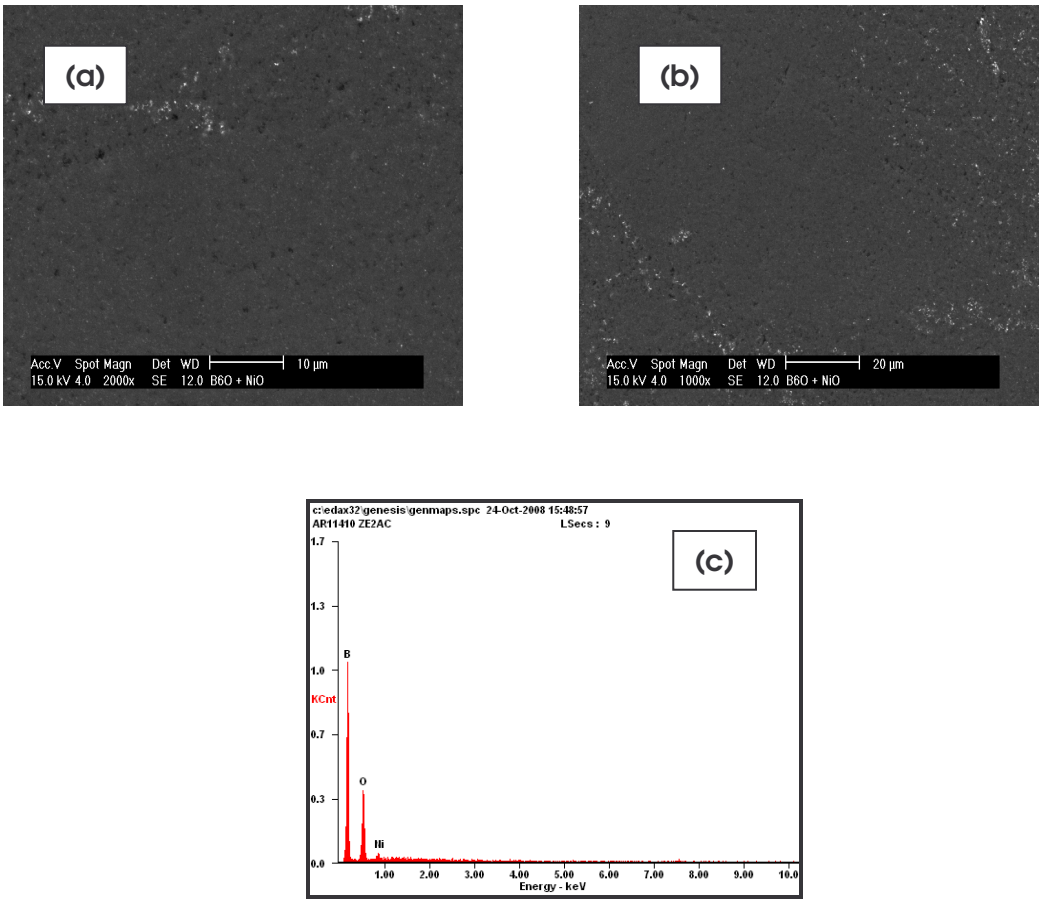

Figure 4.21: SEM image of B_6O + NiO sintered material. (a) *x*2000, (b) *x*1000, and (c) EDS on white phase.

4.4.4 B_6O with cobalt compounds

The cobalt derived compounds used in this study were cobalt boride (Co_2B) and cobalt oxide (CoO). These compounds were added to the B_6O powder and sintered using the hot pressing profile shown in section 3.7 of chapter 3. The results obtained from the hot pressed materials are presented in table 4.7.

Table 4.7: Densities and mechanical properties of B_6O powder with cobalt derived compounds, hot pressed at 1800°C for 20minutes.

Materials	**Wt % of additive**	**Vol % of additive**	**Load (MPa)**	**Density (g/cm^3)**	**% Theo density**	**Open porosity (%)**	**Hardness, H_v (GPa)**	**Fracture toughness, K_{ic} ($MPa.m^{0.5}$)**	**Secondary phase**
$B_6O + Co_2B$	2.1	0.65	80	2.51	96.9	1.47	34.9 ± 1.1	5.2 ± 0.5	CoB
B_6O + CoO	2.7	1.10	80	2.55	98.5	1.58	32.6 ± 2.9	5.8 ± 1.1	CoB

The densities obtained from these materials are over 96% of their respective theoretical densities. This is attributed to the hot pressing profile used. The Vickers hardness values obtained for these materials display a good increase when compared to that of pure B_6O. Co_2B additive-derived composite gives a hardness value of 34.9, and CoO, a value of 32.6 GPa. These materials also show good fracture toughness values of 5.2 and 5.8 $MPa.m^{0.5}$ for Co_2B and CoO additives respectively.

XRD analyses of the mixed powders are shown in appendix C3, which confirm the presence of the added phases in the different mixtures. The position of the main peak for cobalt boride additive was at $2\Theta = 39.4°$, and that of cobalt oxide additive at $2\Theta = 37.3°$. The formation of boride secondary phase in the matrix after sintering (figures 4.22, and 4.23) was observed by XRD. Comparing the admixed powders with the hot pressed material, it was obvious that these additives reacted completely, thus oxidizing the B_6O to form the boride phase in the final composite.

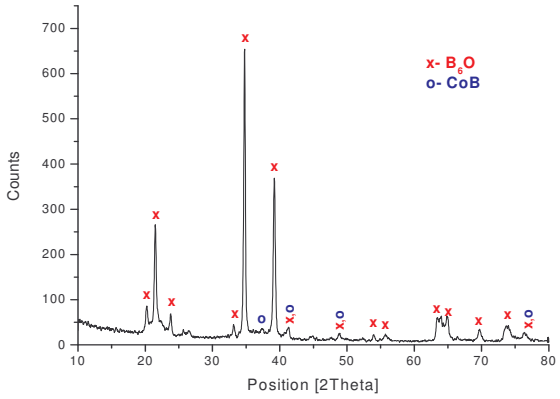

Figure 4.22: XRD pattern of sintered B_6O with Co_2B additive

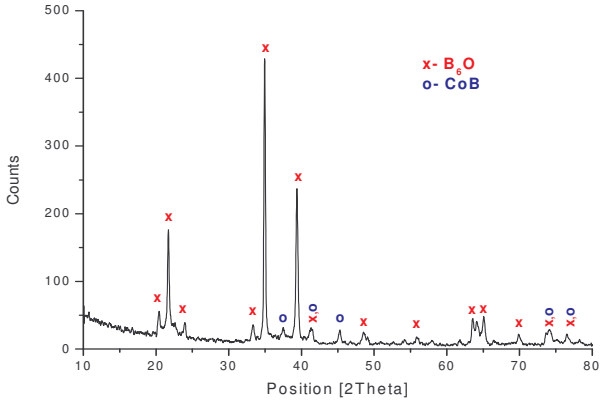

Figure 4.23: XRD pattern of sintered B_6O with CoO additive

The SEM images in figures 4.24 and 4.25 show that these materials display a homogeneous distribution of the secondary phase and EDX analyses reveal that the sintered materials have two phases (B_6O and the respective borides) with some pores retained in the sample which might be due to decomposition at the sintering temperature or pull-out of the softer secondary phase during grinding of the sample. At higher magnification, one can observe no grain growth in the hot pressed compact.

By comparing figures 4.24(a) and 4.25(b), it can be observed that the B_6O materials with cobalt oxide show a better (homogeneous) distribution of the boride secondary phase than the materials with cobalt boride. The reason for this observation could be a result of high degree of oxidation by this oxide. On the other hand, a good combination of hardness-to-fracture toughness properties was achieved for the B_6O materials with cobalt boride. Although the reason for these differences could not be established in this work, it is presumed that further optimization of the additive content and composition are needed to better understand the microstructure formation, mechanical properties and toughening mechanisms existing in these materials, thereby enhancing the probability of producing materials with better properties useful for industrial applications.

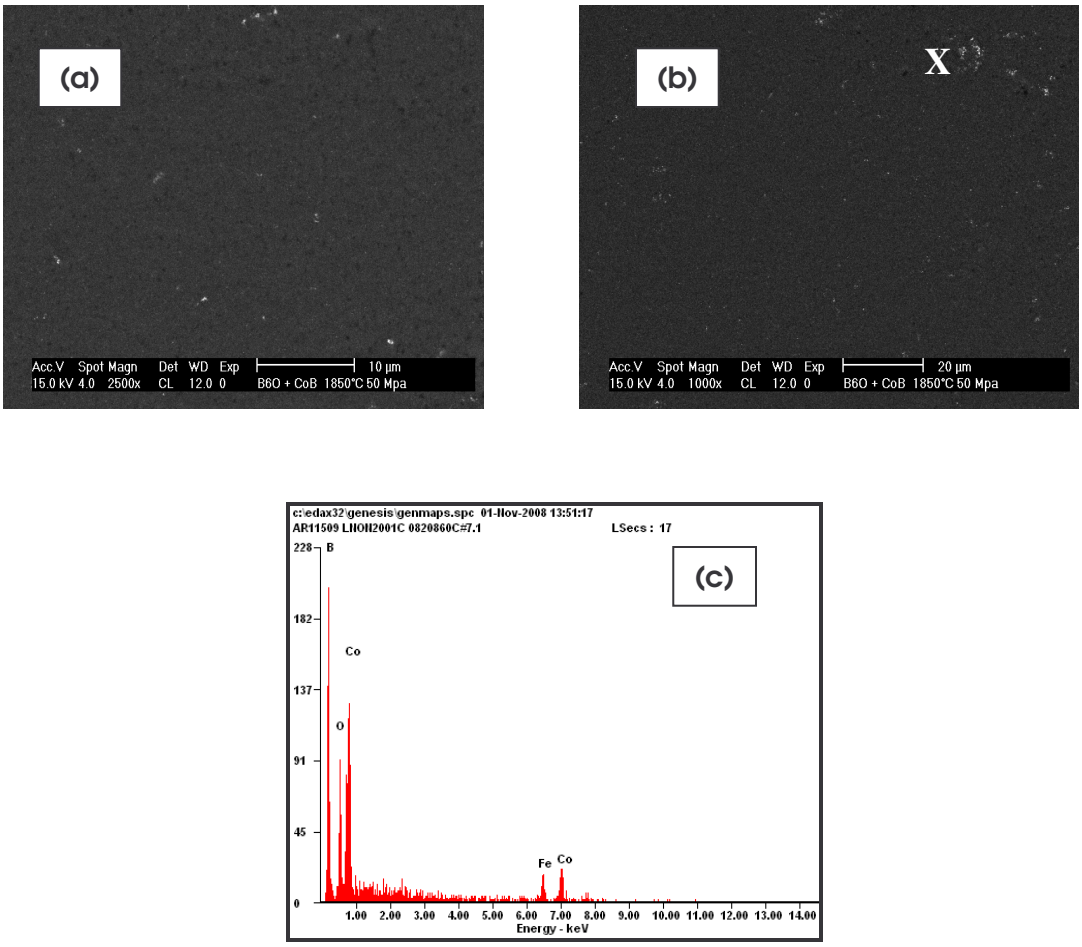

Figure 4.24: SEM image of B_6O + Co_2B sintered material. (a) *x*2500, (b) *x*1000, and (c) EDS of point 'X' at 1000 magnification.

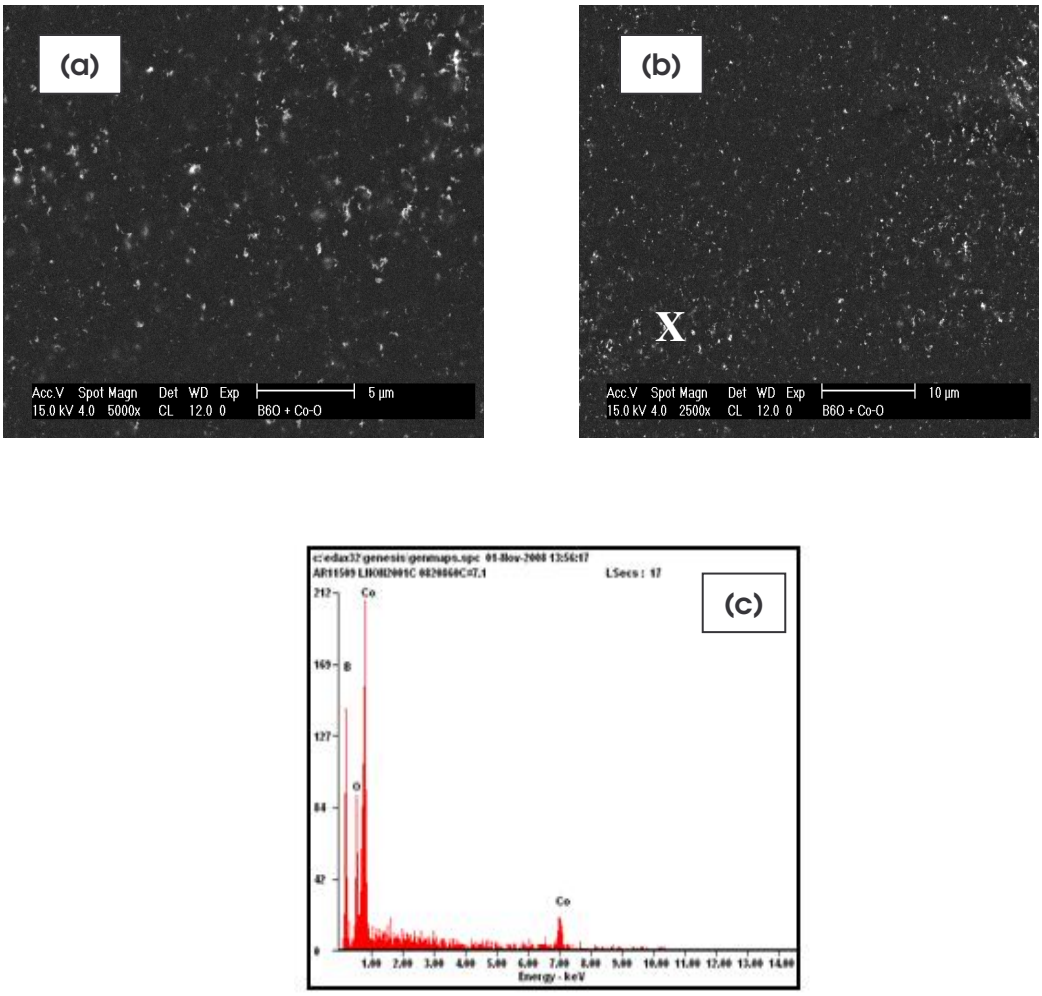

Figure 4.25: SEM image of B_6O + CoO sintered material. (a) *x*5000, (b) *x*2500, and (c) EDS of point 'X' at 5000 magnification.

4.4.5 B_6O with chromium compound

Having produced and obtained good combinations of properties for B_6O materials so far in this study, the concept of adding chromium compound was introduced. The only chromium compound used in this study was chromium boride (CrB_2). B_6O powder was mixed with CrB_2 and then sintered using the hot pressing profile

discussed in section 3.7 of chapter 3. CrB_2 was added in order to test the general effect on the mechanical properties of the sintered material.

Sub-micron B_6O powder was mixed with 1.7wt % of chromium boride and then sintered. The result of the mechanical properties obtained from this experiment is presented in table 4.8

Table 4.8: Density and mechanical properties of B_6O powder with chromium boride additive, hot pressed at 1800oC for 20minutes.

Materials	**Wt % of additive**	**Vol % of additive**	**Load (MPa)**	**Density (g/cm^3)**	**% Theo density**	**Open porosity (%)**	**Hardness, H_v (GPa)**	**Fracture toughness, K_{ic} ($MPa.m^{0.5}$)**	**Secondary phase**
$B_6O + CrB_2$	1.7	0.40	80	2.51	97.7	1.35	32.1 ± 1.6	4.5 ± 0.4	CrB_2

A density higher than 96% of the theoretical density was achieved. The high density achieved could be linked to the hot pressing temperature used which resulted in high amounts of liquid phase present to accelerate mass transport via liquid phase sintering. The Vickers hardness (Hv_1) value of 32.1 GPa measured for this composite shows a slight increase from that of the hot pressed B_6O (30.5 GPa), which could have been a result of the change in the load applied.

From the XRD patterns obtained it was discovered that the chromium boride (CrB_2) crystalline grain boundary phase was retained beside B_6O for both the mixed powder and the sintered compact. No variation of lattice constants for both B_6O and CrB_2 was observed, suggesting that neither formation of solid solution nor new compound was formed under the sintering conditions employed. The XRD pattern of the hot pressed composite is shown in figure 4.26.

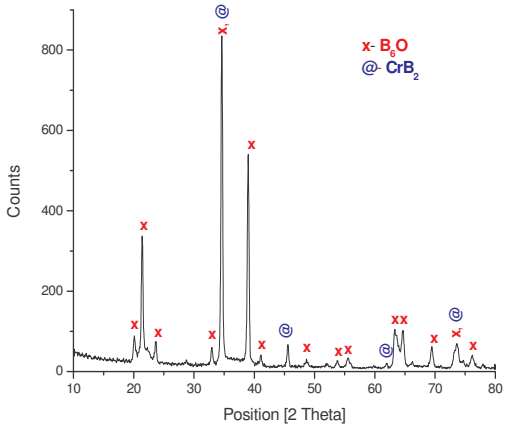

Figure 4.26: XRD pattern of sintered B_6O with CrB_2 additive

The SEM image in figure 4.27 shows that the secondary phase is not homogeneously distributed in the sintered material. EDX analyses revealed that the sintered material has two phases (B_6O and CrB_2) with some pores retained in the sample which might be due to decomposition at the sintering temperature or pull-out of the softer secondary phase during grinding of the sample. The CrB_2 is seen to form clusters around the grains of B_6O, therefore the hardness values obtained in this area having

CrB_2 clusters was low while the fracture toughness was high. At higher magnification no grain growth was observed in the hot pressed material. There are no differences in the distribution of the additives between the centre and the near surface area of the sintered materials. The addition of CrB_2 to boron suboxide powder resulted in a significant improvement in the fracture toughness considering the brittleness of B_6O material.

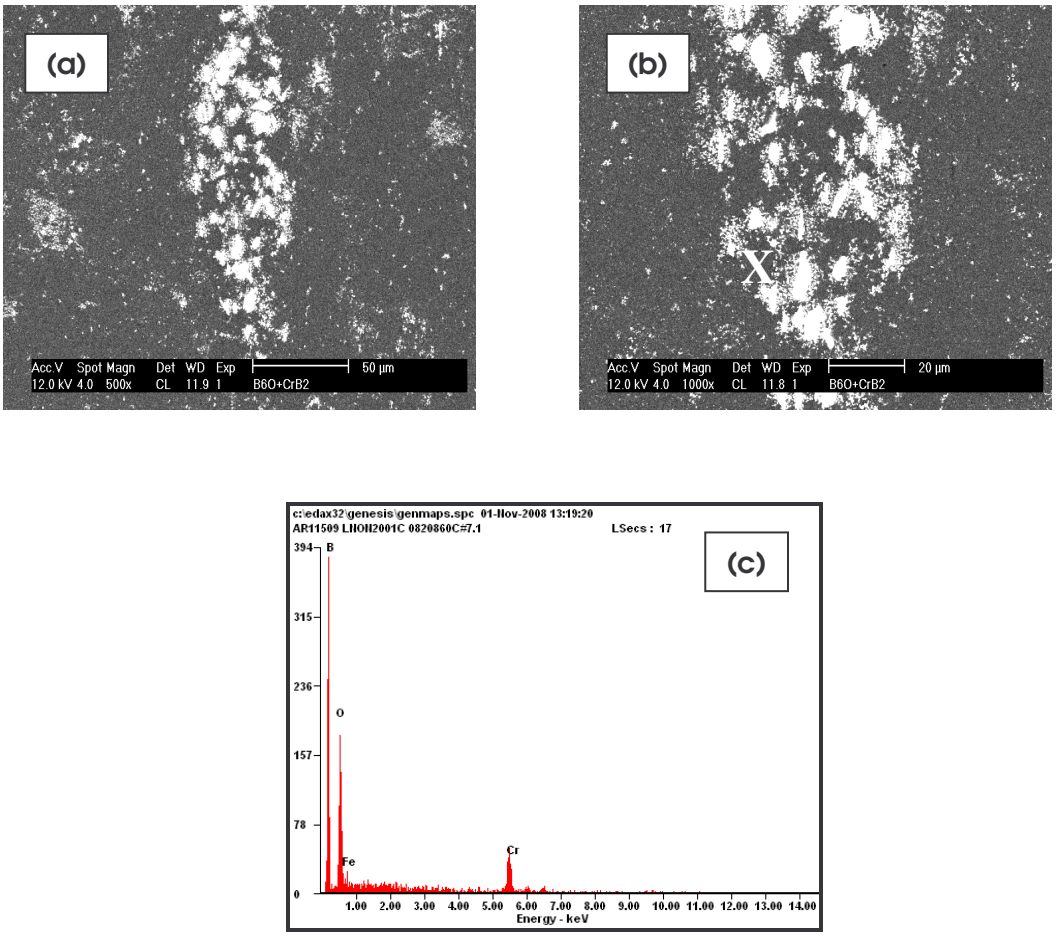

Figure 4.27: SEM images of B_6O + CrB_2 sintered material. (a) *x*500, (b) *x*1000, and (c) EDS of point 'X' at 1000 magnification.

Chapter Five

5 Discussions

5.1 Introduction

This chapter discusses the results presented in chapter four in terms of the relationship between sintering, densification, microstructure, and properties of the hot pressed materials.

5.2 Sintering, densification and microstructure of materials

Sintering has been defined as a processing technique used to produce density-controlled materials and components from metal or/and ceramic powders by applying thermal energy (Suk-Joong, 2005). It aims at producing sintered parts with reproducible and, if possible, designed microstructure through control of sintering variables such as grain size, sintered density and size and distribution of other phases including pores, in order to produce a fully densified body with a fine grain structure.

B_6O is a typically unsinterable material under normal pressure conditions. A fully densified compact of B_6O is difficult even applying high pressure sintering techniques such as hot pressing (Brodhag and Thévenot, 1986) and no appropriate sintering aid has been found. This is because B_6O is easily oxidized to form B_2O_3

with the mechanical strength of the resultant sintered compact degraded (Sasai et al., 2001). The degradation of mechanical properties by B_2O_3 has been corroborated by the work done by Andrews (2008). The presence of B_2O_3 also lowers the theoretical density of B_6O (Shabalala, 2007).

The theoretical densities of the hot pressed materials were calculated using the rule of mixtures (Appendix A2). Errors in these calculations are inevitable since the density of B_6O changes with oxygen and B_2O_3 content. The dependence of the theoretical density on the oxygen content ($\boldsymbol{x}$) in B_6O is shown in figure 5.1. The theoretical values in the figure were adapted from the International Centre for Diffraction Data (ICSD) card. It can be seen from the graph that the theoretical density increases with increasing oxygen content ($\boldsymbol{x}$). In this work, the theoretical density of B_6O has been assumed to be 2.55 g/cm^3, which corresponds to an oxygen content of 0.9. Therefore the determined value would be close to an upper limit of the density. It was also assumed that all the additives in the powder completely transformed to their respective secondary phase(s) after sintering. Another assumption made in the calculation of theoretical densities was the weight percentage of B_2O_3 (1 wt. %) which is present in the starting powder.

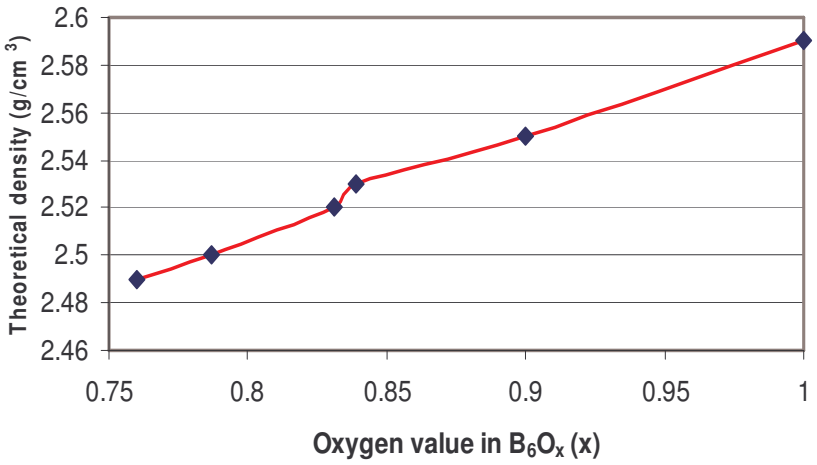

Figure 5.1: The dependence of the theoretical density on ***x*** in B_6O_x (ICSD Cards 81-2192, 87-2286, 87-2287, 87-2288 and 50-1505)

B_6O powders hot pressed either under vacuum or argon conditions at temperatures in the range of 1600°C- 1900°C, (Bairamashvili et al., 1979;, Kayhan and Inal 1999; Brodhag and Thévenot, 1986; and Shabalala, 2007), have produced B_6O materials with densities in the range of 85-97% of the theoretical density. This study produced a density of 2.45 g/cm^3 for pure B_6O, which was 95.3% of the theoretical density. The difference between the value obtained in this work and others is that the amount of porosity in the sintered material is very low. The SEM image of the hot pressed sample reveals some small holes representing porosity. It is possible that the small amount of B_2O_3, which may have volatilized at high temperatures, partly acts as the source of small pores in the microstructure (see appendix D). Part of the pores observed in the image may also have been caused by the removal of the remaining B_2O_3 during polishing or due to bad polishing. The density of the hot pressed B_6O

samples does not reach 100% theoretical. The theoretical density of B_2O_3 is 2.46 g/cm^3, which is less than that of B_6O at 2.55 g/cm^3; therefore a small amount of B_2O_3 in the samples will lower the overall theoretical density of a hot pressed B_6O sample. Figure 5.2 below shows the comparison of densities of hot pressed B_6O samples obtained from different studies.

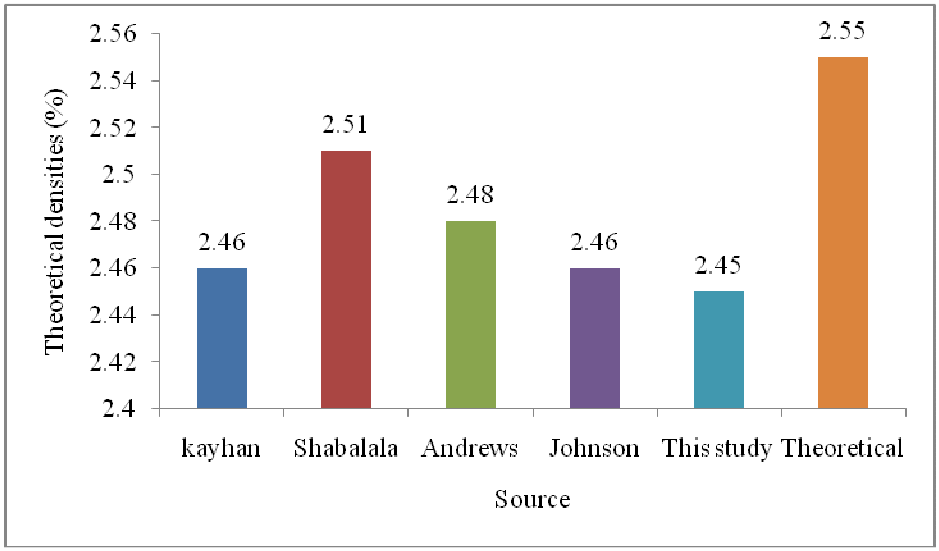

Figure 5.2: Comparison of densities of hot pressed B_6O samples obtained from different studies

The use of ultra-high pressures does not guarantee a completely dense B_6O compact. An ultra-high pressure high temperature study at pressures in the range of 3-5 GPa, by Itoh et al. (1998), did not produce fully densified materials. The density of the materials was reported to be above 95% theoretical. Petrak et al. (1974) claimed to have produced B_6O materials with densities greater than 99% of the theoretical via

reactive hot pressing. A fully dense B_6O material made by hot pressing, with a density of 2.60 g/cm^3, was reported by Goosey (1974), although this density is higher than the theoretical density.

B_6O powders were mixed with different additives (alkaline earth-metal oxide, nickel compounds, cobalt compounds, and chromium boride). These materials were hot pressed at 1850^{o}C for 20 minutes at loads of 50 and 80 MPa. The sintered materials resulted in higher densification as compared with that of pure B_6O hot pressed at 1900^{o}C, although a lower load was used for the pure B_6O. XRD patterns of the sintered materials show the formation of a boride secondary phase for calcium oxide, nickel compound, cobalt compound and chromium boride additives, a borate phase for magnesium oxide additive, and a carbide and boride phase for the $CaCO_3$ additive. The theoretical densities of the composites were calculated (Appendix A2) to ascertain the percentage densification obtained by the hot pressing process. It was assumed that all the additives in the powder completely transformed to their respective secondary phase(s) after sintering.

There are two possible explanations for the improvement in the densities obtained for the materials; one is that the additives form a liquid phase in which B_6O partially dissolves, and which assists with the densification of the materials at the sintering temperature and which recrystallizes during cooling to form the respective secondary

phase(s) at the grain boundaries as shown in the XRD patterns. On the other hand, the formation of B_2O_3 as a result of the oxidation reaction occurring in most cases between the B_6O and the sintering additives, suggest that a more liquid phase is formed, thereby improving the densification behaviour. Hence, a precise control of the oxygen content would be necessary for the reproducible densification of the materials.

Figure 5.3 shows the comparison of the percentage theoretical densities between sintered pure B_6O and sintered B_6O-alkaline earth metal oxide (CaO, MgO and $CaCO_3$).

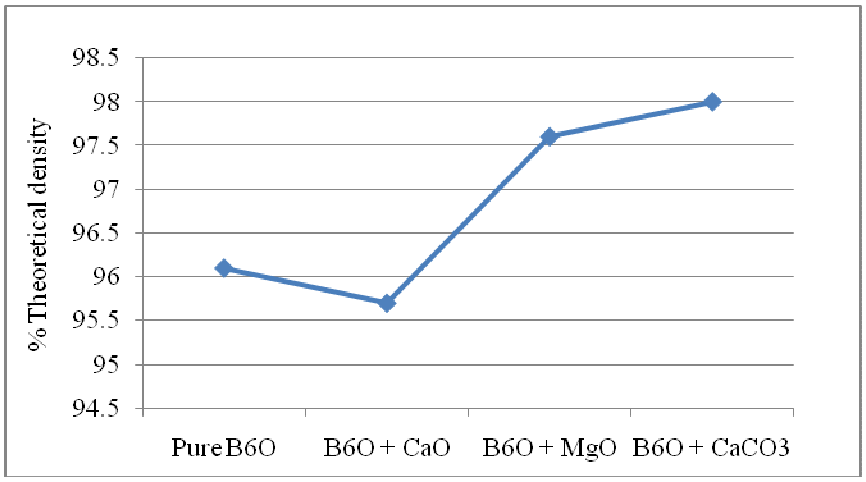

Figure 5.3: Comparison of the percentage theoretical density of sintered pure B_6O with the alkaline earth metal oxide additives.

The trend obtained and the observed microstructures are an indication that these composites are to some extent densified via liquid phase sintering. A sharp increase in densification was observed from the B_6O-CaO material to the B_6O-$CaCO_3$ material. This trend is in agreement with the SEM images of these materials shown in figure 5.4. The reactions for the alkaline earth metal oxide additive with B_6O powders after sintering, showing the products formed are shown in equations 5.1 and 5.2.

$$CaCO_3 \rightarrow CaO + CO_2 \uparrow \qquad [5.1]$$

$$4CaO + 5B_6O = 4CaB_6 + 3B_2O_3 \uparrow \qquad [5.2]$$

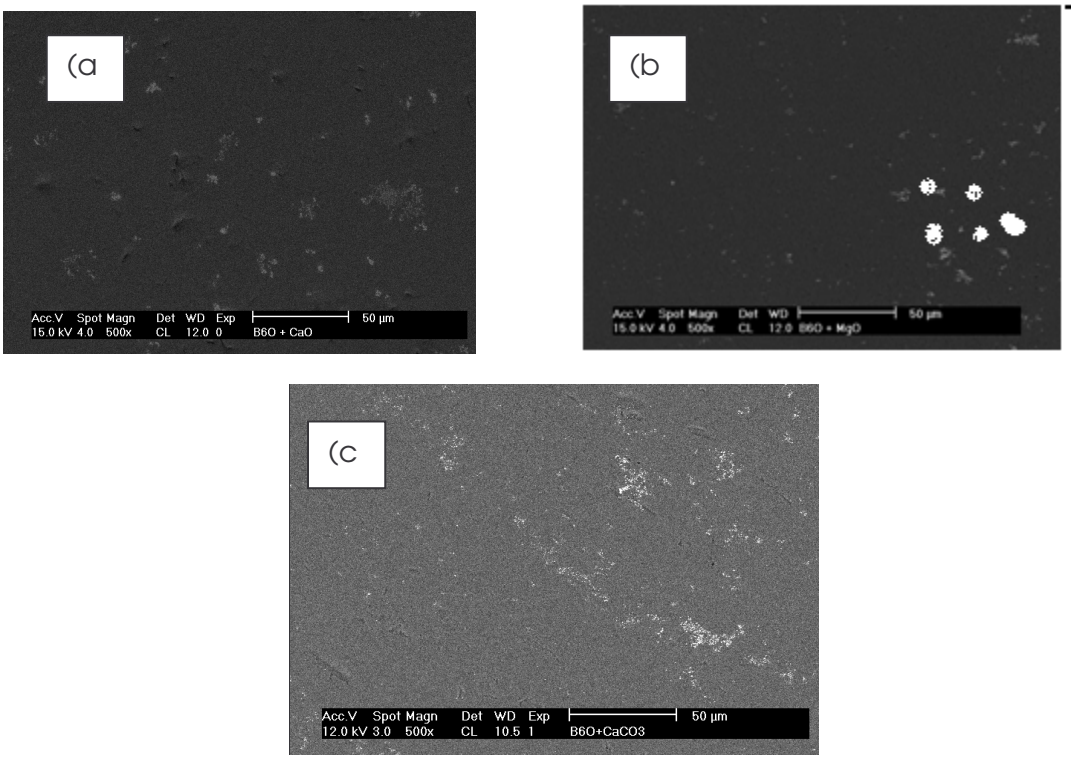

Figure 5.4: SEM images of sintered B_6O with alkaline-earth metal oxides (a) CaO (b) MgO and (c) $CaCO_3$

In B_6O-CaO materials, there was segregation (pockets) of liquid phase in the microstructure which might be as a result of poor mixing of CaO and B_6O powder under the mixing condition. This liquid tends to decompose at sintering temperature leaving pores within the material, which has a negative influence on the densification at such temperature.

In the B_6O-MgO material there was segregation of the secondary phase (Magnesium borate, $Mg_2B_2O_5$) within the matrix, although there was an increase in the density of the material. Two reasons can be attributed to this, one that the pressure applied (when compared with that of pure B_6O) is different, and the other can be understood from a thermodynamic point of view. To understand and properly explain the densification of this material, there is a need to consider the phase diagram of the MgO-B_2O_3-B_6O system. There is no known phase diagram for this system, but one can consider that of the MgO-B_2O_3 system. From figure 5.5, at the sintering temperature, there is enough liquid present which accelerates mass transport and therefore improves densification. The segregation could have been as a result of poor wettability of the MgO on B_6O (see appendix D figure D3). The oxidation reaction between the B_2O_3 and MgO resulted in the formation of a liquid phase, which re-crystallized during cooling and formed magnesium borate ($Mg_2B_2O_5$) at the grain boundaries.

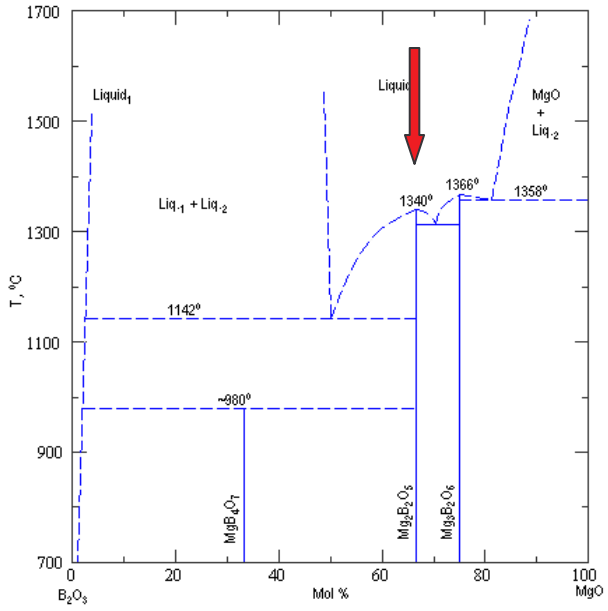

Figure 5.5: Phase diagram of MgO-B_2O_3 system. (ACerS-NIST phase equilibrium diagram, figure 93-028) The arrow indicate the material under consideration

For B_6O-$CaCO_3$ material, the pockets were seen as a cluster with an even distribution of the secondary phase. The microstructure also shows that this hot pressed material was nearly dense without any evidence of porosity. The pockets of the secondary phases in this microstructure were analyzed more closely using energy dispersive X-ray analysis (EDX) and were found to contain calcium with traces of iron. A backscattered SEM image of the sintered material (B_6O-$CaCO_3$) showing segregation of the grain boundary phase is shown in figure 5.6a while figure 5.6b shows the EDX spectrum of the glassy pocket.

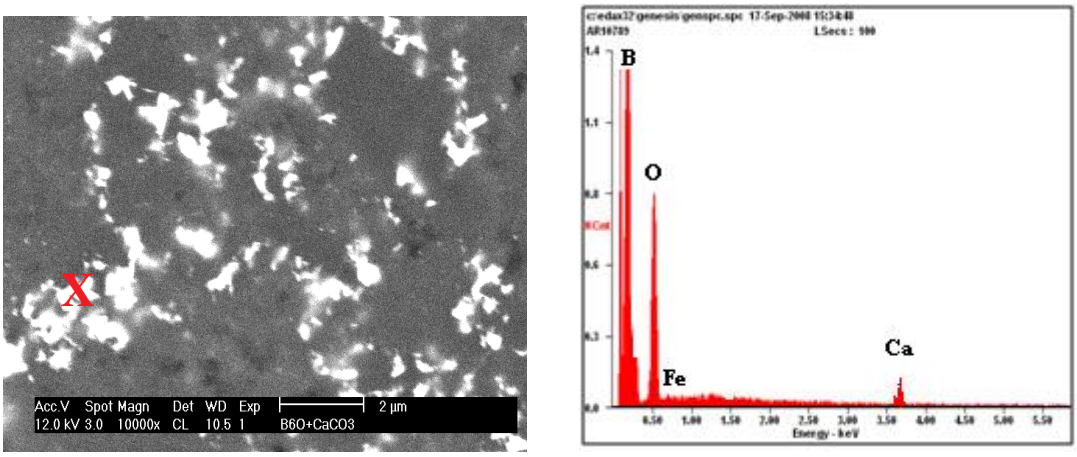

Figure 5.6: SEM image and EDX analysis of sintered B_6O-$CaCO_3$ material, (a) SEM image (b) EDX analysis of spot 'x' in the segregated region of the grain boundary phase.

For nickel and nickel compound additives, the phase diagram indicates that at the sintering temperature, there is enough liquid present to accelerate mass transport thus improving densification. Densities higher than 96% theoretical, (except for Ni additive at 95.8%, although higher than that of pure B_6O by 0.3%) were obtained. Although SEM images of these materials did not indicate homogeneous distribution of the nickel boride secondary phase within the matrix, yet the densification achieved differs in each material. The difference in the densification achieved is connected to the amount of B_2O_3 produced by the interaction of these additives with B_6O. With the assumption of 1 wt% of B_2O_3 in the starting powder, it was deduced (see equations 5.3 and 5.4) that more B_2O_3 was produced in the B_6O-Ni and B_6O-NiO materials, while a constant value was present in the B_6O-Ni_2B material, where there was no further formation of B_2O_3 through the interaction of B_6O and NiB.

$$16Ni + 3B_6O = 16NiB + B_2O_3 \uparrow \quad \textbf{[5.3]}$$

$$16NiO + 5B_6O = 16NiB + 7B_2O_3 \uparrow \quad \textbf{[5.4]}$$

From the above reactions, it is expected that the same mol% of additive (Ni or NiO) will produce the same volume of second phase after hot pressing (NiB), but for one (1) part by volume of B_2O_3 produced for the B_6O-Ni material, seven (7) parts by volume will be produced in the B_6O-NiO material. With the addition of 3.7 wt% Ni to the B_6O powder, 0.27 wt% B_2O_3 was produced, while 2.8 wt% NiO added resulted in the formation of 1.14 wt% B_2O_3 after sintering. This gives an indication of the higher amount of B_2O_3 in the B_6O-NiO material. The theoretical density of B_2O_3 is 2.46 g/cm^3, which is less than that of B_6O at 2.55 g/cm^3; therefore a small amount of B_2O_3 in the samples may lower the overall theoretical density. Theoretically, the presence of 1wt% B_2O_3 in the B_6O powder will cause a reduction of 0.4% in the density of the B_6O material.

Figure 5.7 represents the phase diagram of the Ni-B system while figure 5.8 shows the comparison of the percentage theoretical density of sintered pure B_6O with nickel and nickel compound additives.

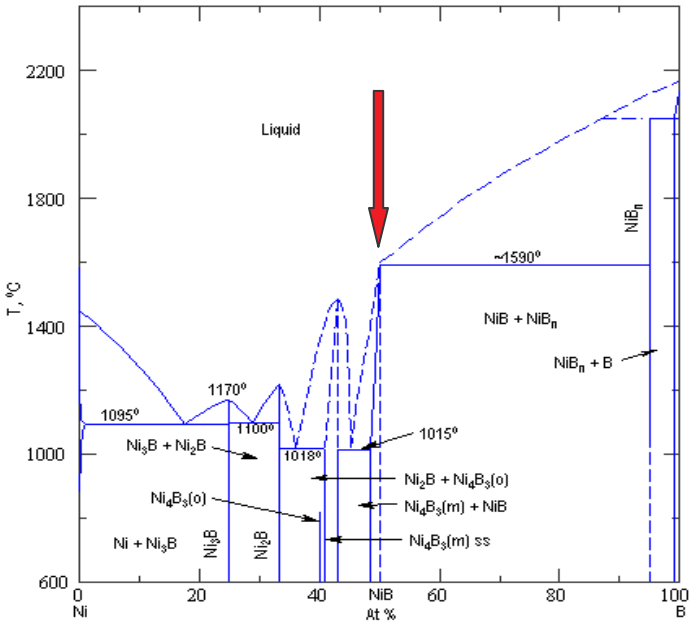

Figure 5.7: Phase diagram of the Ni-B system (ACerS-NIST phase equilibrium diagram, figure 08814). The arrow represents the composite under consideration.

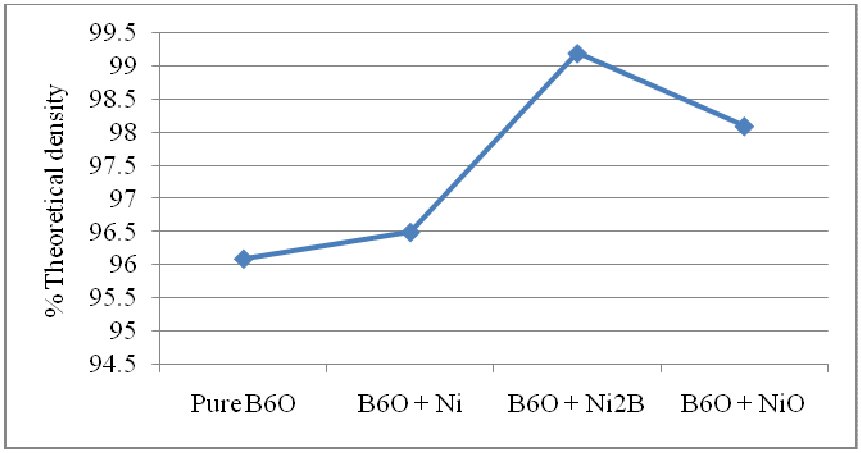

Figure 5.8: Comparison of the percentage theoretical density of sintered pure B_6O with nickel and nickel compound additives.

The phase diagram of the Co-B system is shown in figure 5.9. The composition under consideration has been indicated with an arrow. According to the phase diagram, at 1850^{o}C there is a liquid phase formed, which accelerates mass transport and therefore improves densification. Hence, densities of more than 97% of the theoretical densities were achieved. By comparison, the cobalt containing materials had higher densification than the pure hot pressed B_6O. However, the high amount of B_2O_3 in the system can also have had a negative effect on the densification because of its high vapour pressure resulting in some decomposition of the materials.

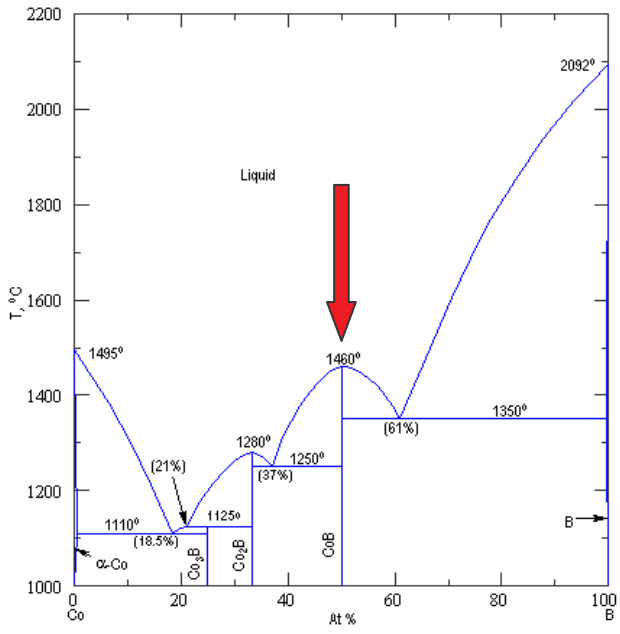

Figure 5.9**:** Phase diagram of Co-B system (ACerS-NIST phase equilibrium diagram, figure 08803). The arrow represents the composite under consideration.

B_6O material mixed with cobalt compound (cobalt boride and cobalt oxide) was also studied. The melting of cobalt-boron in the starting powder took place below 1500°C, which was far below the sintering temperature, suggesting that there was enough liquid phase present to accelerate mass transport thus improving densification. Hence, a nearly fully densified material was achieved. During heating, the oxide decomposed into cobalt boride (CoB) liquid at the grain boundaries, and B_2O_3, evaporated as described in equation 5.5.

$$16CoO + 5B_6O = 16CoB + 7B_2O_3 \uparrow \qquad [5.6]$$

The combination of properties obtained for this material suggest that if this material is suitably prepared and optimized, it could be potentially used in cutting tool and other wear part applications in industry.

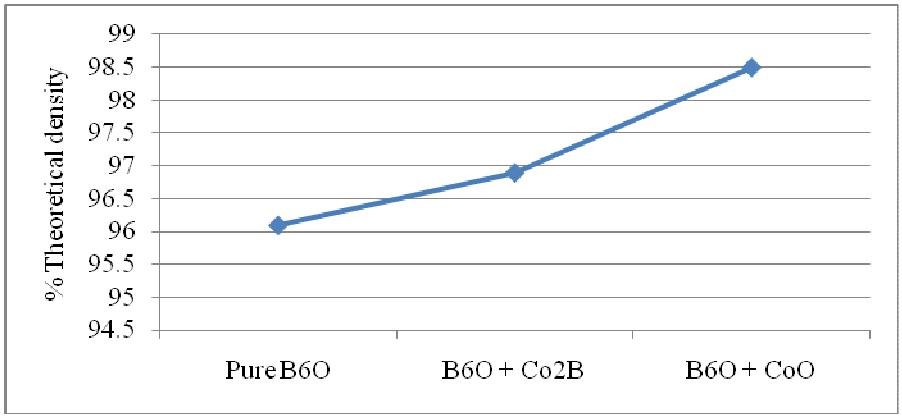

Figure 5.10: showing the comparison of the percentage theoretical density of pure B_6O with cobalt compound additives.

The influence of Chromium boride additive on densification was also studied. The phase diagram of the Cr-B system is shown in figure 5.11. The type of chromium boride (CrB_2) form was identified with the XRD pattern shown in figure 4.10, which gives an indication of the composition under consideration (see arrow in figure 5.11). According to the phase diagram, at 1850°C there will not be any liquid present in the material at sintering temperature. Nevertheless, there is some level of solubility of B_6O in the system resulting in the formation of transient liquid or it could be that the composition is not pure CrB_2 and therefore a liquid is formed which lowers the melting point in this system, creating enough liquid for densification to occur via liquid phase sintering.

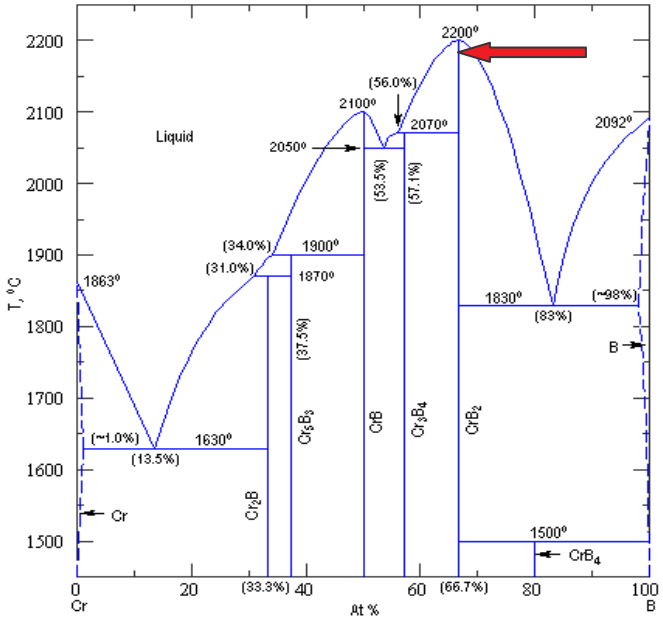

Figure 5.11: Phase diagram of Cr-B system (ACerS-NIST phase equilibrium diagram, figure 08865a). The arrow represents the composite under consideration.

Density of more than 95% of the theoretical density was achieved. A higher densification was observed. SEM micrographs of the sintered material revealed a non-homogeneous distribution of the boride secondary phase within the matrix (see figure 5.12). At higher magnification some dark spots which represent pull-out of the binder phase were observed; these were formed as a result of the incomplete polishing of the material. Since B_6O is a superhard material, it requires a long polishing time to obtain a scratch free surface after grinding.

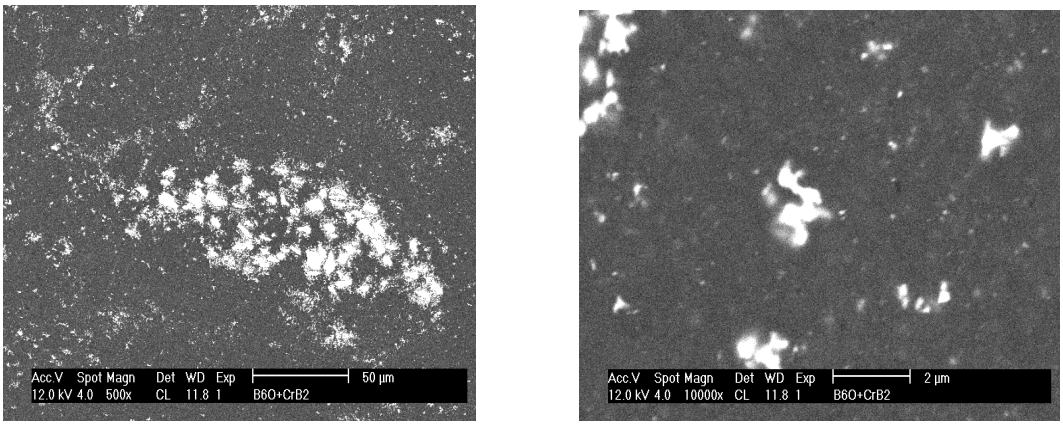

Figure 5.12: SEM images of sintered B6O with CrB_2 additive at different magnifications.

5.3 Microstructure and hardness of materials

The hot pressing profile for pure B_6O has been described in section 3.7 of chapter 3. A Vickers hardness of 30.5 ± 2.1 GPa was obtained with a load of 1kg (1000g). A B_6O single crystal (100µm) grown at a pressure of 5.5 GPa was reported to have a Vickers microhardness of 45 GPa under a load of 100g (Duanwei et al., 2002).

A comparison of hot pressed pure B_6O samples made by other authors is shown in figure 5.13. Although the Vickers hardness (30.5 GPa) of the B_6O sample measured in this study seems to be lower when compared with the 38 GPa (100g load) obtained by Holcombe et al., (1972), and the 34.8 GPa (500g load) by Shabalala (2007), and the 31-33 GPa (200g load) achieved by Itoh et al. (1998) at high pressures, a load of 1kg was used to indent the sample, which is 10 times and 2 times bigger than those of Holcombe et al., and Shabalala, respectively. The Vickers hardness value obtained in this study is also higher than those obtained by Andrews (2008) and Johnson (2008), even at the same load of 1kg. Also the Vickers hardness value obtained in this study is higher than the 30.4 GPa obtained via hot pressing by Petrak et al (1974).

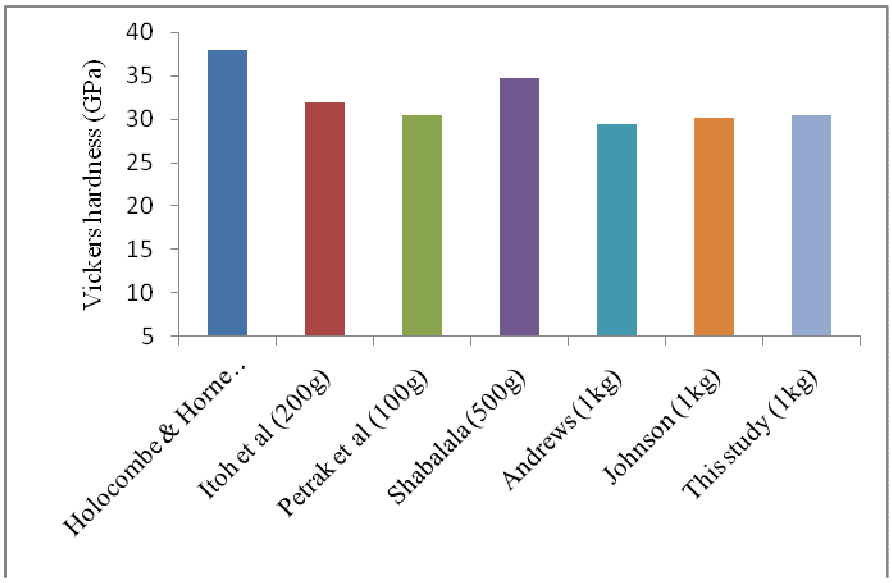

Figure 5.13: A comparison of hot pressed pure B_6O samples made by other authors with this study.

It should also be noted that the stoichiometry of the boron suboxide material (B_6O_x) made in this study might be different from those reported in other studies. Also, a variation of the sintering conditions in terms of temperature, pressure, time and atmosphere could affect the amount of porosity present which has a negative effect on hardness.

Figure 5.14 compares the Vickers hardness values of hot pressed B_6O-alkaline earth metal oxide materials produced by sintering at 1850^oC for 20 minutes. The measurements were taken under a load of 5kg. The hardness values obtained for the B_6O-alkaline-earth metal oxide sintered material were higher than that of the pure B_6O compact. The hardness value obtained for the alkaline-earth oxide shows a similar range as seen from the error bars. The variation in the hardness values obtained gives an indication of the intrinsic hardness values of the secondary phases formed after hot pressing.

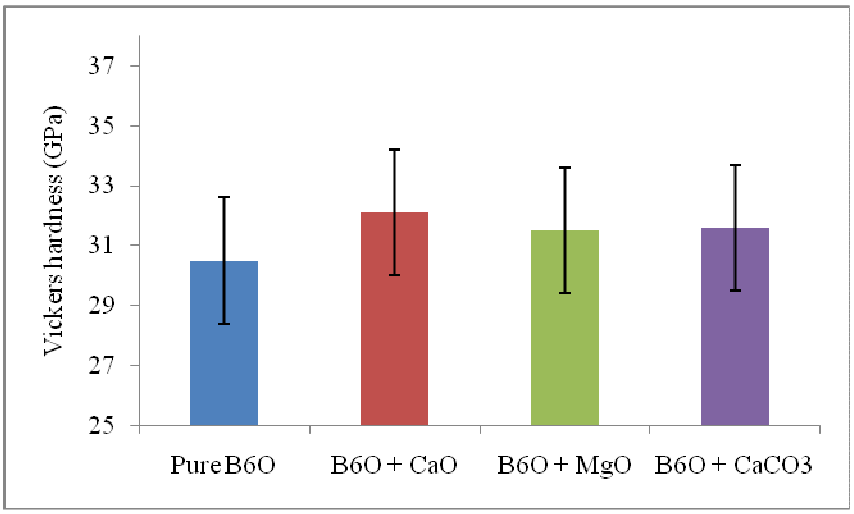

Figure 5.14: Comparison of the Vickers hardness values of hot pressed B_6O-alkaline earth metal oxide materials.

Although full densification was not achieved for these materials, the average hardness value obtained was encouraging. This also suggests that improvement of the densification of this group might result in better hardness values.

The hardness values obtained for the B_6O-Ni and B_6O-Ni_2B sintered materials were similar, except for that of the B_6O-NiO system which recorded a value of 27.1 GPa, which is less than that of pure B_6O. The reason could be connected to the formation of considerable B_2O_3 which might have volatilised at high temperature and/or the possibility that indentations could have been made on the segregated boride phase in the matrix with lower intrinsic hardness compared with B_6O. This is confirmed by the presence of pores at higher magnifications (see figure 5.15a). A typical indentation obtained during a Vickers hardness measurement, under a load of 5kg is shown in

figure 5.15b for a sample with 2.8 wt% NiO addition to the B_6O. Figure 5.16 gives a comparison between the hardness values obtained for B_6O-nickel and B_6O-nickel compound sintered materials. Although the absolute values of hardness measured differ, a similarity in hardness values were observed if one considers the error bars.

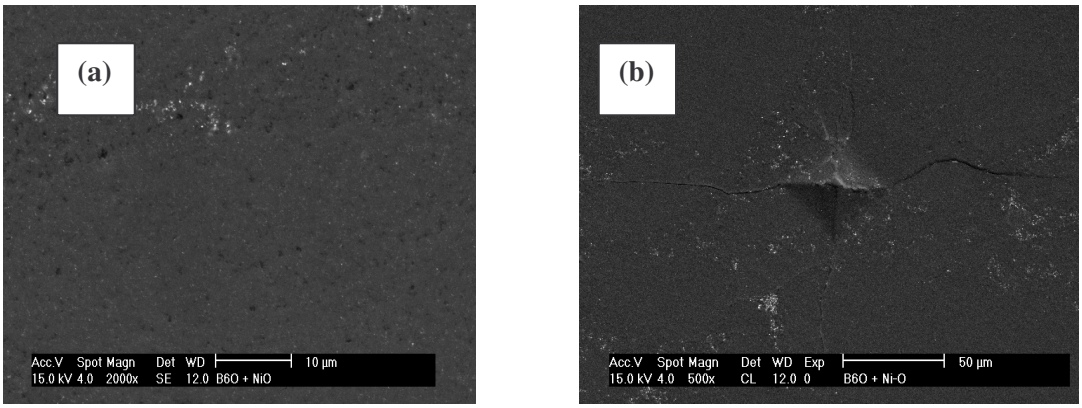

Figure 5.15: SEM image and typical indentation obtained for sintered B_6O-NiO material (a) SEM image (b) typical indentation obtained for this material.

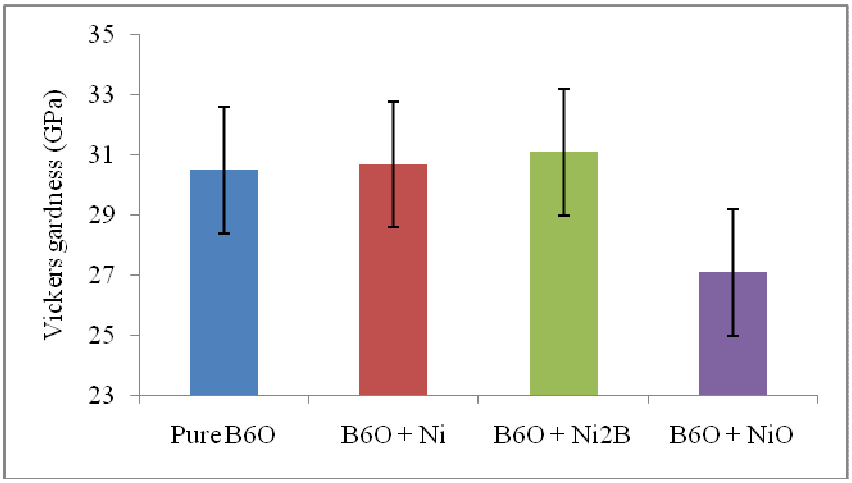

Figure 5.16: Comparison of the Vickers hardness values of hot pressed B_6O-nickel and B_6O-nickel compounds.

Hot pressed B_6O-cobalt compound materials produced good Vickers hardness values, ranging between 32.1 and 34.9 GPa. This could be connected to the homogenous distribution of the secondary phase (CoB) in these materials (see figure 5.18). Although porosity of 1.47% and 1.58% was retained in the hot pressed materials, the even distribution of indentations around the matrix and also at points which are B_6O-rich resulted in an overall high hardness value. It should be noted that full densification was not achieved for these materials, the average hardness values are higher than those of other groups of sintering additives used in this study. It suggests that improvement of the densification of this group might result in better hardness values. Figure 5.17 compares the Vickers hardness values obtained for sintered B_6O-cobalt compound materials.

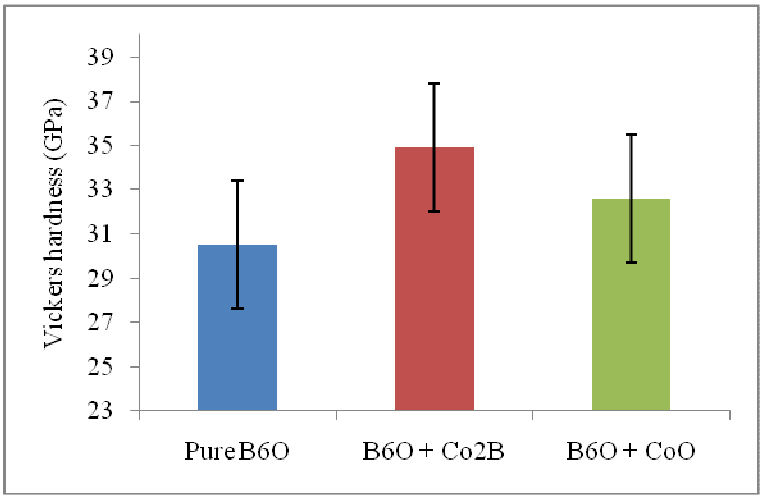

Figure 5.17: Comparison of the Vickers hardness values of hot pressed B_6O-cobalt compounds.

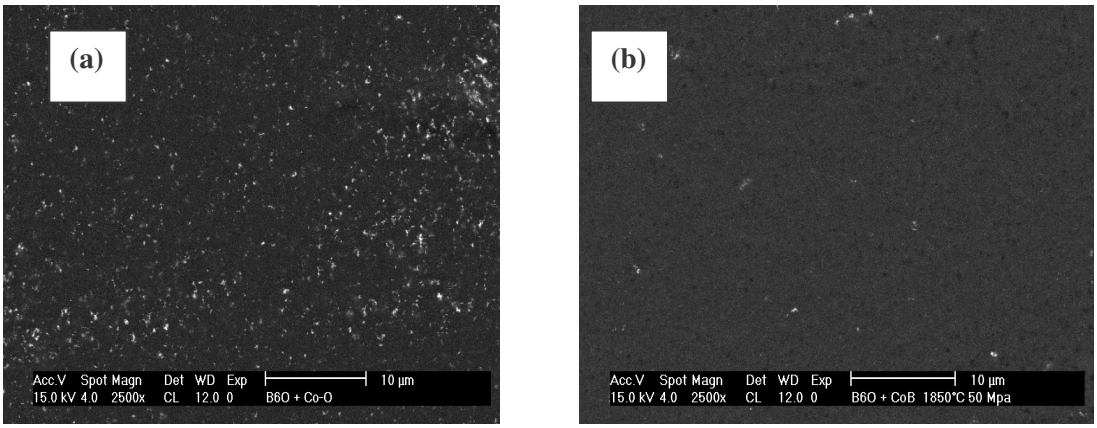

Figure 5.18: SEM image showing the distribution of the secondary phase in sintered B_6O with cobalt compound additives (a) CoO (b) Co_2B

Although the SEM image shows a non-homogenous distribution of the secondary phase in sintered B_6O-CrB_2 material, this material showed an increase in Vickers hardness value when compared with that of pure B_6O. The Vickers hardness increased from 30.5 GPa for the sintered pure B_6O to 32.1 GPa in sintered the B_6O-CrB_2 material. The reason for this increase might be as a result of the addition of CrB_2. Figure 5.19 gives a comparison between the Vickers hardness obtained for sintered pure B_6O and sintered B_6O-CrB_2 material.

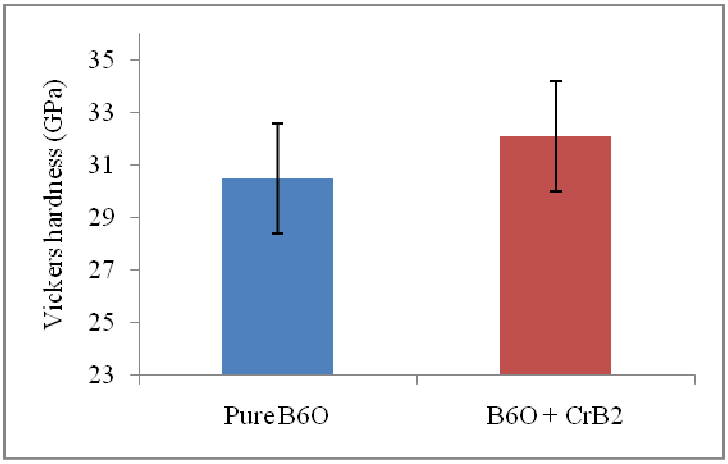

Figure 5.19: Comparison between the Vickers hardness obtained for sintered pure B_6O and sintered B_6O-CrB_2 material.

5.4 Microstructure and fracture toughness of materials

A single crystal of B_6O made at high pressures of between 3-5 GPa recorded a fracture toughness of 4.5 MPa.$m^{0.5}$ (Duanwei et al., 2002). Generally, a pure sintered B_6O compact is believed to be brittle. The reason for the very low toughness is not very clear. In this study during the course of hardness measurement on a sintered pure B_6O compact, on increasing the load above 1kg, the material showed a high scattering property with chipping during indentation. It was thus concluded that the material had low fracture toughness. It is not clear how fracture occurs in this material but there was some evidence of both intergranular and transgranular fracture. Fracture toughness values of sintered B_6O with additives reported in this study were measured using a load of 5kg.

Fracture toughness values obtained for the hot pressed B_6O-alkaline earth metal oxide material were 6.1, 6.1 and 6.8 MPa.m$^{0.5}$, for B_6O-$CaCO_3$, B_6O-MgO and B_6O-CaO materials respectively. The trend obtained showed a similar value. This shows a significant improvement in the fracture toughness considering the fact that the pure sintered B_6O compact is very brittle. Figure 5.20 gives a comparison of the fracture toughness obtained from the alkaline-earth metal oxide additives.

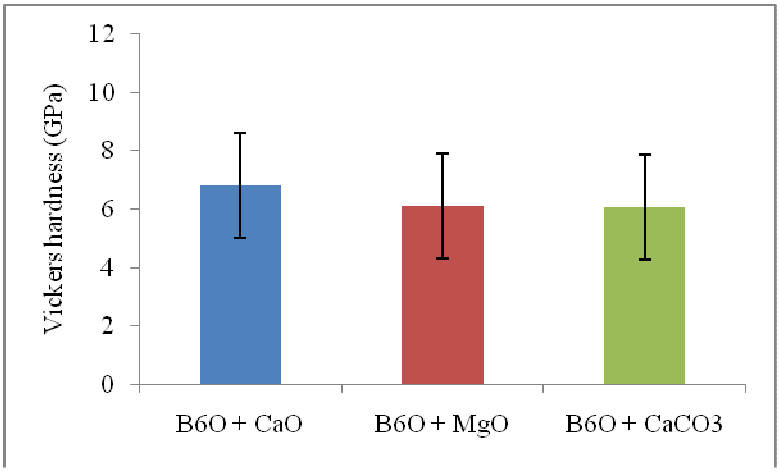

Figure 5.20: Comparison of the fracture toughness of sintered B_6O-alkaline-earth metal oxide materials.

SEM images of the crack propagation on the polished surfaces of sintered B_6O-alkaline earth metal oxide materials are shown in figure 5.21. A straight-line crack which cuts across the grains of B_6O was observed mainly in B_6O-CaO materials indicating a transgranular fracture mode. Crack deflection was observed in the B_6O-CaO and B_6O-$CaCO_3$ materials. It must be mentioned that not all cracks were deflected. The fractures were predominantly transgranular. The deflection observed

can be explained by the stresses that exist in the material. The B_6O matrix has a different thermal expansion coefficient (CTE) to the secondary phase(s). This could result in the formation of large internal stress when the material is cooled down from the sintering temperature.

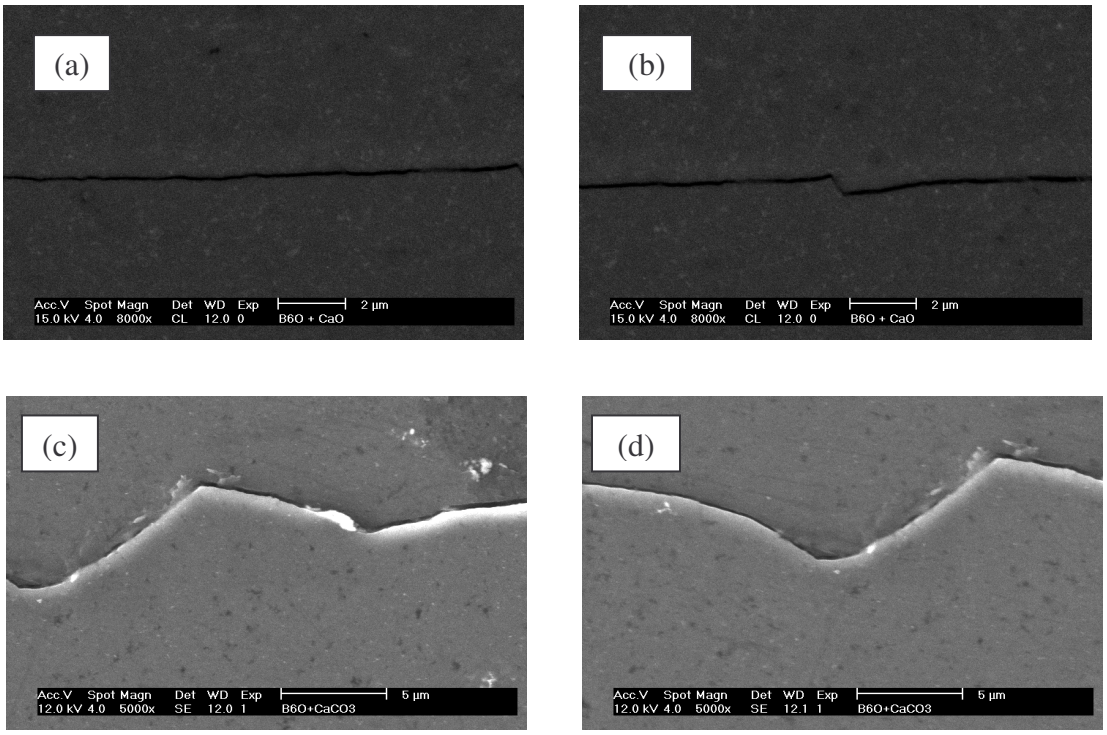

Figure 5.21: Indentation crack path on sintered B_6O-alkaline earth metal oxide materials (CaO = a & b; $CaCO_3$ = c & d)

Figure 5.22 shows the fracture toughness of the sintered B_6O-nickel and sintered B_6O-nickel compound material. The fracture toughness sharply increased with a small addition of each additive. The values obtained were 6.1, 6.4 and 6.5 $MPa.m^{0.5}$ for B_6O-NiO, B_6O-Ni and B_6O-Ni_2B additives respectively. This is due to the

similarity in grain sizes and grain boundary chemistry in the different hot pressed materials. When compared with the sintered pure B_6O compact, there were significant increases in fracture toughness. Although the secondary phase was not evenly distributed in these materials, as seen by the segregation of the boride phase, yet there was no evidence of grain growth observed.

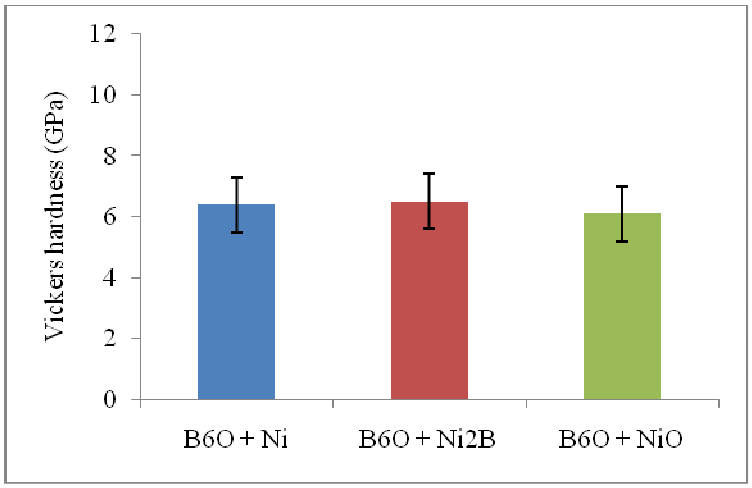

Figure 5.22: Comparison of the fracture toughness of sintered B_6O-nickel and sintered B_6O-nickel compound materials.

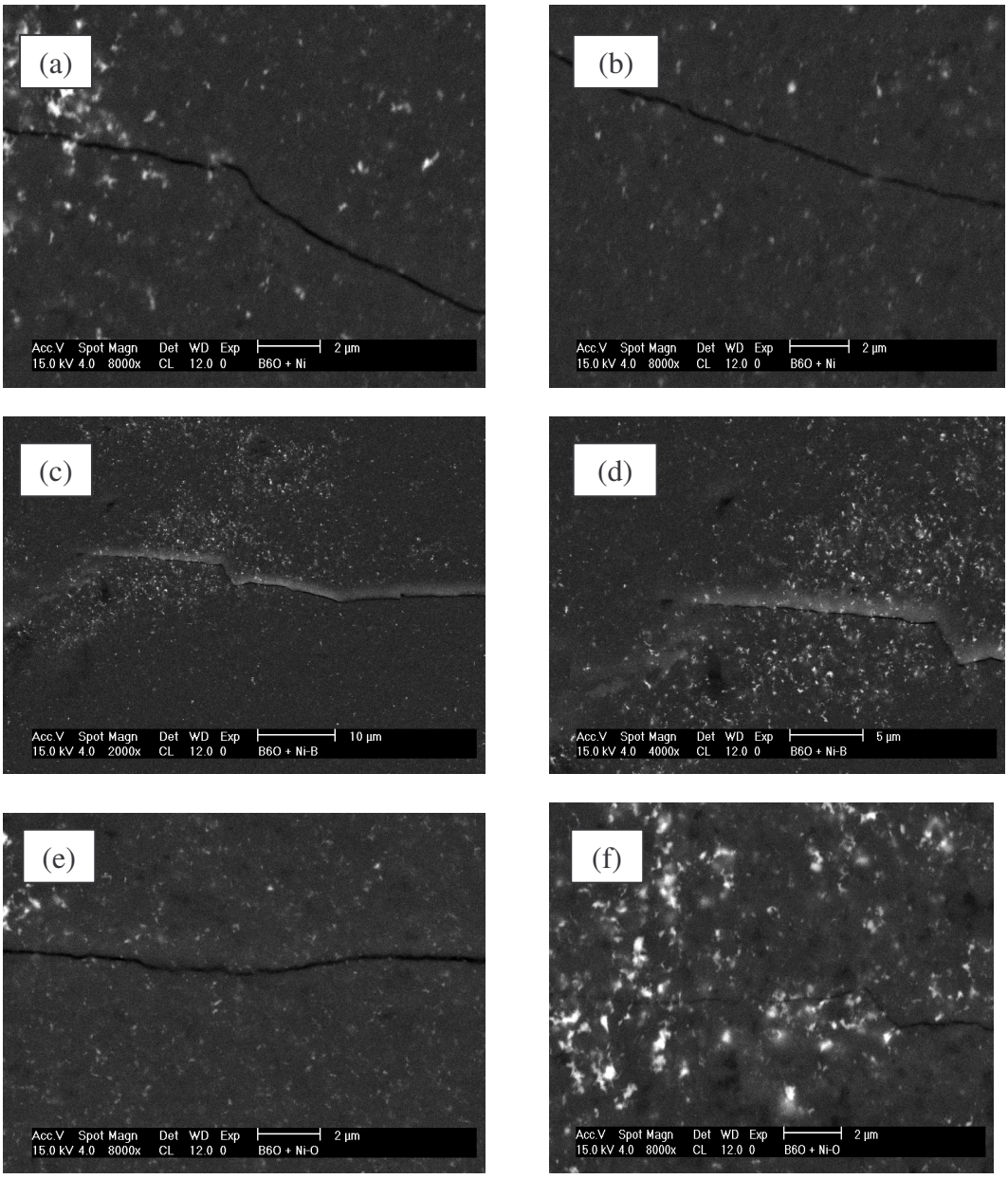

Figure 5.23: Indentation crack path on sintered B_6O-nickel and sintered nickel compound materials (Ni = a & b; Ni_2B = c & d; NiO = e & f)

Figure 5.23 shows the SEM images obtained for the various crack paths for the B_6O-nickel and nickel compound sintered materials. Crack deflections and bowing can be observed from the images (figure 5.23). Transgranular fractures were observed in the

sintered materials and in some cases cracks were deflected. This is an indication that the binding forces of grain boundary were so strong that cracks tended to advance transgranularly and could consume more energy. Bowing of propagating cracks could also be observed when the B_6O grain underwent compressive stresses. The presence of a twin boundary in B_6O crystals, which is a characteristic of boron compounds, can make major cracks deflect and branch, and also make the development of main cracks consume more energy. This consequently resulted in the high toughness of the materials.

An excellent combination of hardness and fracture toughness values were obtained in the B_6O-cobalt compound materials, 34.9 GPa and 5.2 $MPa.m^{0.5}$ and 32.6 GPa and 5.8 $MPa.m^{0.5}$, for B_6O-Co_2B and B_6O-CoO sintered materials respectively. Figure 5.24 shows a comparison of the two additives used.

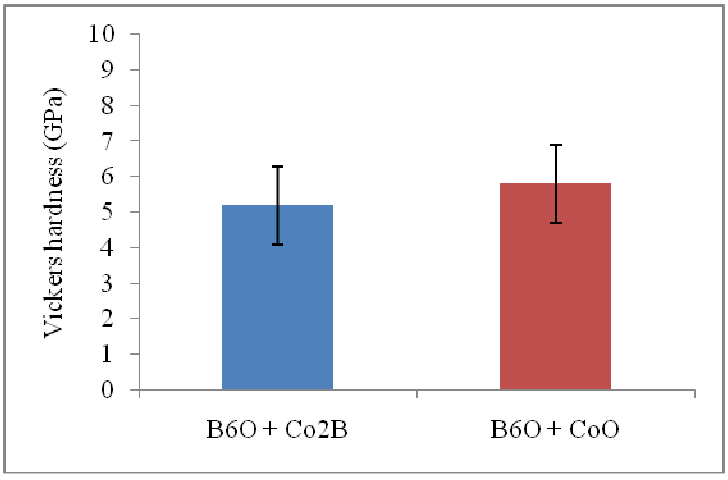

Figure 5.24: Comparison of the fracture toughness of sintered B_6O-cobalt compound materials.

SEM images showing the crack paths are shown in figure 5.25. The high fracture toughness measured in these composites was enhanced by a combination of fracture mechanisms. A combination of crack bridging and deflection caused by bimetallic stresses gave rise to high fracture toughness in the B_6O-CoO material.

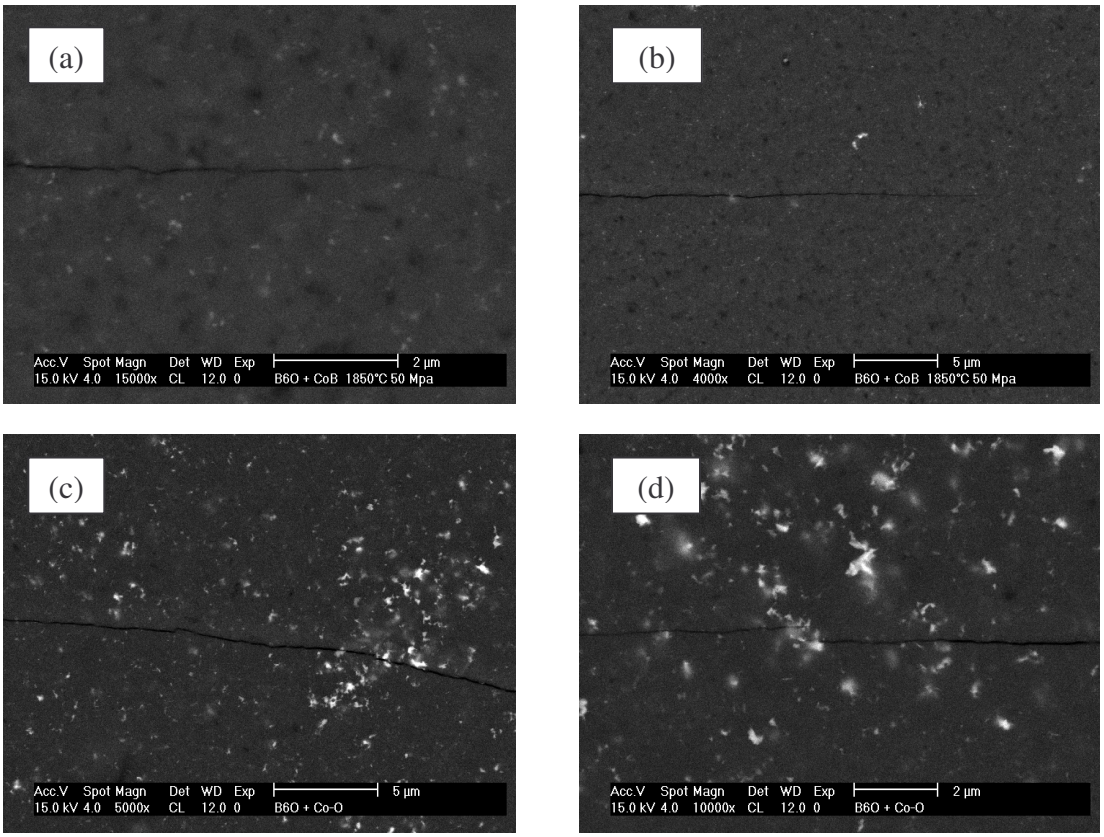

Figure 5.25: Indentation crack path on sintered B_6O-cobalt compound materials (Co_2B = a & b; CoO = c & d).

A good combination of hardness (32.1 GPa) and fracture toughness (4.5 $MPam^{0.5}$) was obtained when 1.7 wt% of CrB_2 was sintered. CrB_2 was formed at the grain boundaries. It is believed that the grain boundary composition increased the

toughness of this composite. The difference between the thermal expansion coefficients of the B_6O matrix and the chromium boride secondary phase induces a tangential compressive stress near the particle/matrix interface and diverts the crack around the particle. This makes the material tough. Figure 5.26 shows the crack paths in B_6O-CrB_2 sintered material.

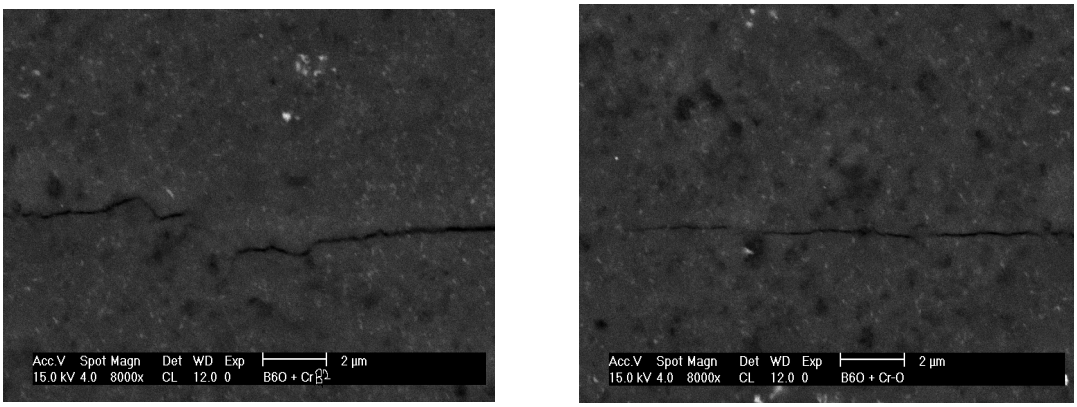

Figure 5.26: Indentation crack path on sintered B_6O-chromium boride materials.

The residual stress (σ) between B_6O and CrB_2 was estimated, using equation 5.7 [Liversage (2005), Jianxin (2000)], to be between 571-751MPa, assuming the change in temperature is about 1000°C.

$$\sigma = \left(\frac{(\Delta\alpha.\Delta T)}{[(1+\nu_m)/2E_m + (1-2\nu_s)/E_s]} \right) \qquad \textbf{[5.7]}$$

Where:

$\Delta\alpha$ = Difference in thermal expansion coefficient between B_6O ($\alpha_{B6O} = 5.5\times10^{-6}$ / $^oC^{-1}$ (Bairamashvili *et al.,*1979, Shabalala 2007) and the secondary phase, CrB_2 [$\alpha_{B6O} = 7.8\times10^{-6}$ / $^oC^{-1}$ (Johnson, 2008)].

ΔT = Change in temperature at which sufficient softening occurs to alleviate the stresses (~1000^{o}C)

$\nu_{m,s}$ = Poison ratios of B_6O (0.197) and CrB_2 [0.2 - 0.3]

$E_{m,s}$ = Elastic moduli of B_6O (540 GPa) and CrB_2 =211.04 GPa (www.memsnet.org)

The thermal expansion of cobalt boride (CoB) and nickel boride (NiB) is given as 7.24×10^{-6} / $^oC^{-1}$ & 12.3×10^{-6} / $^oC^{-1}$ (Borisov et. al 1987), which differs from that of B_6O ($\alpha_{B6O} = 5.5\times10^{-6}$ / $^oC^{-1}$ (Bairamashvili *et al.,*1979, Shabalala 2007). This differences also induces stresses in the final material. Fracture toughness enhancement via this mechanism is very common in ceramic materials. The effect of residual stresses on fracture toughness that result from the mismatch between the thermal expansion coefficients of the two components in ceramic materials, was also reported by Wahi and Ilschner (1980) and Bingqiang et al. (2007) in Al_2O_3-TiC composites, with Al_2O_3 as the matrix. Other studies include the SiC-TiC ceramic composites (Liversage 2005), the SiC_x/TiB_2 composites (Jianxin 2000) and SiC-AlN particulate composites (Pan *et al*., 1998).

A good combination of fracture toughness and hardness was obtained in this work. Fracture toughness has been enhanced by the introduction of secondary phases to the B_6O matrix with a slight reduction and considerable increase in hardness. The reason for the increase in fracture toughness could be due to many reasons such as crack deflection due to bimetallic stresses, or due to crack arrest in the secondary phase, or due to the solidification of the grain boundaries between B_6O particles being present as films or by many other mechanisms. The additives used had the potential of removing the B_2O_3 present at the surfaces of B_6O particles thereby forming other phases that cause bimetallic strain toughening at the grain boundaries.

A table showing the comparison of all the sintered materials is shown in appendix A1.

Chapter Six

6 Conclusions and recommendations

B_6O powders were milled in an attrition mill to reduce to particle sizes to submicron range. Optimum milling conditions were 20 hours milling time in propan-1-ol using 2.5 mm diameter steel balls. The average particle size obtained was 0.5 µm. Impurities introduced during milling were acid leached in HCl and the remaining impurities therein were quantified using chemical analysis (ICP-OES). The reduction in the particle sizes of B_6O before hot pressing improved the mechanical properties of the 'pure' hot pressed B_6O compacts.

The washed powders were dried in a rotavap. Some of the washed powders were admixed with different additives. B_6O powders were hot pressed with and without additives. Pure B_6O powder was hot pressed at a temperature of 1900^oC, 50 MPa, in an argon atmosphere while the mixed powders were hot pressed at a temperature of 1850^oC, with pressures from 50 – 80 MPa. The loads applied for pure B_6O and mixed powder were for 20 minutes.

The following conclusions were drawn from this work;

1. Dense pure B_6O sintered compacts (95% of theoretical) were achieved with an average hardness of 30.5 GPa using a load of 1kg. The hardness value

obtained is higher than that produced by Holocombe et al., (1972), Itoh et al., (1998), Petrak et al., (1974), Shabalala (2007), Andrews (2008) and Johnson (2008). The hardness is however less than that obtained by Kayhan and Inal (1999). They reported a fracture toughness of 8.5 MPa.$m^{0.5}$ for Al-doped B_6O composite using a load of 100g. It must be mentioned here that even before infiltrating B_6O with Al, the fracture toughness measured by Kayhan and Inal was very high (5.5 MPa.$m^{0.5}$) and does not corroborate the measured strength values. Additionally, they used a load of 100g whereas 5kg load was used in this work to measure fracture toughness. The wide variation of hardness values reported for B_6O is due to the different processing routes taken. The most obvious reasons for the variation in hardness values are differences in sintering temperature, pressure, impurities introduced during sintering, and sintering time. The fracture toughness was however low and agrees with what has been reported by other researchers (Itoh et al., [47] 2000; Sasai et al., 2001; Itoh et al., [83] 2000; Shabalala, 2007).

2. More than 96% of theoretical densities were achieved for B_6O sintered materials with additives at 1850^oC.

3. Good combinations of properties were achieved for all B_6O materials produced in this work (appendix A1), Vickers hardness ranging from 27.1 – 34.9 GPa and fracture toughness from 4.5 – 6.8 MPa.$m^{0.5}$. The fracture toughness improved with the addition of different additives which included alkaline-earth metal oxides, nickel and nickel compounds, cobalt compounds and chromium boride.

4. Fracture toughness was enhanced by the introduction of secondary phases to the B_6O matrix. The fracture toughness increase could be due to different mechanisms which include crack deflection due to bimetallic stresses, or due to crack arrest in the secondary phase, or due to the changes in the grain boundaries between the B_6O grains. The additives used had the potential of forming other phases that caused bimetallic strain toughening at the grain boundaries. Fracture toughness was mainly transgranular.
5. Fracture mechanism is not completely clear. Further work is necessary to understand the toughening mechanism.
6. Materials produced from Co_2B and CoO showed an excellent combination of properties (34.9 GPa and 5.2 MPa.m0.5 for Co_2B and 32.6 GPa and 5.8 MPa.$m0^{-5}$ for CoO) with homogeneous distribution of the secondary phase. This makes these materials potentially good candidates for ultrahard materials produced at low pressure.

In conclusion, the materials developed in this work are promising candidates for a new class of liquid phase sintered materials produced without ultrahigh pressure. Mixing with even a small amount of oxide additive resulted in a pronounced improvement in both the hardness and fracture toughness values. Properties obtained in this work are comparable to other hard materials used for cutting applications (e.g. amborite, DBC50 (Element Six) and Al_2O_3-TiC composite). Further optimization of

the additive content, composition, and mechanical properties are needed to better understand the microstructure formation and toughness mechanisms existing in the materials. This will allow fabrication of B_6O composite material for industrial applications such as cutting tool, drill bits, grinding wheels and abrasives.

References

ACerS-NIST phase equilibrium diagrams, NIST Standard References Database, Vol. 31, version 3.1.

Andrews A. (2008): "*Development of boron suboxide composites with improved toughness"* University of the Witwatersrand. PhD Thesis.

Andrews A., Hermann, M., Shabalala, T.C., Sigalas, I (2007): "Liquid phase assisted hot pressing of born suboxide-materials" Journal of the European Ceramic Society 28 (2008) 1613-1621.

Anstis, G.R., Chantikul, P., Lawn, B.R. and Marshall, D.B., *J. Am. Ceram. Soc*., Vol. 64, 1981, p. 533.

Badzain, A.R. (1988): "*Superhard material comparable in hardness to diamond*", Appl. Phys. Lett., Vol. 53, pp. 2495-2497.

Bairamashvili, I.A., Kalandadze, G.I., Eristavi, A.M., Jobava, J.S., Chotulidi, V.V. and Saloev, Y.L. (1979): "*An investigation of the physicomechanical properties of B_6O and SiB_4*", J. Less Comm. Met., Vol. 67, pp. 455-561.

Barry, I. (1999): "Synthesis of superhard icosahedral boron-rich solids", *Research experience for undergraduate,* http:/mrsec.la.asu.edu/outreach/reu/reu1999.

Binder, F. (1975): Radex-Rundschau, Refractory Metallic Hard Materials. Vol. 4, 531 - 537.

Bingqiang, L., Chuanzhen, H., Xinyu, L., Meilin, G. and Hanlian, L. (2007): "In situ growth of TiC whiskers in Al_2O_3 matrix for ceramic machine tools." *Ceramics International,* Vol. 33, pp.1475–1480.

Borisov Y.S, Kunitskii, Y.A, Korzhik, V.N, and Yaprakova, M.G (1986): "Structure and some physical properties of plasma-sprayed coatings of the nickel boride". Journal of powder metallurgy and metal ceramics, Vol. 25, pp. 966 – 969.

Brazhkin, V.V., Lyapin, A.G., and Hemley, R.J. (2002): Harder than diamond: dreams and reality, Philos. Mag. A., vol. 82, no. 2, pp. 231 – 253.

Brodhag, C. and Thévenot, F. (1986): "*Hot pressing of boron suboxide $B_{12}O_2$*", J. Less Comm. Met., Vol. 117, pp. 1-6.

Brookes, C.A (1986): Mechanical properties of cubic boron nitride- a perspective. Institute of Physics, Conference Series. Issue 75, pp 207-220.

Bundy, F.P., Hall, H.T, Strong, H.M and Wentorf, R.J. (1955): Man-Made Diamonds. Nature 176, 51 - 55.

Clarke, D.R. and Faber, K.T. (1987): "Fracture of ceramics and glasses." *Journal of Physics and Chemistry of Solids,* Vol. 48, pp. 1151-1157.

Cook, B.A., Harringa, J.L., Lewis, T.L. and Russell, A.M. (2000): "*A new class of ultrahard materials based on $AlMgB_{14}$*", Scripta Mater., Vol. 42, pp. 597-602.

Duanwei He, Yusheng Zhao, Daemen, L., Qian, J. and Shen, T.D. (2002): Boron suboxide: As hard as cubic boron nitride. Applied Physics Letters. vol. 81, No. 4, pp. 643-645.

Ellison-Hayashi, C., Emond, G.T. and Kuo, S.Y. (1995): "*Method of abrading with boron suboxide (B_xO) and the boron suboxide (B_xO) articles and composition used*", *5,456,735*, US Patent.

Ellison-Hayashi, C., Emond, G.T. and Kuo, S.Y. (1994): "*Abrasives material and method of removing material from surface*", *0 0621 327 Al*, EU Patent.

Ellison-Hayashi, C., Morteza, Z., and Frank, J. (1994): Boron suboxide material and method of preparation, US patent 5,330,937.

Ellison-Hayashi, C., Zandi, M., Murray, Csillag, F.J. and Kuo, S. (1992): "*Boron suboxide material and method for its preparation*", *5,135,895*, US Patent.

Ellison-Hayashi, C., Zandi, M., Shetty, D.K., Kuo, P., Yeckley, R. and Csillag, F. (1994): "*Boron suboxide material and method for its preparation*", *5,330,937*, US Patent.

Endo, T., Sato, T. and Shimada, M. (1987): "*High-pressure synthesis of B_2O with diamond-like structure*", J. Mater. Sci. Lett., Vol. 6, pp. 683-685.

Evans, A.G. (1972): The Strength of Brittle Materials Containing Second phase dispersions, *Philosophical Magazine*. Vol .26, pp. 1327-1344.

Evans, A.G. (1988): High Toughness Ceramics. *Materials Science and Engineering*, A105/106, pp. 65-75.

Gao, F., Hou, L. and He, Y. (2004): "*Origin of superhardness in icosahedral B_{12} materials*", J. Phys. Chem. B, Vol. 108, pp. 13069-13073.

Gao, F., Qin, X., Wang, L., He, Y., Sun, G., Hou, L. and Wang, W. (2005): "*Prediction of new superhard boron-rich compounds*" J. Phys. Chem. B, Vol. 109, pp. 14892-14895.

Garvie, L.A.J., Hubert, H., Petuskey, W.T., McMillan, P.F. and Buseck, P.R. (1997): "*High-pressure, high-temperature synthesis in the B-C-N-O system, II. Electron energy-loss spectroscopy (EELS)*", J. Solid State Chem., Vol. 133, pp. 365-371.

Gladkaya, I.S., Dyuzheva, T.I., Ekimov, E.A., Nikolaev, N.A. and Bendeliani, N.A. (2001): "*Crystal growth at high pressure and the problem of characterisation of the interstitial phases in the B-C-O system*", J. Alloys and Compds., Vol. 329, pp. 153-156.

Goosey B.F (1974): Method of fabricating boron suboxide articles. United State Patent - US 3816586.

Goosey, B.F. and Anderson, S.C. (1974): "*Method of fabricating boron suboxide articles*", *3,816,586*, US Patent.

Hall, H.T. and Compton, L.A. (1965): "*Group IV analogs and high pressure, high temperature synthesis of B_2O*", Inorg. Chem., Vol. 4, pp. 1213-1216.

Hansson, T., Warren, R. and Wasen, J. (1993): Fracture anisotropy and toughening mechanisms of a hot-pressed alumina reinforced with silicon carbide whiskers, Journal of the American Ceramic Society, vol. 76, pp. 841-848.

He, D., Akaishi, M., Scott, B.I. and Zhao, Y. (2002): "*Growth of boron suboxide crystals in the B-B_2O_3 system at high pressure and high temperature*", J. Mater. Res., Vol. 17, pp. 284-290.

He, D., Zhao, Y., Daemen, L., Qian, J., Shen, T.D. and Zerda, T.W. (2002): "*Boron suboxide: As hard as cubic boron nitride*", Appl. Phys. Lett., Vol. 81, pp. 643-645.

Hoard, J.L., Sullenger, D.B., Kennard, G.H.L. and Hughes, R.E. (1970): "*The structure analysis of β-rhombohedral boron*", J. Solid State Chem., Vol. 1, pp. 268-277.

Holcombe, Jr., Cressie, E., Horne, Jr., and Ottis J.H. (1972): Method for preparing boron suboxide. . United State Patent- US 3 660 031.

Holleck, H. (1986): J. Vac. Sci. Technol. A4, 2661.

Hubert, H., Devouard, B., Garvie, L.A.J., O'Keeffe, M., Buseck, P.R., Putuskey, W.T. and McMillan, P.F. (1998): "*Icosahedral packing of B_{12} icosahedra in boron suboxide (B_6O)*", Nature, Vol. 391, pp. 376-378.

Hubert, H., Garvie, L., Devouard, B., Buseck, P., Petuskey, W., and McMillan, P. (1998): *Chemistry of materials*, vol. 10, pg 1530-1537.

Hubert, H., Garvie, L.A.J., Devouard, B., Buseck, P.R., Petuskey, W.T. and McMillan, P.F. (1996): "*High-pressure, high-temperature synthesis and characterisation of boron suboxide (B_6O)*", Chem. Mater., Vol. 10, pp. 1530-1537.

Itoh, H., Maekawa, I. and Iwahara, H. (1998): "*High pressure sintering of B_6O powder and properties of the sintered compact*", J. Soc. Mat. Sci., Vol. 47, pp.1000-1005.

Itoh, H., Maekawa, I. and Iwahara, H. (2000): "*Microstructure and mechanical properties of B_6O-B_4C sintered composites prepared under high pressure*", J. Mat. Sci., Vol. 35, pp. 693-698.

Itoh, H., Yamamoto, R. and Iwahara, H. (2000): "*B_6O-c-BN composite prepared by high pressure sintering*", J. Amer. Ceram. Soc., Vol. 83, pp. 501-506.

Itoh, H (2004): Preparation of Superhard Ceramic Materials and Evaluation of their Mechanical Properties. *Journal of the Ceramic Society of Japan*, vol. 112, pp. 121-129.

Jianxin, D. (2000): Effect of thermal residual stress on the high temperature toughening behaviour of TiB_2/SiC composites." *Journal of Materials Processing Technology*, Vol. 98, pp. 292-298.

Johnson, O. T (2008): "*Improvement on the mechanical properties of boron suboxide (B_6O) based composites using other compounds as second phase"*. University of the Witwatersrand. MSc Dissertation.

Kayhan, I.O. and Inal, O.T. (1999): "*Synthesis of aluminium infiltrated boron suboxide drag cutters and drill bits*", J. Mater. Sci., Vol. 34, pp. 4105-4120.

Kharlamov, A.I., Kirillova, N.V., Loichenko, S.V. and Kostyuk, B.D. (2002): "*Properties of boron suboxide $B_{13}O_2$*", Powder Metall. Metal Ceram., Vol. 41, pp. 97-106.

Kleebe, H. J, Lauterbach, S., Shabalala, T.C., Hermann, M., Sigalas, I (2008): "B_6O: A correlation between mechanical properties and microstructure evolution upon Al_2O_3 addition during hot pressing" J. Am. Ceram. Soc., 91 [2] 569-575 (2008)

Kobayashi, M., Higashi, I., Brodhag, C. and Thévenot, F. (1993): "*Structure of B_6O boron suboxide by Rietveld refinement*", J. Mater. Sci., Vol. 28, p. 2129.

Kurisuchiyan, E., Jiyooji, T.E. and Shii, R.K. (1995): "*Grinding by using composition containing boron suboxide*", *7,034,063*, Japan Patent.

Lange, F. F. (1970): Interaction of a Crack front with a Second phase Dispersion, *Philosophical Magazine*, vol .22, pp. 983-992.

Lee, F., Sandlin, M.S. and Bowman, K.J. (1993): Toughness anisotropy in textured ceramics, Journal of the American Ceramic Society, vol. 76(7), pp. 1793-1800.

Lee, S., Kim, S.W., Bylander, D.M. and Kleiman, I. (1991): "*Crystal structure, formation enthalpy, and energy bands of B_6O*", Phys. Rev. B, Vol. 44, pp. 3550-3554.

Liu, X., Zhao, X., Hou, W. and Su, W. (1995): "*A new route for the synthesis of boron suboxide (B_7O)*", J. Alloys and Compds., Vol. 223, pp. L7-L9.

Liversage, J.H (2005): "An enhancement of the mechanical properties in functionally graded liquid-phase SiC-TiC ceramic composites". *PhD Thesis*, University of Witwatersrand.

Lundström, T. (1997): "*Structure and bulk modulus of high-strength boron compounds*", J. Solid State Chem., Vol. 133, pp. 88-92

Lundström, T. and Andreev, Y.G (1996): "*Superhard boron-rich borides and studies of the B-C-N system*", Mater. Sci. and Eng. A, Vol. 209, pp. 16-22.

Lundström, T. and Bolmgren, H. (1994): "11th international symposium on boron, borides and related compounds", [ed.] Higashi, I. and Uno, R. Vol. 10, p. 1.

Makarov, V.S. and Ugai, Ya. A. (1986): Thermochemical study of boron suboxide B_6O. *Journal of the Less-Common Metals*, vol. 117, pp. 277-281.

Masago, A., Sharai, K. and Katayama-Yoshida, H. (2006): "*Crystal stability of α- and β-boron*", Phys. Rev. B, vol. 73, 104102.

McMillan, P.F., Hubert, H., Chizmeshya, A., Petuskey, W.T., Garvie, L.A.J. and Devouard, B. (1999): "*Nucleation and growth of icosahedral boron suboxide clusters at high pressure*", J. Solid State Chem., Vol. 147, pp. 281-290.

Meguid, S. A. (1996): Mechanics and Mechanisms of Toughening of Advanced Ceramics. *Journal of Materials Processing Technology*, vol. 56, pp. 978-989.

Nieto-Sanz, D., Loubeyre, P., Crichton, W. and Mezouar, M. (2004): "*X-ray study of the synthesis of boron oxides at high pressure: Phase diagram and equation of state*", Phys. Rev. B, Vol. 70, pp. 214108-6.

Olofsson, M. and Lundström, T. (1997): "*Synthesis and structure of non-stoichiometric B_6O*", J. Alloys and Compds., Vol. 257, pp. 91-95.

Pan, **Y.B**., Qiu, J.H., Morita, M., Tan, S.H. and Jiang, D. (1998): "The mechanical properties and microstructure of SiC–AlN particulate composite." *Journal of Material Science,* Vol. 33, pp. 1233–1237

Petrak, D.R., Ruh, R. and Atkins, G.R. (1974): "*Mechanical properties of hot-pressed boron suboxide and boron*", Ceram. Bull., Vol. 53, pp. 569-574.

Rizzo, H.F., Simmons, W.C. and Bielstein, H.O. (1962): "*The existence and formation of the solid B_6O*", J. Electro. Soc., Vol. 109, pp. 1079-1082.

Sasai, R., Fukatsu, H., Kojima, T. and Itoh, H. (2001): "*High pressure consolidation of B_6O-diamond mixtures*", J. Mater. Sci., Vol. 36, pp. 5339-5343.

Seung, K.L. and Chong, H.K. (1994): Effects of α-SiC versus β-SiC starting powders on microstructure and fracture toughness of SiC sintered with Al_2O_3-Y_2O_3 additives, *Journal of the American Ceramic Society,* vol. 77(6), pp. 1655-1658.

Shabalala T.C, McLachlan D.S, Sigalas I, Herrmann M, (2006): Hard and tough boron suboxide based composites. Advances in Science and Technology, vol. 45, 1745 – 1750.

Shabalala, T. C (2007): The preparation and characterisation of boron suboxide based composites. University of the Witwatersrand. PhD Thesis.

Spear, K. E. (1989): "Diamond: Ceramic coating of the fibre." Journal of American Ceramic Society, vol. 72, 171 - 191.

Srikanth, V., Roy, R., Graham, E.K. and Voigt, D.E. (1991): "*B_xO: Phases present at high pressure and temperature*", J. Amer. Ceram. Soc., Vol. 74, pp. 3145-3147.

Suk-Joong L. Kang (2005): Sintering: densification, grain growth and microstructure. Elsevier Butterworth Heinemann. Pg 3 - 18.

Takeda, M., Fukuda, T., Domingo, F. and Miura, T. (2004): "*Thermoelectric properties of some metal borides*", J. Solid State Chem., Vol. 177, pp. 471-475.

Torsten Lundström (1997): Structure and Bulk Modulus of High- Strength Boron compounds. Journal of Solid state chemistry, vol. 133, pp. 88-92.

Uno, R. and Higashi, I. (Eds.), (1994): Japan. Journal of Applied Physics, Series 10.

Veprek, S. "Nanostructured superhard materials", In *Handbook of ceramic hard materials,* [ed.] R. Rieldel, Weinheim, New York, Wiley, 2000, vol. 1, pp 104 - 134.

Wachtman, J.B. (1996): "*Mechanical properties of ceramics*", New York, John Wiley and Sons.

Wahi, R.P. and B. Ilschner, B. (1980): "Fracture behavior of composites based on Al_2O_3–TiC." *Journal of Material Science,* Vol. **15**, pp. 875–885.

Wentorf, R.H (1957): Cubic form of boron nitride. Journal of Chemistry and Physics, 26, 956 - 962.

Wentorf, R.H (1961): Synthesis of the cubic form of boron nitride. Journal of Chemistry and Physics, 34, 809 - 812.

Yu, S., Wang, G., Yin, S., Zhang, Y. and Liu, Z. "*Nanostructured films of boron suboxide by pulse laser deposition*", Phys. Lett. A., Vol. 268, 2000, pp. 442-447.

Zerr, A. and Rieldel, R. (2000): "Introduction: Novel ultrahard materials", In *Handbook of ceramic hard materials,* [ed.] R. Rieldel, vol. 1, pp XLV – LXXIII.

Zhongwu, W. and Yusheng Z. (2005): In situ pressure Raman spectroscopy and mechanical stability of superhard boron suboxide. Applied Physics Letters. Vol.86. No 041911, pp. 1-3.

www.chemtopics.com

www.uni-duisburg.de

www.memsnet.org

Appendices

Appendix A: Summary of the measured properties of all the hot pressed materials.

Table A1: summary of the measured properties of all the hot pressed materials.

Material	Load applied (MPa)	Wt % of additives	Vol. % of additives	Density (g/cm^3)	Theoretical density (g/cm^3)	% Theoretical density	Open porosity (%)	Hv_5 (GPa)	K_{IC} ($MPa.m^{0.5}$)	Phases after sintering
B_6O	50	-	-	2.45	2.55	96.1	0.9	30.5 ± 2.1	-	B_6O
B_6O + CaO	80	1.4	1.08	2.44	2.55	95.7	1.45	32.1 ± 1.9	6.8 ± 1.6	B_6O, CaB_6
B_6O + MgO	50	1.5	1.08	2.49	2.55	97.6	0.86	31.6 ± 2.1	6.1 ± 1.3	B_6O, $Mg_2B_2O_5$
B_6O + $CaCO_3$	80	0.7	1.08	2.50	2.55	98.0	0.97	31.6 ± 1.7	6.1 ± 1.7	B_6O, B_4C
B_6O + Ni	80	3.7	1.10	2.53	2.62	96.5	1.97	30.7 ± 1.1	6.4 ± 0.6	B_6O, NiB
B_6O + Ni_2B	80	1.5	0.75	2.57	2.59	99.2	0.75	31.1 ± 1.1	6.5 ± 0.8	B_6O, NiB
B_6O + NiO	80	2.8	1.10	2.54	2.59	98.1	3.97	27.1 ± 2.1	6.1 ± 0.9	B_6O, NiB
B_6O + Co_2B	80	2.1	0.65	2.51	2.59	96.9	1.47	34.9 ± 1.1	5.2 ± 0.5	B_6O, CoB
B_6O + CoO	80	2.7	1.10	2.55	2.59	98.5	1.58	32.6 ± 2.9	5.8 ± 1.1	B_6O, CoB
B_6O + CrB_2	80	1.7	0.40	2.51	2.57	97.7	1.35	32.1 ± 1.6	4.5 ±0.4	B_6O, CrB_2

Appendix A2: Estimation of theoretical densities.

Estimation of the theoretical density of the materials formed after sintering of the admixed powders was calculated in order to ascertain the densification obtained from the hot pressing process. It was assumed that all the additives in the powder completely transformed into their respective secondary phase after sintering. The theoretical density was determined from the rule of mixture expression given below

$$Theoretical\ density = \frac{100}{\left(\frac{Wt\ \%\ of\ B_6O}{\rho_{B_6O}}\right) + \left(\frac{Wt\ \%\ of\ A}{\rho_A}\right) + \ \ldots}$$

The theoretical density of B_6O was assumed to be 2.55g/cm^3

ρ_A= density of the resulting sintered phase.

<u>B_6O + CaO material</u>

Amount of CaO added = 1.4 wt%

Molar mass of CaO = 56.1 g/mol

Molar mass of CaB_6 = 104.9 g/mol

Assuming all the CaO was converted after sintering into CaB_6 with (calculated) density of 2.43 g/cm^3 (card no = 00-031-0254). Amount of B_2O_3 present = 1 wt %.

If X (in wt %) is the amount of CaB_6 formed after sintering, then

$$X = \left\{\frac{wt\ \%\ of\ CaO \times Molar\ mass\ of\ CaB_6}{Molar\ mass\ of\ CaO}\right\}$$

X = 2.62 wt%.

Therefore, the amount of B_6O in the material = (100 – 2.62 – 1) wt % = 96.38 wt %.

$$Theoretical\ density = \left\{\frac{100}{\left(\frac{97.38}{2.55}\right)+\left(\frac{2.62}{2.43}\right)+\left(\frac{1}{2.46}\right)}\right\}$$

Theoretical density = 2.55 g/cm^3

Table A2: Theoretical densities of sintered materials.

Materials	Amount of additives (g)	Secondary phase(s) after sintering	Calculated density of the secondary phase (g/cm^3)	Theoretical density (g/cm^3)
B_6O + CaO	1.4	CaB_6	2.43	2.55
B_6O + MgO	1.5	$Mg_2B_2O_5$	2.90	2.55
B_6O + $CaCO_3$	0.7	B_4C	2.52	2.55
B_6O + Ni	3.7	NiB	7.17	2.62
B_6O + Ni_2B	1.5	NiB	7.17	2.59
B_6O + NiO	2.8	NiB	7.17	2.59
B_6O + Co_2B	2.1	CoB	7.37	2.59
B_6O + CoO	2.7	CoB	7.37	2.59
B_6O + CrB_2	1.7	CrB_2	5.20	2.57

Appendix A3: Calculations of the weight percentage and volume percentage of the additives.

1.5g MgO was used as the basis. This was mixed with boron suboxide (B_6O) powder and then sintered. The equivalent amount of other additives was calculated to retain the volume percentage of the secondary phase in the mixture.

Mass of MgO in B_6O = 1.5g, Density of MgO = 3.6g/cm^3

Therefore, the volume occupied by MgO in the mixture was;

$$\rho = \frac{mass}{volumes}$$

Therefore, the volume occupied by MgO in the material was;

$$volume = \frac{mass}{density} = \frac{1.5}{3.6} = 0.42cm^3$$

Mass of B_6O = 98.5g, Density of B_6O = 2.55g/cm^3, therefore the volume occupied by B6O = 38.62cm^3. Hence, the total volume of the compact = (38.62 + 0.42)g/cm^3 = 39.04cm^3. Therefore, the percentage of volume occupied by MgO will be

$$Volume\ \%\ MgO\ in\ the\ compact = \frac{0.42}{39.02} \times 100 = 1.08\%$$

Table A3: Weight and volume percentages of the additives.

Additives	Density (g/cm3)	Amount of additives (g)	Volume percentage of additives
CaO	3.34	1.4	1.08
MgO	3.60	1.5	1.08
$CaCO_3$	2.71	0.7	1.08
Ni	8.91	3.7	1.10
Ni_2B	5.1	1.5	0.75
NiO	6.7	2.8	1.10
Co_2B	8.1	2.1	0.65
CoO	6.4	2.7	1.10
CrB_2	4.24	1.7	0.40

Appendix B: Milling results

Table B1: Milling results

	Duration (hrs)	Speed (Rpm)	$d_{0.1}$(µm)	$d_{0.5}$ (µm)	$d_{0.9}$ (µm)
Average	**10**	**400**	**0.29**	**0.623**	**1.344**
Average	**19**	**400**	**0.252**	**0.484**	**0.949**
Average	**20**	**400**	**0.252**	**0.509**	**1.093**

The graphical representation of the milled powder is given in figure B1 – B2

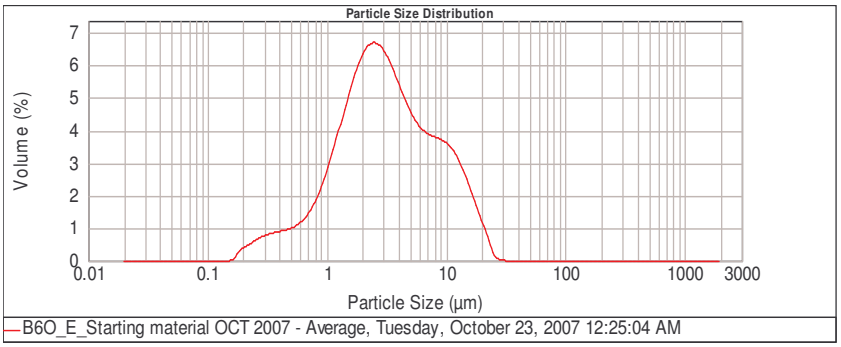

Figure B1: Graph of B_6O powder before milling.

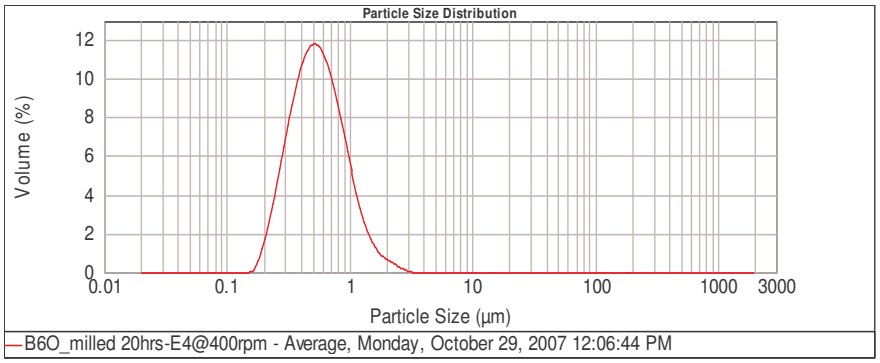

Figure B2: Graph of B_6O powder after milling for 20 hours.

Appendix C: XRD patterns of mixed powders after drying in the rotavap evaporator.

Appendix C1: XRD patterns of B_6O powders mixed with alkaline earth metal oxides

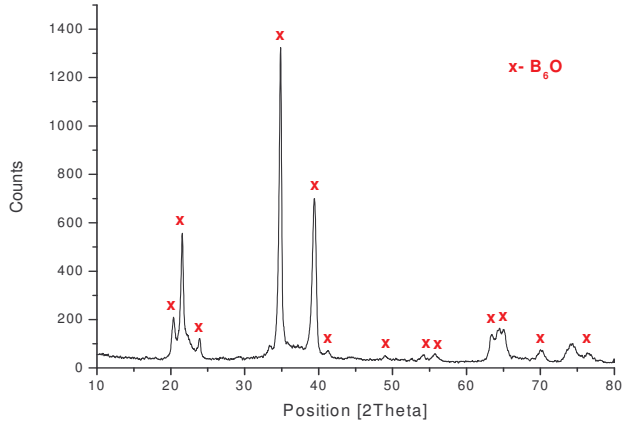

Figure C1a: XRD pattern of B_6O powder with CaO additive

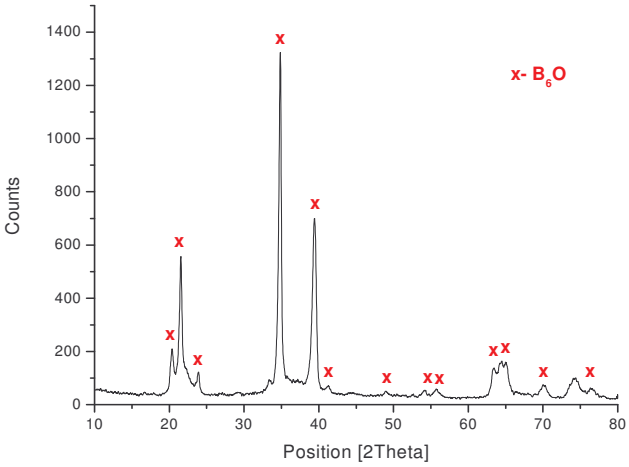

Figure C1b: XRD pattern of B_6O powder with MgO additive

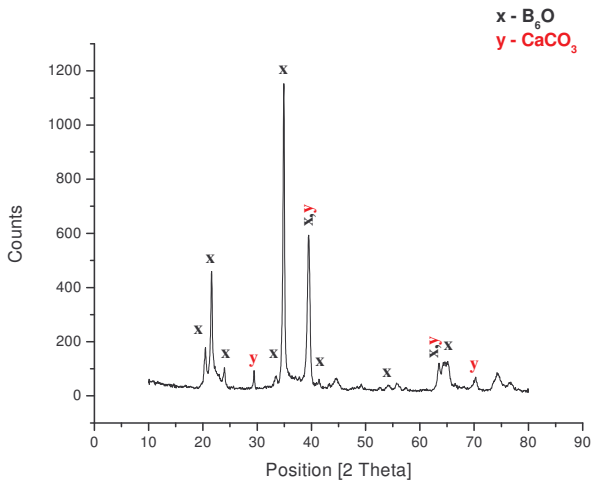

Figure C1c: XRD pattern of B_6O powder with $CaCO_3$ additive

Appendix C2: XRD patterns of B_6O powders mixed with nickel and nickel compound additives.

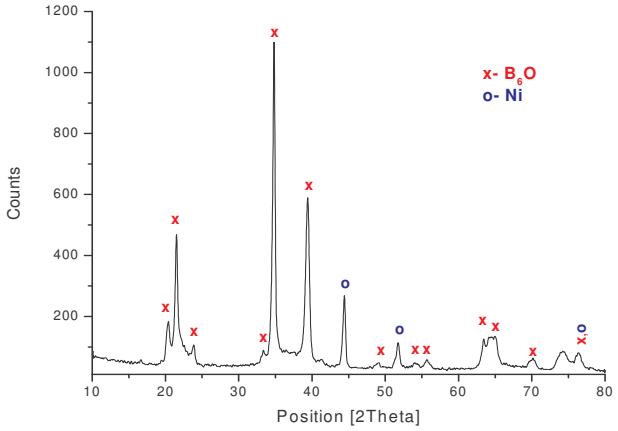

Figure C2a: XRD pattern of B_6O powder with Ni additive

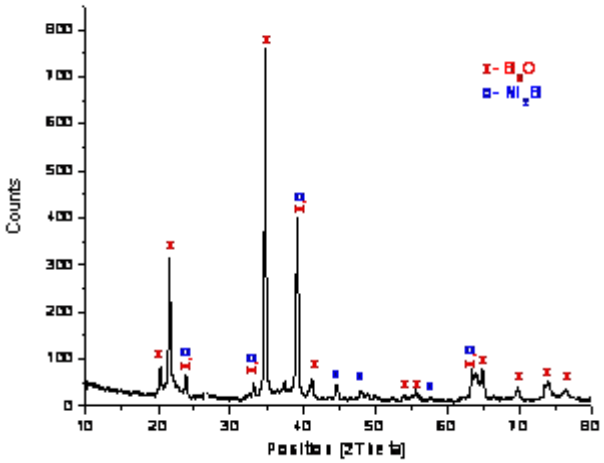

Figure C2b: XRD pattern of B_6O powder with Ni_2B additive

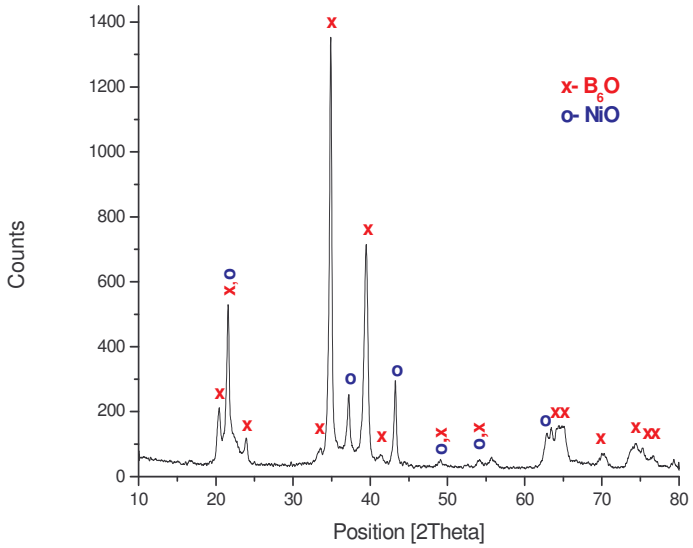

Figure C2c: XRD pattern of B_6O powder with NiO additive

Appendix C3: XRD patterns of B_6O powders mixed with cobalt compound additives.

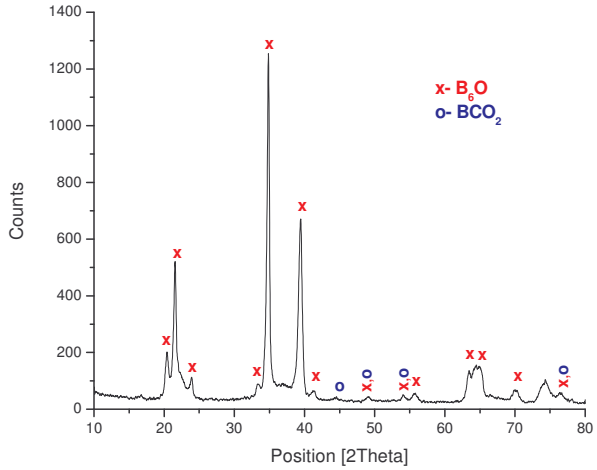

Figure C3a: XRD pattern of B_6O powder with Co_2B additive

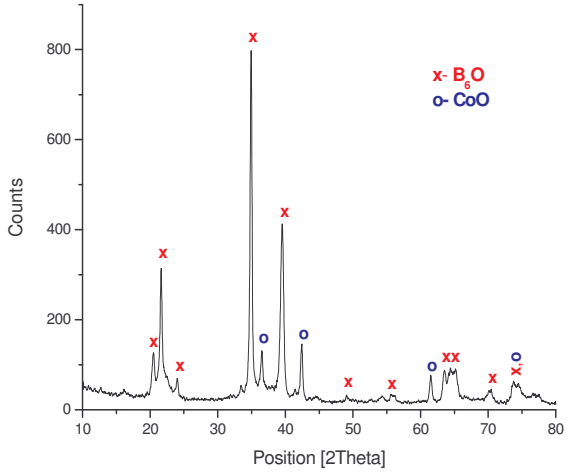

Figure C3b: XRD pattern of B_6O powder with CoO additive

Appendix C4: XRD patterns of B_6O powders mixed with chromium boride additives.

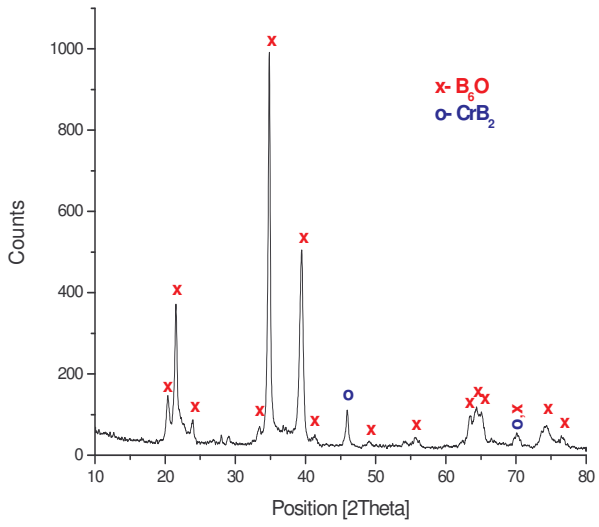

Figure C4: XRD pattern of B_6O powder with CrB_2 additive

Appendix D: SEM images of pure B_6O showing porosity.

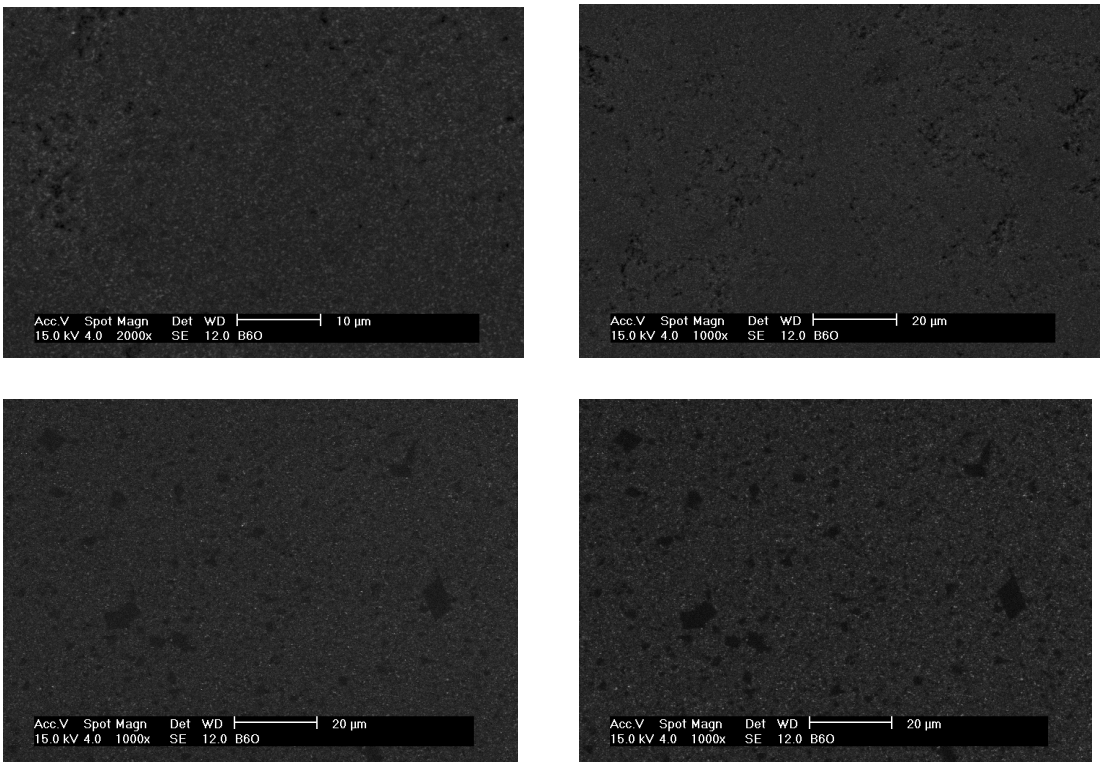

Figure D1: SEM images of pure B_6O showing pores.

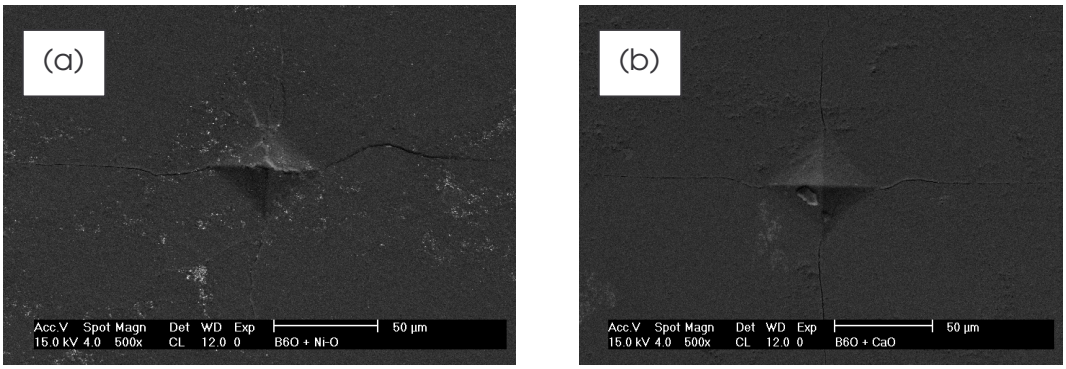

Figure D2: SEM images showing good indentations from different materials (a) NiO (b) CaO

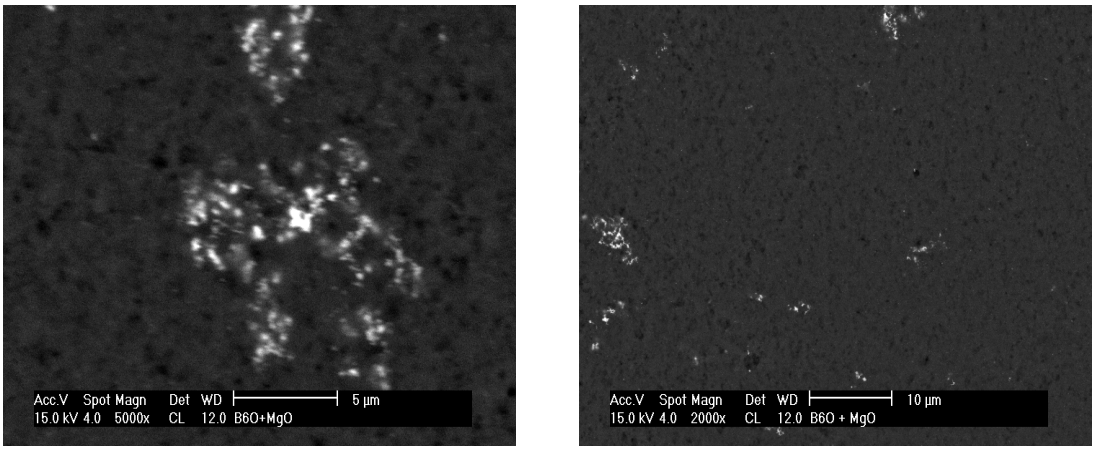

Figure D3: SEM images showing segregation in B_6O-MgO sintered material.